Copyright © National Academy of Forensic Engineers (NAFE). Redistribution or resale is illegal.
Originally published in the Journal of the NAFE volume indicated below.

Journal of the National Academy of Forensic Engineers®

http://www.nafe.org

ISSN: 2379-3252

DOI: 10.51501/jotnafe.v39i2

Vol. 39 No. 2 December 2022

National Academy of Forensic Engineers®

Journal Staff

Editor-in-Chief:

Bart Kemper, PE, DFE, F.ASME

Managing Editor:

Ellen Parson

Technical Review Process

The Technical Review Committee Chair chooses the reviewers for each Journal manuscript from amongst the members and affiliates of the NAFE according to their competence and the subject of the paper, and then arbitrates (as necessary) during the review process. External reviewers may also be utilized when necessary. This confidential process concludes with the acceptance of the finished paper for publication or its rejection/withdrawal. The name(s) of authors are included with their published works. However, unpublished drafts together with the names and comments of reviewers are entirely confidential during the review process and are excised upon publication of the finished paper.

National Academy of Forensic Engineers®

Board of Directors

President
Samuel Sudler, PE, DFE
Senior Member

President-Elect
Joseph Leane, PE, DFE
Fellow

Senior Vice President
Steven Pietropaolo, PE, DFE
Senior Member

Vice President
Michael Aitken, PE, DFE
Senior Member

Treasurer
Bruce Wiers, PE, DFE
Senior Member

Secretary
Richard Rice, PE, DFE
Fellow

Past Presidents
Liberty Janson, PE, DFE
Senior Member

James Petersen, PE, DFE
Fellow

John Certuse, PE, DFE
Fellow

Directors at Large
Daniel Couture, PEng, DFE
Senior Member

Robert Peruzzi, PhD, PE, DFE
Member

Executive Director
Rebecca Bowman, PE, Esq.
Member

Journal of the National Academy of Forensic Engineers®

Editorial Board

Editor-in-Chief
Bart Kemper, PE, DFE, F.ASME
Senior Member

Managing Editor
Ellen Parson
Affiliate

Senior Associate Editor
James Green, PE, DFE
Fellow, Life Member

Associate Editor
Zohaib Alvi, PE, DFE
Associate

Associate Editor
Rebecca Bowman, PE, Esq.
Member

Associate Editor
David Icove, PhD, PE, DFE
Fellow

Associate Editor
Mark McFarland, PE, DFE
Member

Associate Editor
Robert Peruzzi, PhD, PE, DFE
Member

Associate Editor
Steven Pietropaolo, PE, DFE
Senior Member

Associate Editor
Michael Plick, PE, DFE
Fellow

Associate Editor
Paul Stephens, PE, DFE
Fellow

Associate Editor
Paul Swanson, PE, DFE
Life Member

OJS Technical Editor
Mitchell Maifeld, PE, DFE
Member

Submitting Proposed Papers to NAFE for Consideration

Please visit the Journal's author page at
http://journal.nafe.org/ojs/index.php/nafe/information/authors for submission details.

We are looking for NAFE members who are interested in giving presentations on technical topics that will further the advancement and understanding of forensic engineering at one of the academy's biannual meetings and then developing those presentations into written manuscripts/papers, which will go through a single-blind peer review process before publication. Only papers presented at a NAFE regular technical seminar and that have received oral critique at the seminar will be accepted for review and publication. We recommend that you review the About the Journal page for the journal's section policies as well as the Author Guidelines listed on the Submissions page. Authors need to register with the journal prior to submitting, or (if already registered) they can simply log in and begin the process. The first step is for potential authors to submit a 150-word maximum abstract for consideration at an upcoming conference into the online journal management system.

Copies of the Journal

The Journal of the National Academy of Forensic Engineers® contains papers that have been accepted by NAFE. Members and Affiliates receive a PDF download of the Journal as part of their annual dues. All Journal papers may be individually downloaded from the NAFE website. There is no charge to NAFE Members & Affiliates. A limited supply of Volume 33 and earlier hardcopy Journals (black & white) are available. The costs are as follows: $15.00 for NAFE Members and Affiliates; $30.00 for members of the NSPE not included in NAFE membership; $45.00 for all others. Requests should be sent to NAFE Headquarters, 1420 King St., Alexandria, VA 22314-2794.

Comments by Readers

Comments by readers are invited, and, if deemed appropriate, will be published. Send to: Ellen Parson, Journal Managing Editor, 3780 SW Boulder Dr, Lee's Summit, MO 64082. Comments can also be sent via email to journal@nafe.org.

Material published in this Journal, including all interpretations and conclusions contained in papers, articles, and presentations, are those of the specific author or authors and do not necessarily represent the view of the National Academy of Forensic Engineers® (NAFE) or its members.

© 2022 National Academy of Forensic Engineers® (NAFE). ISSN: 2379-3252

Table of Contents

Ø Paper presented at the NAFE seminar held in July 2018 in Buffalo.
ᴗ Paper presented at the NAFE seminar held virtually in January 2021.
‡ Paper presented at the NAFE seminar held in July 2021 in Providence.
ϕ Paper presented at the NAFE seminar held in January 2022 in Tucson.
§ Paper presented at the NAFE seminar held in July 2022 in Toronto.

FE Investigation into Manufacturing- and Design-Related Issues Contributing to the Failure of a Climbing Treestand

By Jahan Rasty, PhD, PE, DFE (NAFE 768S), Mathew Mills, PE (NAFE 1199C), and Olin Parker

Abstract

The foot platform of a climbing treestand fractured while a user was standing on it in the process of securing his harness to a tree. Analysis of the frame's fracture surface revealed a manufacturing defect in the form of a ¼-inch diameter hole next to the fracture area, likely created during the welding process. To prove that this defect was the proximate cause of the treestand's failure (under reasonably expected and foreseeable use conditions), a series of tests on exemplar treestands as well as finite element analysis were performed. It was concluded that the defect reduced the fracture toughness of the treestand by 40%. In addition, it was found that the manufacturer failed to account for additional stress caused by dynamic loading experienced during normal use. The authors opined that both the reduced strength and the omission of dynamic loading in the design resulted in the treestand's frame failure. Appropriateness of the manufacturer's reliance on users always wearing their full body harness is also discussed. This paper examines the contribution of the drilled hole to the integrity and suitability of the ASTM-required Factor of Safety (FOS) of 2.

Keywords

Treestand, aluminum weld, manufacturing defect, dynamic overload, forensic engineering

Introduction

Hunters often use a variety of equipment to augment their experience. One such piece of equipment is a treestand — a platform affixed to a tree that allows the hunter to take an elevated position (typically between 15 and 30 feet above the ground). Treestands are commonly utilized to allow hunters to ambush their prey at short ranges, making the use of bows and other short range or less precise weaponry more viable. According to conducted marketing research, treestands are utilized by around 87% of hunters in North America, making it one of the most utilized pieces of hunting equipment[1,2].

A treestand typically consists of a two-by-two-foot platform seat with straps and cords that affix the device to the trunk of the tree. As expected of such a well-utilized device, treestands come in a variety of distinctive styles and configurations. Fixed or hang-on treestands utilize straps, chain, and/or serrated metal teeth to secure the stand to the trunk of a tree. To reach a fixed stand that has been previously set up, hunters use climbing sticks that they insert into the trunk of the tree. Ladder stands, on the other hand, provide the user with a ladder they can use to reach the stand platform. These stands offer greater stability because the load is carried by the ladder and the tree. Another commonly used variant is the climbing treestand. These two-piece stands (consisting of a foot-platform and a seat-platform) allow users to ascend the tree by wrapping the stand's cables around the tree trunk and moving one piece at a time until they reach their desired height.

According to available literature, falls from treestands are currently the most common cause of hunting-related injuries (50%), while accidental gun wounds account for 29% of injuries[3,4]. Of those who fell from a treestand, 80% were noted to have required surgery and 10% experienced permanent neurological disability or death[5]. Therefore, it is clear that falls from treestands present a significant hazard to the average hunter.

Treestands are known to experience failure from a variety of different mechanisms. For example, the plastic deformation or fracturing of the load-bearing sections of a treestand can result in loss of load-bearing capability,

Jahan Rasty, PhD, PE, 805 Boston Ave., Lubbock, TX 79409-9831, (806) 834-6571, jahan.rasty@ttu.edu

causing the user to plummet to the ground. Repeated usage can gradually induce fatigue in the load-bearing components, which can reduce the load-bearing capacity of the treestand to the point where normal operation can result in failure. Treestands that rely upon supporting cables or chains can have these components snap, resulting in the stand and its user falling. A treestand and its load-bearing components can also experience excessive corrosion, which renders the stand unfit for use. The mechanism engaging the stand to the trunk of a tree may also experience failure or a loss of efficiency, leading to the stand disengaging from the tree.

Background

In the present case, a 5-foot, 9-inch male user (weighing approximately 200 lb) suffered injury after the foot platform he was standing on snapped in two pieces, resulting in his fall from the tree while standing on the foot platform section of the stand. Based on the climber's testimony, the incident occurred while he was in the process of finalizing his climb and setting the stand in place. The climber had reached a fork in the tree about 18 to 20 feet above the ground, and was attempting to throw a rope around the tree to tie off his safety harness. In the process of throwing the rope, the foot section slipped, causing the treestand to fall a short distance with him on it before re-engaging. This motion of the foot section of the treestand caused the frame rail to experience dynamic loading that resulted in its fracture and the ensuing fall of the user to the ground.

Figure 1
Photograph showing a new treestand of the same model as the subject treestand.

The authors were retained to review provided documents pertinent to this case — as well as to determine the root cause of the treestand's failure — to render an expert opinion within a reasonable degree of engineering and scientific certainty, regarding the safety and suitability of the foot section as it related to the incident.

ASTM standards require the treestand to withstand static load twice the rated load. Initial review of the failed treestand revealed a manufacturing defect in the form of a weld hole at the failure site. This paper examines the contribution of the drilled hole to the integrity and the suitability of the ASTM-required FOS of 2.

Analysis of the Treestand

The treestand at issue — a climbing treestand constructed from an aluminum frame — was stated to have a rated weight capacity of 300 lb. Manufacturing documents failed to state what grade/alloy of aluminum was utilized in the construction of the treestand.

The treestand was comprised of two main sections, the seat (upper) section and the foot (lower) section, as shown in **Figure 1**. As described earlier, while the user was standing on the foot platform, the treestand lost its grip on the tree and slipped down a short distance before re-engaging. The dynamic loading created by this motion caused the foot platform to fracture into two pieces, as shown in **Figure 2**.

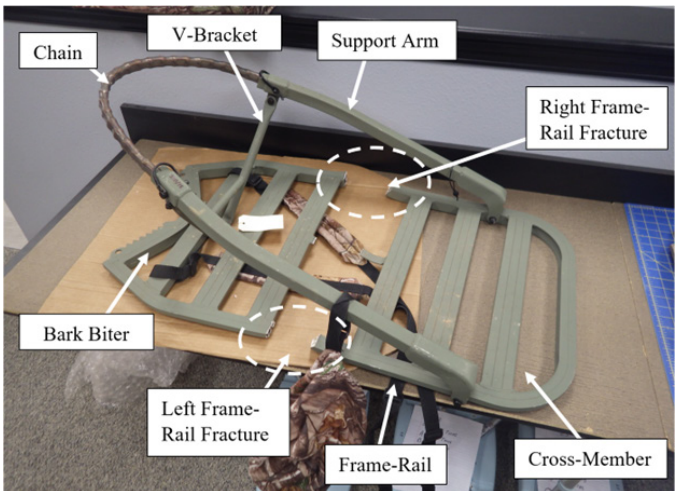

Figure 2
Photograph showing overall foot section of treestand with circles indicating failure locations.

The frame rail for the foot section of the treestand fractured at both the right and left sides of the frame rail (approximately halfway between the contact point with the tree and support arm). The bolt, which is used to connect the "V-bracket" to the support arms, was also fractured with its tab plastically deformed.

Closer examination of these three failure locations on the foot section revealed the presence of a ~¼-inch hole near a fillet welded cross-member connection to the frame rail (**Figure 3**). This hole, which appears to have been caused by improper welding during manufacturing, was located approximately 0.18 inches from the bottom of the frame rail adjacent to a weldment connecting the cross-member to the frame-rail.

When a climber is standing on the foot platform, the lower portion of the frame-rail's cross section (where the hole is) would be subjected to tensile bending stresses during normal usage of the device when the user is standing at the center of the platform. The presence of a ~¼-inch hole in the portion of the frame railing subjected to tensile bending stesses resulted in increased stresses (due to stress concentration effect of a hole) that exceeded the material's strength, causing the failure observed in **Figure 4** and **Figure 5**.

The presence of the protective coating on the inner surface of the hole (**Figure 6**) indicates that the hole existed at the time of the treestand's manufacture. Testimony from the manufacturer representative confirmed that this hole was accidentally created during the process of welding the treestand — and that the presence of such holes was common.

This hole was observed by the climber and his family

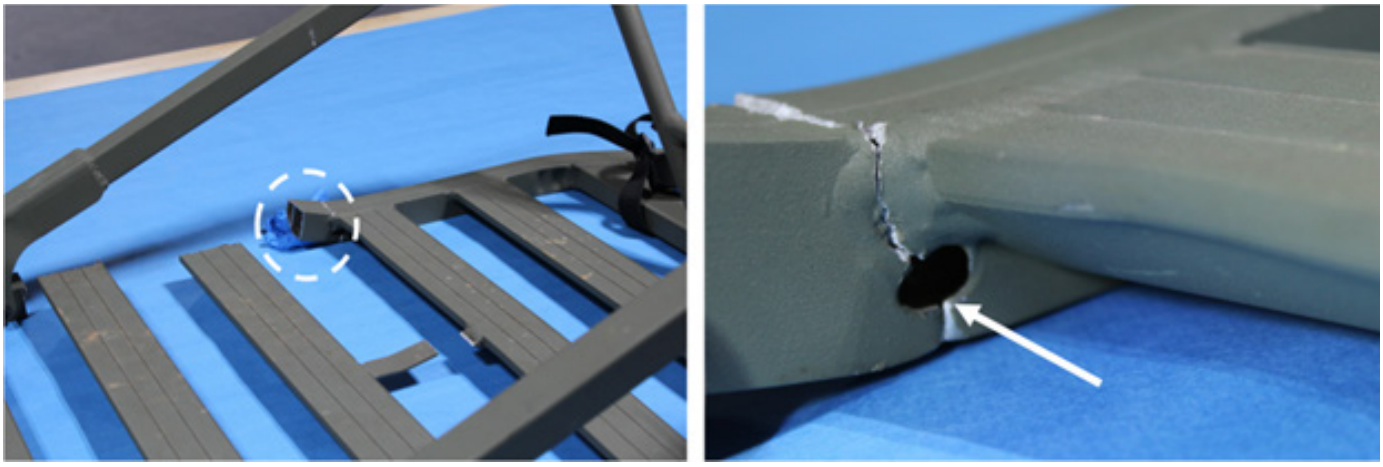

Figure 3
Photograph of the left frame-rail fracture in the treestand's foot section (left) and close-up of the hole (right), showing failure origin and direction of failure.

Figure 4
Photograph of the right frame-rail fracture in the treestand's foot section (left) and close-up of the fracture (right).

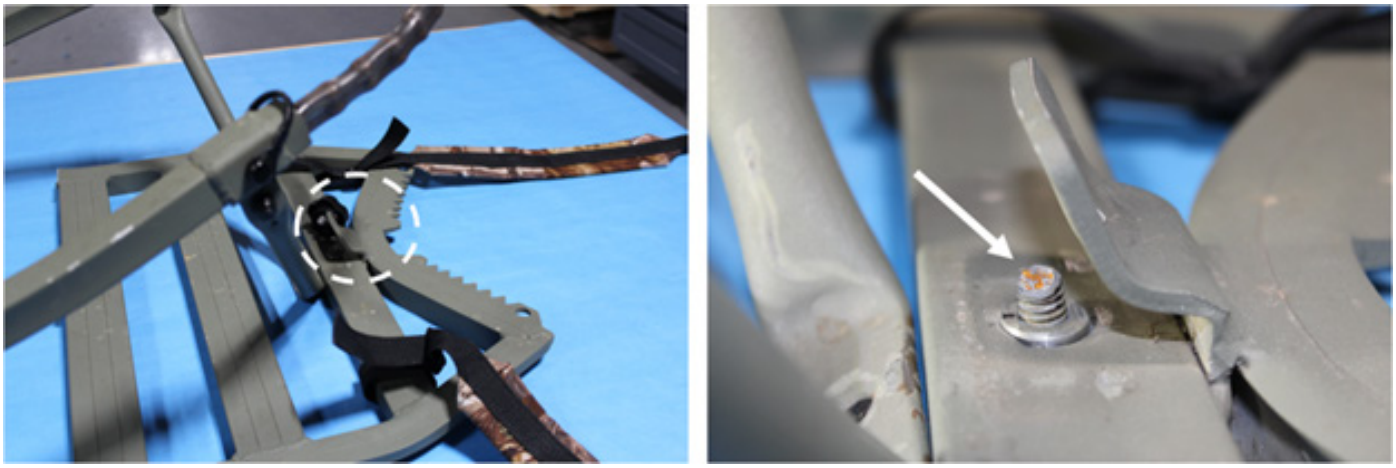

Figure 5
Photograph of the bolt fracture in the treestand's foot section (left) and close-up of the bolt fracture and bent tab (right).

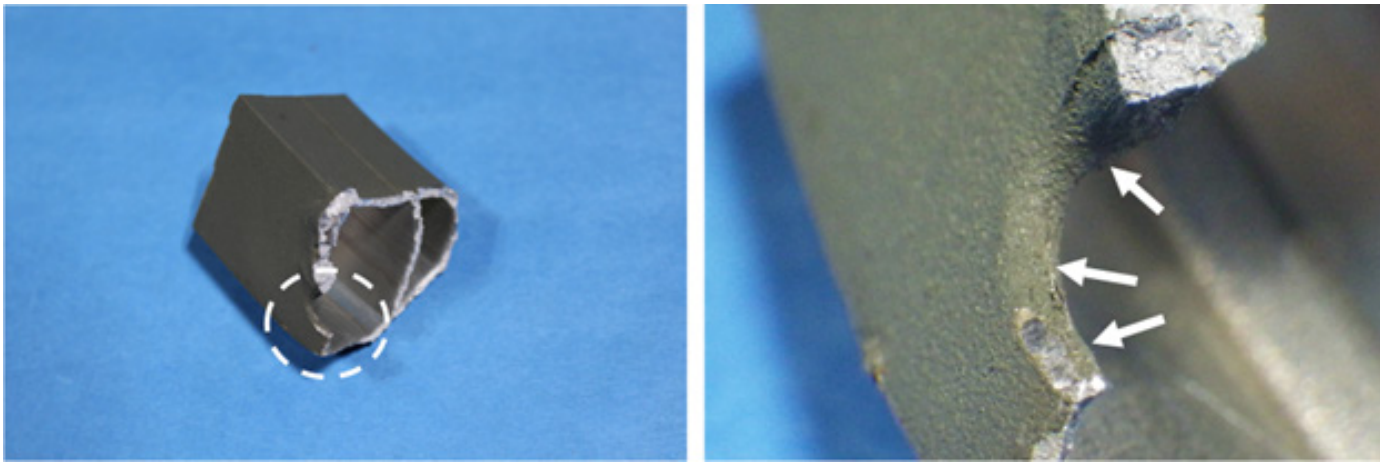

Figure 6
Overall (left) and close-up (right) of the failure area, showing the presence of protective coating around the periphery of the hole, indicative of hole being present prior to the application of coating.

during their inspection of the failed treestand after his fall. This observation led them to pursue legal compensation on the basis of a manufacturing defect.

Finite Element Analysis

To assess the stress-concentration effect of the discovered ¼-inch diameter hole (**Figure 6**) on magnifying the tensile stresses present in the side rail under the weight of the user (~200 lb), a finite element analysis (FEA) model of the treestand was created. A mesh sensitivity analysis was performed to arrive at the optimum mesh size for this analysis. The boundary conditions for the FEA model consisted of geometrical constraints where the foot platform is attached to the tree and supported by the support arms, as indicated by the white squares (**Figure 7**). The total weight of the user (200 lb) was equally distributed on the cross-members where the user would have been standing, as shown in **Figure 7**. The FEA model was run in a comparative study (with and without the discovered ¼-inch diameter hole) to assess the additional stresses created in the railing due to the presence of the hole. As this was comparative in purpose, the V-brace was not considered in the constructed model. The results of the FEA analysis revealed that the presence of the hole (a manufacturing defect) resulted in a 52.2% increase in Von Mises stress at this location — from 7.1 ksi to 10.7 ksi.

Experimental Analysis

Since the failure in this instance occurred as a result of the energy delivered by the user to the foot platform cross-members, it was sought to determine (through a series of experiments) the reduction in the energy absorption capability of the foot-platform's frame with and without the presence of the hole. To this end, two exemplar treestands were acquired. One was tested in as-received condition; the other was modified by drilling a ¼-inch hole at the

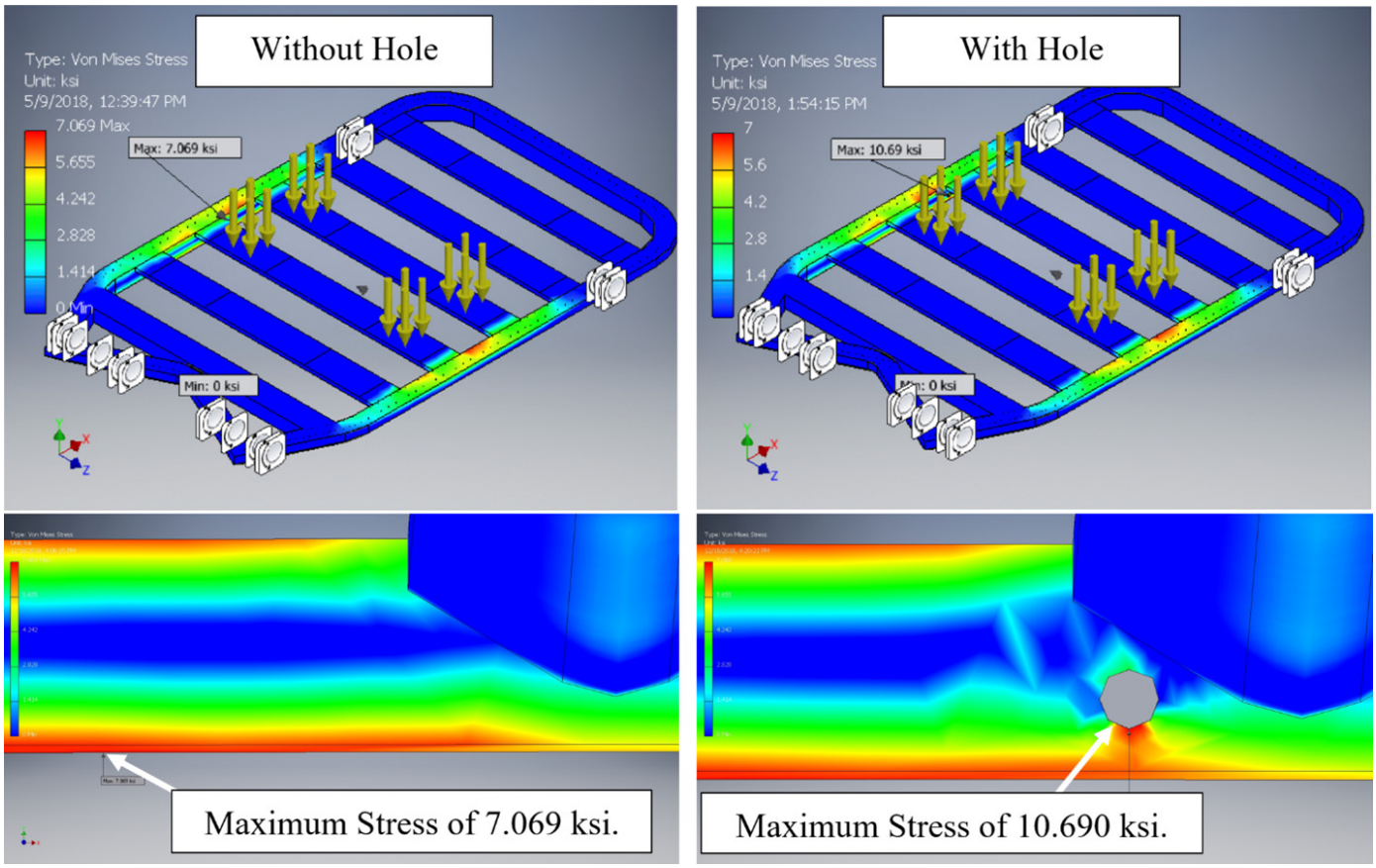

Figure 7
FEA analysis results comparing the Von Mises stresses of the frame railing with (right) and without (left) the discovered hole.

same location as the ~¼-inch hole identified on the frame rail of the treestand (**Figure 8**).

The experimental test setup (**Figure 9**) consisted of a ~10-inch diameter wooden pole on which the treestand was mounted. A 10-inch by 10-inch square steel plate was used to apply an increasing load to the cross-members of the frame in accordance with the TMS 11 standard for load testing of treestands. As the applied load to the cross-members was increased, the corresponding deflection of the frame was measured to arrive at the load-displacement response of the treestand's foot platform. The load was continually increased until the foot platform experienced failure of the frame railing. The area under the load-displacement response curve for each test was then utilized to arrive at the energy necessary to cause failure of the treestand's foot platform. The results indicated that the treestand without a manufacturing defect was capable of withstanding of 2,380 lb-in. of energy (max load of 1,120 lb) while the treestand with the hole was only able to withstand 1,425 lb-in. of energy (max load of 950 lb), representing ~40% reduction in energy absorption capability of the treestand.

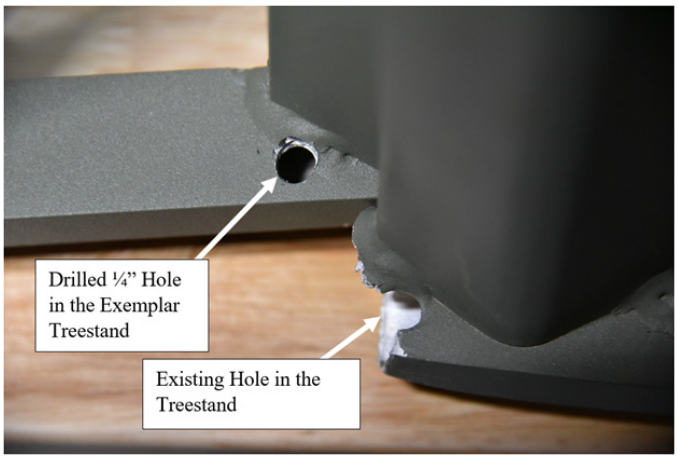

Figure 8
Photograph of hole drilled in exemplar next to manufacturing-induced hole.

Following completion of the tests, comparison of failure characteristics (crack origin and propagation direction) of the exemplar test treestand to that of the subject treestand revealed identical features, which is evidence of the validity of this test setup and

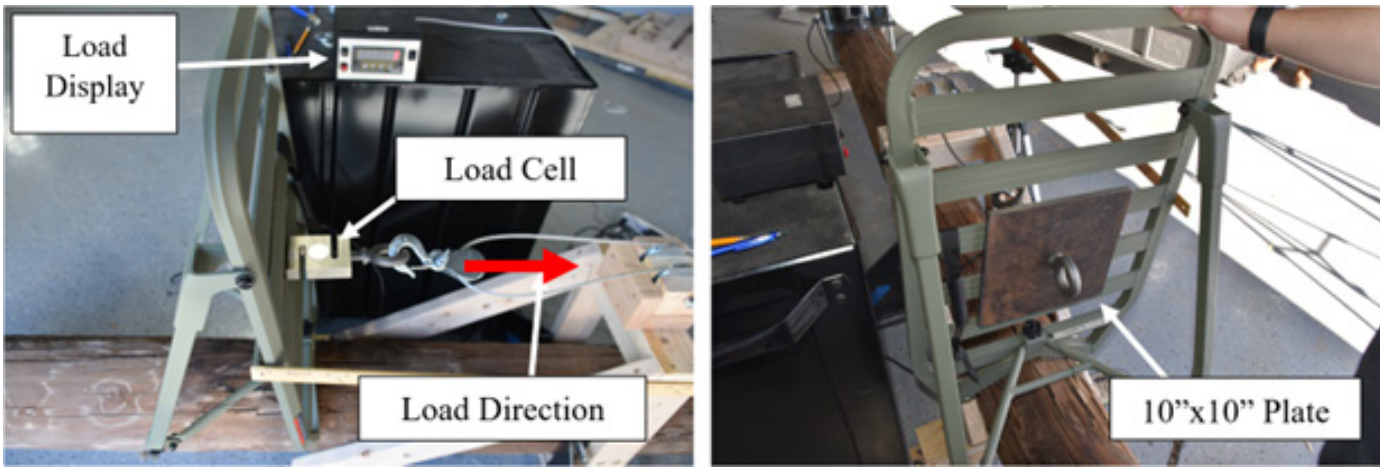

Figure 9
Photographs of test setup with red arrow indicating the direction of the applied load.

procedures used for the experimental phase of this study (**Figure 10**).

Based on the results of the experimental tests previously described, the 200-lb climber must have fallen a distance of at least 7.125 inches for his body to create the necessary energy of 1,425 lb-in. to cause failure of the foot platform's rail. Had the manufacturing-induced hole not existed at the time of the incident, the same 200-lb climber would have had to have fall 11.9 inches to reach the failure threshold energy of 2,380 lb-in. energy for a non-defective treestand. Given the climber's testimony that the foot platform slipped by a few inches before it reengaged with the tree, it is reasonable to conclude that the presence of the hole was the proximate cause of the treestand's failure.

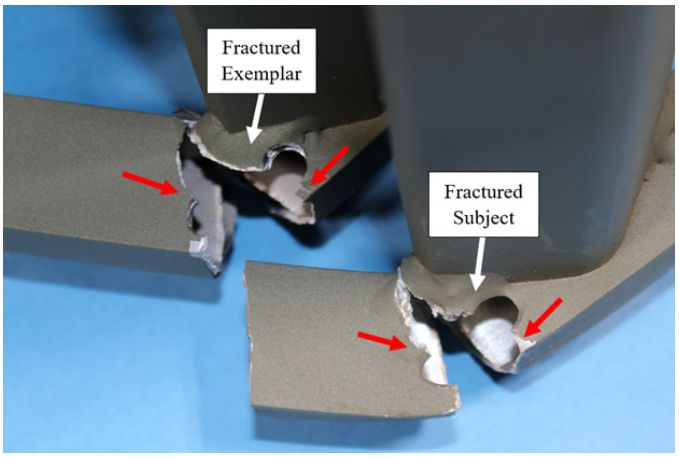

Figure 10
Near identical failure features between exemplar and subject treestands as evidence of the validity of experimental setup and procedures.

Manufacturer's Inadequate Quality Control Procedures

The Treestand Manufacturer's Association (TMA) Standard TMS 09[6] section 5.1 states that:

"A procedure shall be in effect so that appropriate inspections are made on manufactured parts and subassemblies to ensure conformance with engineering specifications."

In addition, section 5.3 of the same standard states that:

"A procedure shall be in effect so completed units are inspected prior to delivery."

As such, a manufacturer that is responsible for the design and/or distribution of the treestand should implement quality control procedures to ensure each part and each completed unit is properly inspected. If the treestand's frame rail or the assembled treestand had been properly inspected by the manufacturer, the presence of the hole near a sensitive area (heat-affected zone near the weld) would have been identified, and the treestand should have been rejected.

The manufacturer stated that the presence of welding-induced holes in treestand frames is a common occurrence that does not constitute a defect. While it is true that aluminum is notorious for being difficult to weld and "burn through" (causing a hole in one of the welded members) can occur, the results of the authors' experimental and numerical studies clearly indicate that such holes constitute a manufacturing defect as the stress concentration effect associated with such holes results in significant reduction of the load-bearing and energy-absorption capabilities of the

treestands under normal and anticipated use conditions.

Inadequacy of Treestand Design

The manufacturer testified that it is unreasonable to foresee a treestand being subjected to dynamic loads. However, the manufacturer also testified that treestand users are warned about the treestand disengaging from the tree and then reengaging, a mechanism that can result in the climber imparting a dynamic load upon the treestand (as was the case in this incident). Therefore, the manufacturers knew of the situations that might result in a dynamic loading environment. As such, the design of the treestand should have been commensurate with such a dynamic loading environment foreseen and warned against by the manufacturer.

Moreover, the load rating for the treestand was 300 lb. As indicated earlier, the authors' experimental results showed that this treestand (without any manufacturing defect) was only capable of withstanding 2,380 lb-in. of energy before failure. As such, a 300-lb individual would have to fall only 7.8 inches to reach the failure energy threshold of 2,380 lb-in. This indicates the presence of a design defect because the treestand can fail due to slippage of the foot platform (loaded at its rated capacity) by approximately 8 inches. Such an occurrence is not an unforeseeable event. In fact, it's one the manufacturer knows and warns about.

The manufacturer testified that the treestand was tested to TMS 11-98[7] and ASTM F2126-06[8] standards regarding the load capacity of climbing treestands. Both of these standards require climbing treestands to be tested to twice the rated capacity — or an FOS of 2 with respect to yield for static loading conditions. These standards only require an FOS of 2; however, TMS 11-98 section 4.1 and ASTM F2126-06 section 5.1 state the following regarding the significance and use of the standards:

"This test method is intended for quality assurance and production control purposes."

This indicates that the purpose of the standard is not to provide a guide for the sufficiency or safety of the design under foreseeable loading conditions, but rather to provide a method for providing quality assurance. In fact, in section 1.3 of both standards, it is clearly stated that:

"This standard does not purport to address all of the safety concerns, if any, associated with its use. It is the responsibility of the user of this standard to establish appropriate safety and health practices and determine the applicability of regulatory limitations prior to use."

Therefore, the manufacturer of the treestand should not have solely relied on these standards for its design or establishing the safety of its design. Instead, it should have identified foreseeable loading conditions that are beyond the scope of the above standards, including dynamic loading associated with a climbing treestand, for which an FOS of 2 is insufficient.

In 29 CFR 1917.118[9], "Fixed Ladders," subsection (d)(1)(ii), OSHA requires fixed ladders, a product designed to support users at an elevated height, to have an FOS of 4. Further, in 29 CFR 1926[10], "Safety and Health Regulations for Construction," subsection 451(a)(1), OSHA requires scaffolds, a product designed to support users at an elevated height, to also have an FOS of 4. Furthermore, in the manufacturer's own quality assurance document, section III(b)(i) states:

"Our quality assurance coordinator determines the pass/fail requirements. This is based on the weight rating, and they type of use. Every component and assembly must pass a 4-time weight rating test. (i.e., 300 lb. weight rated product: all components and assemblies pass up to 1,200 lb.)"

Although the treestand at issue was created for recreational purposes, this alternative use does not change the nature of consequences of the hazards that are present. Since these hazards have been identified and recognized by OSHA, a prudent designer would have incorporated their recommendations. By failing to do this, the manufacturer ignored a hazard present in their device and the well-known methods to alleviate it.

The designers deviated from their holding company's internal quality assurance standards by not testing to an FOS of 4 (which the subject treestand would have failed according to the authors' load-to-failure testing) and also deviated from applicable inspection standards and guidelines that would have rejected the subject frame rail based on the manufacturing defect present at the time the treestand was constructed. As a result of these deviations from design and manufacturing guidelines, the treestand suffered catastrophic failure resulting in the climber's subsequent injuries.

Inadequacy of Treestand Warnings

Figure 11 is a set of photographs showing a warning label attached on the treestand. This warning label states:

Figure 11
Warning label location on the treestand (left) and close-up of the warning (right).

"MAXIMUM WEIGHT CAPACITY: 300 LBS. — MINIMUM TREE DIAMETER: 9 INCHES"

This is a warning informing the user of the treestand's capacity and tree conditions. The warning label continues with the following statement:

"This product has been thoroughly tested and proper usage, and following of guidelines is mandatory for the safety of the user! Failure to follow these guidelines may result in serious injury or death!"

There are several issues with this section of the warning label.

The label shown in **Figure 11** states "this product has been thoroughly tested…" however, the treestand had never been tested. The overall design was tested under static conditions, but not tested to foreseeable dynamic loading conditions that the manufacturer both knew and had warned about. The manufacturer testified that the treestands are shipped directly from the manufacturer to the supplier without each individual treestand being tested. This indicates that the subject treestand was never tested. Additionally, the manufacturer stated that it had no knowledge as to whether or not the treestand's foot section was ever inspected.

Inappropriateness of Reliance on Safety Harness

The climber was criticized for not attaching the safety harness to the tree when beginning to climb prior to the incident. The climber stated that, when having done so in the past, the top portion of the treestand would disengage from the tree, presenting another safety hazard. In addition, the climber stated that he was aware of risks associated with utilizing a safety harness.

Treestand manufacturers recommend the use of safety harnesses, yet the use of such a device is not without risk. An HSC Contract Research report[11], entitled "Harness Suspension: Review and Evaluation of Existing Information," presents a study conducted on the Wright-Patterson Air Force Base in Ohio. In this study, young and healthy individuals were suspended in four different designs of full-body harnesses.

During the study, the tests were terminated when either the test subject voluntarily chose to end the study (due to symptoms including nausea, tingling and numbness of the extremities) or on-site medical professionals chose to end the test. The average suspension time was 14.38 minutes before the test was terminated. Further, an OSHA Safety and Health Information Bulletin (SHIB) 03-24-2004[12] describes the hazards associated with suspension trauma. It states that if a worker using a fall arrest harness can experience venous pooling, which can result in death in as little as 30 minutes.

The climber was hunting with a friend who was able to assist him in getting medical attention after the incident. The friend's testimony states that it took approximately 30 minutes to reach the climber after the incident — and that, if the climber would have still been suspended in the tree by his safety harness, it would have taken additional time to rescue him.

The hierarchy of controls (also known as the engineering hierarchy) represents the necessary steps to reduce exposure to a known hazard[13]. **Figure 12** is a graphic representation of the hierarchy of controls. These controls begin with the most effective steps and go down in order of effectiveness. The steps in order of effectiveness are: elimination, substitution, engineering controls, administrative controls, and PPE.

Providing the user with personal protective equipment

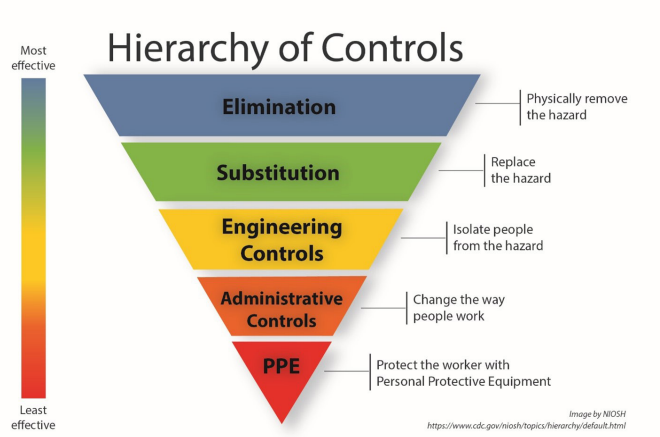

Figure 12
Hierarchy of controls[13].

(PPE) is the final, and therefore least effective, way to protect users from a hazard.

The engineering hierarchy for reducing/eliminating hazards requires that a known hazard should be eliminated by designing the hazard out of the system when possible. If a hazard cannot be eliminated through design, the next step is to guard against the hazard. Providing a safety harness/fall arrest system, which is accompanied by its own set of risks and hazards, does not give the designer/manufacturer free reign to produce and introduce into the stream of commerce defective and unreasonably dangerous treestands.

Summary

It was determined that the foot section contained a preexisting hole near a welded cross-member connection to the frame rails. More likely than not, the hole was generated during manufacturing of the treestand during the welding process.

Two exemplar treestands were experimentally tested to determine the threshold of energy as well as the maximum load to failure. One was tested in its as-received condition; the other was modified before testing to include a similar sized hole located at the same position as the hole found in the treestand. It was determined that a total energy of 1,425 lb-in. (max load of 950 lb) was required to induce an identical fracture in the exemplar treestand with a simulated hole. In contrast, it was determined that the exemplar treestand without a hole required a total energy of 2,380 lb-in. (max load of 1,120 lb) before fracturing. Therefore, it was concluded that the presence of the manufacturing-induced hole in the treestand's foot section resulted in ~40% reduction in load-bearing capacity of the treestand, thereby effectively eliminating the FOS of 2 that is reportedly used in the design of the treestand.

The Treestand Manufacturer's Association (TMA) standard (TMS-09 Rev. C) requires that each individual part and each assembled unit be inspected. The manufacturing-induced hole in the treestand was large enough and at a location on the treestand that would have been easily discoverable upon routine visual inspection. If the frame rail or assembled foot section had been inspected according to the above standard, this manufacturing-induced defect would have been discovered.

The design of the treestand relies on standards (TMS 11-98 and ASTM F2126-06) that require a minimum FOS of 2 with respect to the rated load capacity of the treestand under static loading conditions. However, due to the inherent nature of a climbing treestand (where the user is sliding the treestand up and down the tree during installation and disassembly), it is highly likely that at some point during this process, the user could slip, thereby imparting a dynamic load (impact energy) onto the treestand. As such, the design of the treestand was defective because it was only designed to withstand static loads without any consideration to additional stresses sustained by the treestand in the event of dynamic loading.

OSHA standards (29 CFR 1926.451 and 29 CFR 1917.118) require that scaffolds and fixed ladders, respectively, be designed to withstand four times the rated load capacity, or an FOS of 4. Both these devices are used to suspend individuals at a height, similar in function to the treestand that was only tested to an FOS of 2. This is in contradiction with the manufacturer's own quality assurance document, stating that components and assemblies should be tested to an FOS of 4.

Results of the authors' load-to-failure tests showed that the design of the treestand was defective, because as-designed, the tested exemplar treestands (with or without a hole) required 950 lb and 1,120 lb before fracturing, respectively, which is clearly less than four times the rated capacity (300 lb) of the treestand.

It has been reported that using safety harness/fall arrest systems can cause the user to be suspended for extended periods of time. This can lead to suspension trauma that can lead to death in as little as 30 minutes. A friend of the climber, who was hunting with the climber at the time of the incident, testified that it took him approximately 30 minutes just to find the climber's location after

the incident occurred. It is possible that the climber could have sustained suspension related injuries following the collapse of his treestand had he attached his harness to the tree prior to his fall. By not utilizing the safety harness, the climber in no way contributed to the failure of the subject treestand's foot platform.

Conclusions

The results of the investigation indicated the weld hole reduced the load bearing capacity of the treestand by approximately 40%. In addition, examination of the overall design showed the current ASTM requirement of an FOS of 2 was inadequate because it failed to account for reasonably expectable dynamic loads that might occur during the use of the treestand.

Since the failure of the frame rail sections occurred under bending stresses, alternative designs incorporating a larger cross-sectional moment of inertia (bending resistance) should have been utilized.

Manufacturers must be cognizant that simply meeting a design standard does not ensure their product meet with acceptable engineering and design. The manufacturer should utilize the available codes and standards for design work, but they cannot blindly assume that meeting them is sufficient for a safe and effective design, as the standards are the floor, not the ceiling, for safety considerations. Manufacturers must consider what could be reasonably expected to occur during the life of the product and how these conditions can alter the integrity and efficiency of the device. Finally, the manufacturer's reliance on safety harnesses to make up for the deficient design of its product was inappropriate and does not shield the manufacturer from liability should an incident occur.

Acknowledgements

The authors would like to thank the legal experts they worked with on this case as well as their dedicated team of forensic engineers and interns.

References

1. DDH Staff "One in Three Hunters Will Fall" Deer and Deer Hunting, https://www.deeranddeerhunting.com/deer-hunt/deer-hunting-tips/p3_one_in_three_hunters_will_fall (Accessed Aug. 23, 2022).

2. J. Smith et al. "Injuries Due to Falls from Hunters' Tree Stands in Pennsylvania" American Journal of Preventative Medicine, vol. 37, no. 5, pp. 422-436, Nov. 2009.

3. M. Metz et al. "Tree stand falls: a persistent cause of sports injury" Southern Medical Journal, vol. 97, no. 8, pp. 715-719, Aug. 2004.

4. A. Crocket et al. "Tree stands, not guns, are the midwestern hunter's most dangerous weapon" The American Surgeon, vol. 76, no. 9, pp. 1006-1010, Sep. 2010.

5. C. A. Pierre et al. "Tree stand falls: A persistent cause of neurological injury in hunting" World Journal of Clinical Cases, vol. 2, no. 8, pp. 345-350, Aug. 2014

6. Standard Practice for Treestand Manufacturer Quality Assurance Program, TMS Standard 09, 2009.

7. Standard Test Method for Treestand Static Load Capacity, TMS Standard 11, 1998.

8. Standard Test Method for Treestand Static Load Capacity, ASTM Standard F2126, 2006.

9. Fixed Ladders, 29 C.F.R. §1917.118.

10. Safety and Health Regulations for Construction, 29 C.F.R. §1926.

11. P. Seddon, "Harness Suspension: Review and Evaluation of Existing Information" Health and Safety Executive, Contract Research Report 451/2002, 2002.

12. OSHA, "Suspension Trauma/Orthostatic Intolerance" Occupational Safety and Health Administration, Washington, D.C., SHIB 03-23-2004, Mar. 23 2004.

13. "Hierarchy of Controls" U.S. National Institute for Occupational Safety and Health, https://www.cdc.gov/niosh/topics/hierarchy/ (Accessed Aug. 23, 2022).

Current Assessment of Stand-Up Forklifts' Underride Accidents

By Richard M. Ziernicki, PhD, PE, DFE (NAFE 308F) and Ricky Nguyen, PE, DFE (NAFE 1223M)

Abstract

Stand-up forklift collisions with storage racks are a known hazard in the material-handling industry. When the height of the first rack beam from the floor is close to or above the height of the forklift's operator compartment — and is at a height that is lower than the forklift's overhead guard — the rack beam can intrude into the forklift's operator compartment. These collisions are typically referred to as "horizontal intrusion incidents," also known as "underride" incidents. When the forklift is not equipped with horizontal intrusion guarding, these occurrences often lead to serious (if not fatal) injuries. This paper presents physical testing and analysis of one major forklift manufacturer's accident database records, which show rear-mounted posts are effective guards in reducing or preventing the consequences of horizontal intrusion incidents. Further, this paper shows these rear post guards met and exceeded design requirements of the material-handling industry standards.

Keywords

Forklifts, horizontal intrusion, under-ride, stand-up forklifts, guarding, safety, forensic engineering

Introduction

In the material-handling industry, stand-up forklifts are commonly used to handle materials within a storage facility, such as in an outdoor yard or indoor warehouse. Even though stand-up forklifts come in various sizes, they are smaller than an average gasoline-powered sedan. However, they are heavy pieces of machinery that commonly weigh as much as three times the weight of an average sedan — upward of 9,000 pounds or more without loads. They can also carry loads as heavy as 4,000 pounds, and some can travel as fast as 9 mph. This may not seem fast on public roads, but these forklifts are commonly used in warehouses with narrow aisle storage racks (some less than 10 feet wide) with workers walking around the warehouse floor. In addition, unlike a vehicle and sit-down forklifts, stand-up forklifts are operated from a standing position and controlled by the throttle controls with one hand and the steering controls with the other. These machines can be operated with forward or reverse (also known as "forks-trailing") steering setups.

The operator compartment structure for a stand-up forklift typically consists of four walls with an opening to allow operators to ingress and egress from the compartment. The walls at the end of the forklift (opposite the forks) typically extend up to a height of approximately 4.5 feet tall off the floor. Stand-up forklifts are also equipped with overhead guards that are at a height of typically 7 feet to 8 feet off the floor (**Figure 1**).

Research has shown the most common form of injury occurrences involving stand-up forklifts are collisions[1,2,4]. Since stand-up forklifts are commonly used in storage warehouses, colliding into storage racks has been known and documented for decades. Depending on the forklift and storage rack configuration — when the height of the first rack beam from the floor is close to or above the height of the forklift's operator compartment and is at a height that is lower than the forklift's overhead guard (see **Figure 2**) — the rack beam can intrude into the forklift's operator compartment when forklifts are traveling in reverse toward a rack.

Underride incidents are serious — many times even deadly — when there is a lack of horizontal intrusion guarding to prevent or mitigate the adverse effects of the collision. **Figure 3** and **Figure 4** are 3D graphics that depict the result of a stand-up forklift override incident the authors investigated and reconstructed.

Horizontal Intrusion Guarding

The authors' experience includes investigating

Richard M. Ziernicki, PhD, PE, 7185 S. Tucson Way, Centennial, CO 80112, (303) 925-1900, rziernicki@knottlab.com

Figure 1
A stand-up forklift (green arrows added to outline the walls around the operator compartment). Blue arrow added to show overhead guard.

Figure 2
Storage racking system.

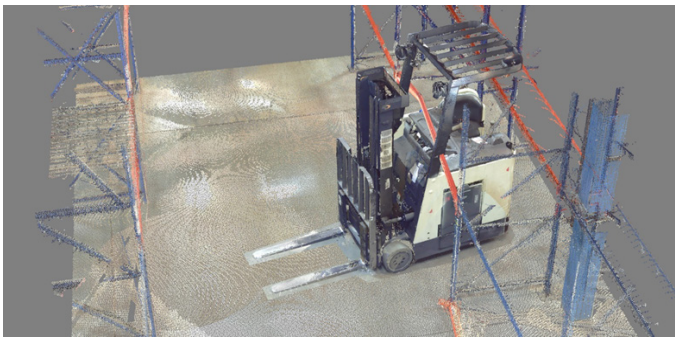

Figure 3
3D graphic of a rack beam that had intruded into a stand-up forklift's occupant compartment.

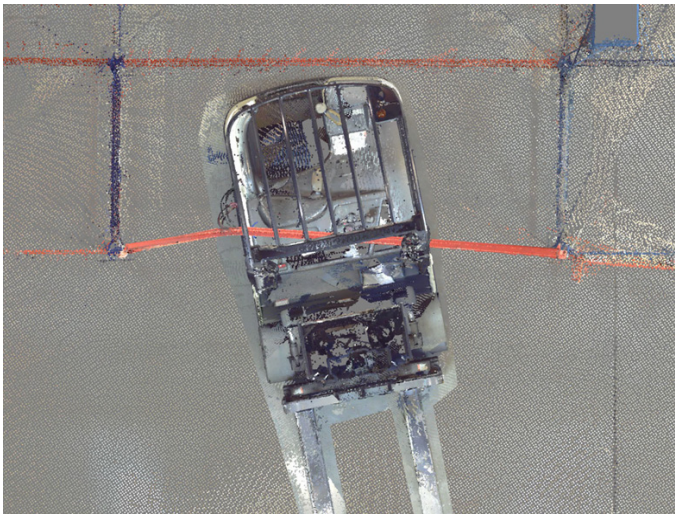

Figure 4
3D graphic of a rack beam that had intruded into a stand-up forklift's occupant compartment (from a top-down view).

numerous stand-up forklift underride incidents, which include inspections of more than two dozen stand-up forklifts and storage rack systems. Based on the authors' experience, most stand-up forklifts have operator compartment heights at about 4.5 feet, and first level beams are also typically configured above that height, such as around 5 feet (as seen in home improvement stores). This mismatch of operator compartment height and first level rack beam is commonly seen in warehouses.

Two well-known methods to safeguard against horizontal intrusions are:

1. Have a forklift equipped with guarding, such as a third corner post, to prevent/minimize horizontal beam intrusion into the occupant compartment. A third corner post is a vertical upright (usually fabricated out of common steel) that is installed between the forklift's main power unit and

overhead guard at the rear left corner the forklift (with the front of the forklift being where the forklift's forks are pointing toward), hence the "third-corner" designation (**Figure 6**). This post needs to be provided by the forklift manufacturer due to Occupational Safety and Health Administration's (OSHA) regulations that state any modifications to the forklift must be approved by the forklift's manufacturer (Title 29, 1910.178(a)(4)). Furthermore, when forklifts are equipped with horizontal intrusion guarding systems, the system must meet performance requirements outlined by the American National Standards Institute (ANSI)/ Industrial Truck Standards Development Foundation's (ITSDF) B56.1 "Safety Standard for Low Lift and High Lift Trucks" for the manufacturer of forklifts.

Some manufacturers do equip or have a post available for the forklift's fourth corner (or the rear right corner) to provide additional horizontal intrusion protection (**Figure 5**). However, others have equipped their stand-up forklifts with a fourth corner extension to provide horizontal intrusion protection instead (**Figure 6**). These extensions are typically either a weldment to the forklift's outer wall plate metal or was formed with the plate metal that surrounds the operator compartment. However, unlike a post that extends from the walls of the operator compartment to the overhead guard, these extensions do not extend to the operator guard — and typically extend to only about a height of 5 to 6 inches above the height of the operator compartment walls.

Aftermarket rear posts manufactured by third-party vendors can be purchased and installed on stand-up forklifts that originally did not come with rear posts. From the authors' communication with the manufacturers, these aftermarket posts have been third-party tested, and the results

Figure 5
A stand-up forklift equipped with a third corner post and fourth corner post as a standard feature.

Figure 6
Stand-up forklift equipped with a third corner post (arrow "1") and a fourth corner extension (arrow "2").

showed their design met the requirements of the ANSI/ITSDF B56.1 standard. The authors had not verified the test results at the time of this paper, but evaluations/verifications of these test results could be performed as part of a future study. The aftermarket post manufacturer further stated that forklift manufacturers do not endorse or provide approval to install these aftermarket posts on their forklifts to meet the 1910.178 regulation regarding forklift modification. Furthermore, the aftermarket posts manufacturer mentioned that end-users have petitioned OSHA to allow them to install these aftermarket posts on their forklifts without approval from the forklift manufacturer.

2. The other method to safeguard against horizontal intrusions is to have a rack system with horizontal rack beams placed at specific heights or add structures, such as a curb, to prevent the occurrence of forklifts under-riding the beams. This needs to be done by the warehouse owner/designer.

   Unless the racking system was initially designed or configured to prevent horizontal intrusion incidents, the existing racking system would need to be modified or retrofitted to provide underride guarding for the forklifts with too low of a fourth corner extension and lack of a third corner post. A common issue with modifying or retrofitting an existing rack system is that the changes can affect the volume and load capacity of the rack system for an entire warehouse, which can be physically and financially impractical.

   The alternative, mounting a post to one or both corners of the forklift, is less of a financial burden (a few hundred dollars for parts and installation) and does not depend on the various configurations of rack systems to be effective.

Forklift Industry Regulations, Standards, and Literature Regarding Rear Posts Guards

In July 2009, OSHA published a Safety and Health Information Bulletin (SHIB) titled "Standup Forklift Under-Ride Hazards." In the bulletin, one of the recommendations OSHA makes was: "*Purchase, where appropriate, standup forklifts that have corner posts, extended backrest, rear post guards, or other features to prevent an under-ride from occurring*"[5].

In August 2004, the National Institute of Occupational Health and Safety (NIOSH) published a Fatality Assessment and Control Evaluation (FACE) report regarding a horizontal intrusion incident that occurred in Iowa in 2003. As a result of the incident, NIOSH recommended: "*manufacturers of stand-up reach forklifts should include vertical framing or post at the rear corners of their machines, from the operator's console to the overhead guard, to protect the operator from horizontal components entering the operator's station*"[6].

Since the early 1990s, the ANSI/ITDSF B56.1, "Safety Standard for Low Lift and High Lift Trucks," contains language that allows manufacturers to equip forklifts with means to protect the operator from the intrusion of horizontal beams, such as rear posts[7]. Further, the standard provides test methodologies and performance criteria for horizontal intrusion guards.

The Industrial Truck Association (ITA) has an engineering committee that included representatives from forklift manufacturers in the industry. In the early to mid-1980s, one of the specific hazards that the committee addressed was the hazard of horizontal intrusion. By 1989, the ITA adopted a recommended practice regarding horizontal intrusion that was similar to the ANSI/ITDSF B56.1 standard's language regarding a means to protect the operator from the intrusion of horizontal beams[8].

Methodology

To analyze the effectiveness and increased safety benefits of equipping stand-up forklifts with rear posts in preventing/minimizing the consequences of horizontal intrusion incidents, the authors analyzed one major forklift manufacturer's accident database to determine if there was a decreasing trend in serious and fatal injuries caused by horizontal intrusion incidents, after the manufacturer equipped their stand-up forklift with a third corner post. The authors then addressed the issues of manufacturers not having these vertical posts as standard equipment on their stand-up forklifts by evaluating their decision with accepted safety engineering practices. Physical testing was also reviewed to analyze the performance of rear posts with criteria outlined in the ANSI/ITDSF B56.1 standard.

Analysis

Manufacturer Statistics

In older studies, Manufacturer A's forklift accident database, consisting of more than 3,000 stand-up forklift accidents, was analyzed. The data indicated there were 250 horizontal intrusion accidents, which resulted in more

than 12 fatalities and 100 serious injuries from 1977 to 2005[1]. The database has since been updated, with records of more than 5,000 accidents that occurred up to the year 2017. **Figure 7** through **Figure 10** are graphs created with information from the updated database.

The updated database showed that by the year 2017, the number of reported horizontal intrusion accidents increased to 303. Furthermore, the number of accidents resulting in fatal injuries increased to 15, and the number of accidents resulting in serious injuries increased to 130.

Analysis of the data showed that the rate of annual horizontal intrusion occurrences started to rapidly decline in the year 1999 and then leveled out to a steady rate starting in the year 2009. The decline in horizontal intrusion occurrences could be attributed to changes in operator training requirements in the 1910.178 regulations for powered industrial trucks. However, the annual rate for the combined number of serious and fatal injuries in horizontal intrusion accidents did not have the same rapid decline (four to eight occurrences per year) until the year 2008 (less than four occurrences per year), as shown in **Figure 11**. It is also worth mentioning that there has been zero reported deaths since the year 2007.

The decline in serious and fatal accidents starting in the year 2008 coincides with the manufacturer's decision to make a third corner post a standard feature on all its stand-up forklifts, starting in 2007. From review of the updated database, the authors also found zero horizontal intrusion accidents that resulted in serious or fatal injuries involving their stand-up forklifts that were equipped with a third corner post as a standard feature. Although there are still reported occurrences of horizontal intrusion accidents that resulted in serious injuries since 2007, the data showed these accidents involved older model forklifts that were not equipped with a third corner post as a

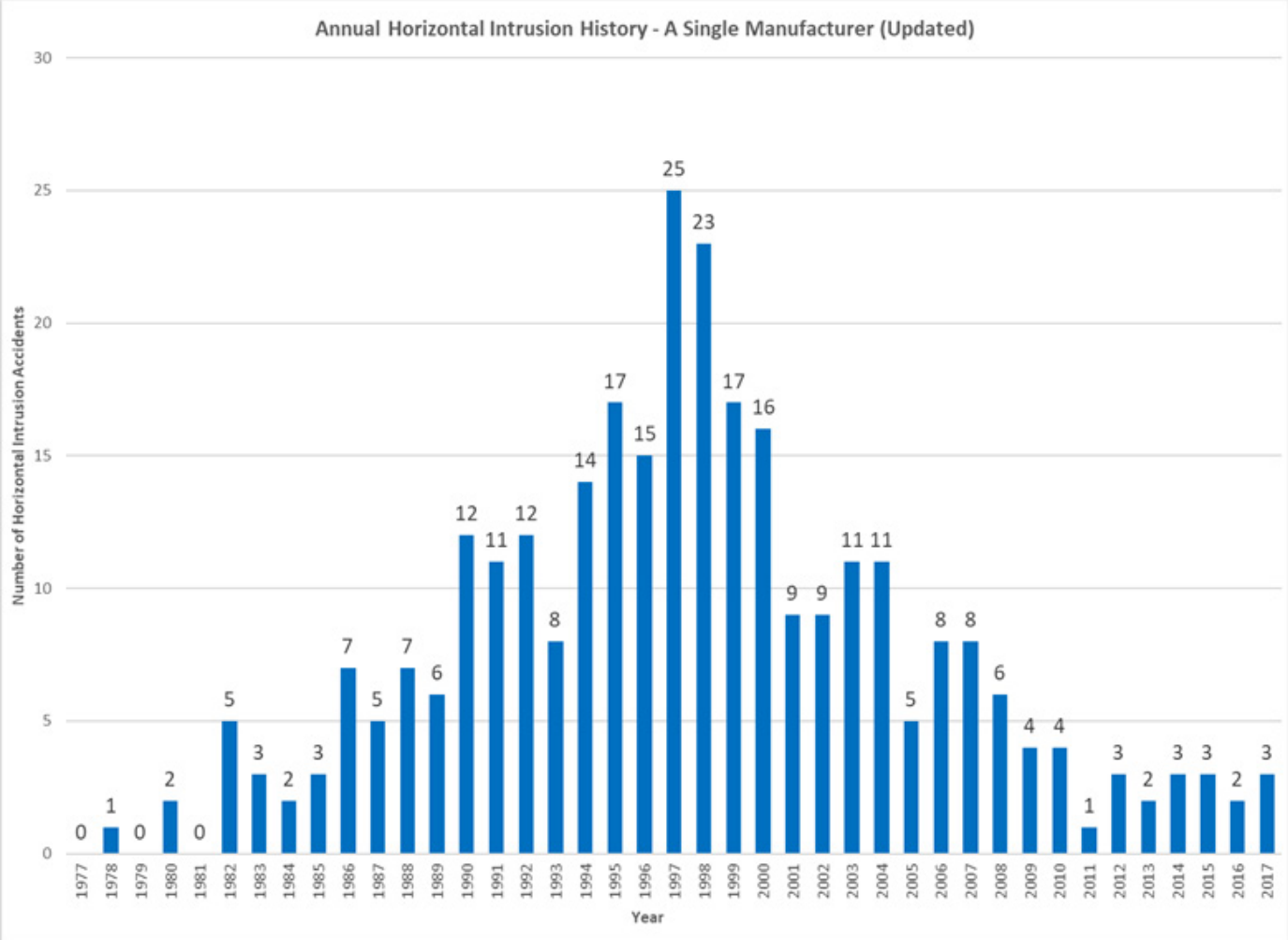

Figure 7
Graph showing the annual number of horizontal intrusion accidents from Manufacturer A's updated database.

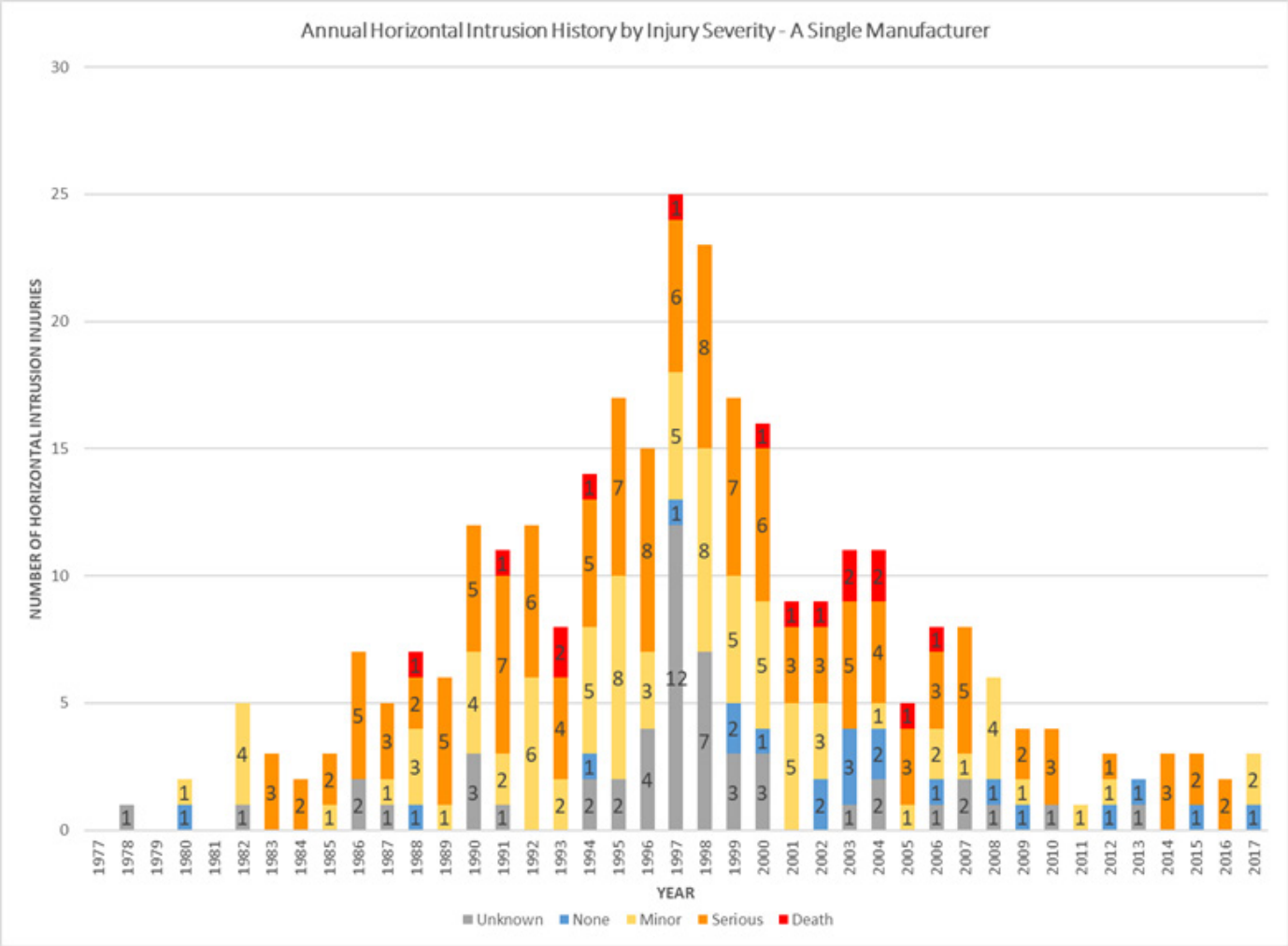

Figure 8
Graph showing the number of annual horizontal intrusion accidents, categorized by injury severity from Manufacturer A's updated database.

standard feature (pre-2007). Therefore, it could be inferred from the accident data that the significant reduction/elimination of serious/fatal horizontal intrusion injury occurrences was due to the addition of the third corner post on modern stand-up forklifts.

Although rear posts have been known to protect operators from the hazard of intruding horizontal beams for decades (and more manufacturers are adopting single or multiple rear posts as a standard feature on their forklifts), some still choose to not make rear posts a standard feature on their stand-up forklifts. Even though the manufacturers may offer one or two rear posts on the forklifts as an optional feature, making the post an optional feature requires the customer to make the decision to add the post for an additional cost. The manufacturers even list some claimed negative considerations associated with rears post in promotional material, further discouraging customers from purchasing the rear post additions. For example, the negative considerations associated with the third corner post that Manufacturer A listed in brochures included the following:

- Doesn't protect in all cases
- Pinch/crush point
- Post may shear/break, striking the operator
- Operator may use post as a bumper
- May create false sense of security with operator

The authors acknowledge that the presence of a third corner post potentially introduces hazards associated with the above negative considerations. However, review of Manufacturer A's accident database from 1977 through 2017 showed the number of serious or fatal injuries (18

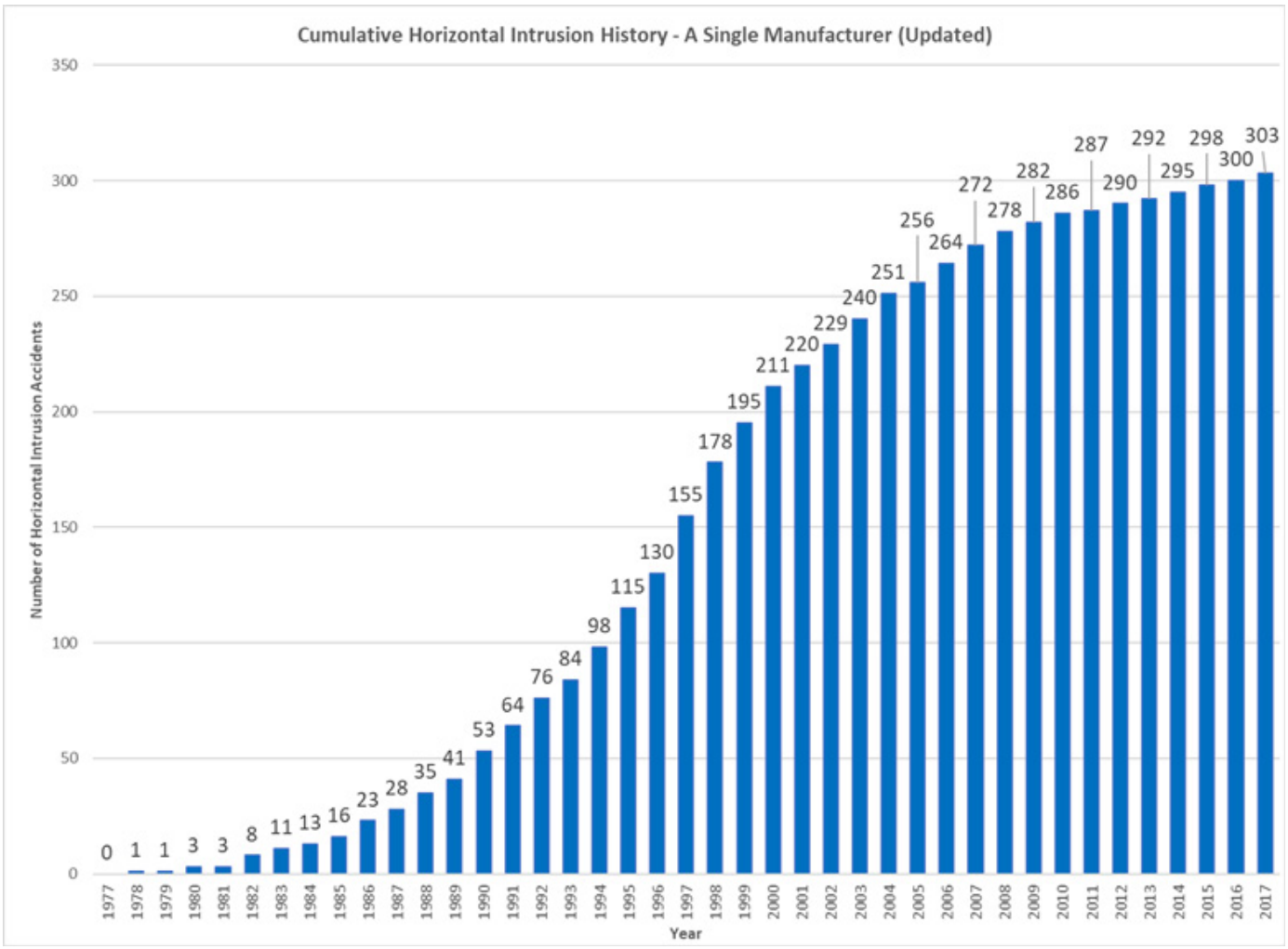

Figure 9
Graph showing the cumulative number of horizontal intrusion accidents from Manufacturer A's updated database.

accidents) that were reportedly caused by claimed hazards associated with the third corner post was an order of magnitude less than the occurrence of serious or fatal horizontal intrusion accidents (more than 140 accidents from 1977 through 2017). The data would indicate that the likelihood of serious/fatal injury caused by the claimed hazards associated with the posts are low compared to the likelihood of injury caused by the lack of post on a forklift. Therefore, the data would also indicate the third corner post's safety benefits outweigh the claimed negative considerations with the post, and the post does provide an overall increase in safety to stand-up forklifts.

Regardless of Manufacturers A's claimed negative considerations, the manufacturer eventually changed its stance on third corner posts being an optional feature, and made them standard on all of its stand-up forklifts since 2007. From information obtained through legal investigations, the reason the manufacturer decided to make the post a standard feature stemmed from the manufacturer's engineers. After reviewing the accident data collected over the last few decades, they subsequently made the determination that the posts did increase the overall safety of the forklift.

In addition to making rear posts an optional feature and inadequately explaining the safety benefits of the rear posts, charging the customer to add the rear posts indicates to the user that this is an unnecessary feature and further discourages the buyer from equipping their forklifts with rear posts. Forklift buyers are also unaware of the safety benefits of rear posts — or even the existence of the posts at all — as the information discussing safety benefits of the posts is relegated to a few brochures or must be explained to the user by the forklift dealer.

Furthermore, the decision to make rear posts a standard feature has been historically divisive in the industry.

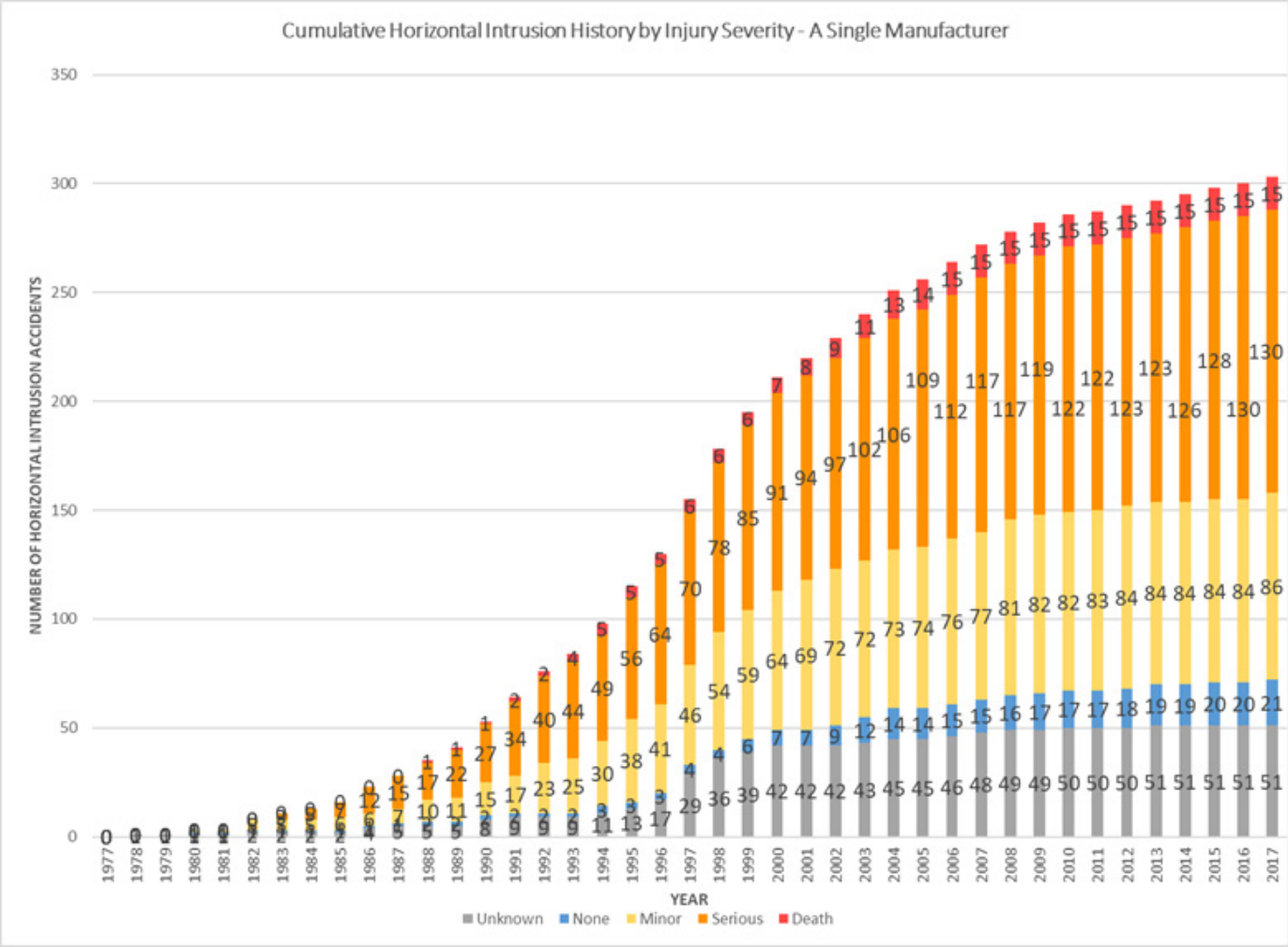

Figure 10
Graph showing cumulative number of horizontal intrusion accidents, categorized by injury severity from Manufacturer A's updated database.

ITA has an engineering committee that included representatives from forklift manufacturers. Although the committee has adopted practices regarding performance requirements of horizontal intrusion guards, they chose to not make effective horizontal intrusion guards (such as rear posts) a required feature on stand-up forklifts. One committee member, a representative from one of the forklift manufacturers (henceforth, will be referred to as "Manufacturer C"), has been critical of the committee's decision to not make the guards a standard feature[15]. Manufacturer C has made rear posts a standard feature on its stand-up forklifts since the 1950s[16].

In conclusion, based on review of Manufacturer A's accident database, it is the authors' opinion that the third corner post should be installed as a standard feature on all-stand-up forklifts rather than an optional feature. If the customer/end-user determines that the third corner post are impractical with their specific application, forklift manufacturers and the B56.1 standard do allow the customer/end-user to request the third corner post to be removed by the forklift manufacturer.

Safeguarding Hierarchy

There are numerous publications that provide methodologies for reducing or eliminating safety hazards. The following are examples of well-known and accepted methodologies that engineers use to design out or reduce hazards associated with products.

International Organization for Standardization (ISO) 12100-1:1992 "Safety of Machinery – Basic Concepts, General Principles for Design" outlines a clear hierarchy to be followed during the design of a product[10]. *"The designer shall, in all circumstances, in the following order:*

- *specify the limits of the machine.*

- *identify the hazards and asses the risks.*
- *remove the hazards or limit the risks as much as possible.*
- *inform and warn the user about any residual risks.*
- *consider any additional precaution."*

The *Mechanical Design Process* by D. Ullman, 1992[11], states:

"There are three ways to institute product safety. The first way is to design safety into the product. This means that the device poses no inherent danger during normal operation or in case of failure. If inherent safety is impossible, as it is with most rotating machinery and vehicles, then the second way to design in safety is to add protective devices to the product."

"The third, and weakest, form of designing for safety is the use of a warning to point out dangers inherent in the use of a product."

"Safety Through Design," published by the National Safety Council, 1999[12], identifies an order of design precedence:

1. *Design for minimum risk.*
2. *Incorporate safety devices.*
3. *Provide warning devices.*
4. *Develop and institute operating procedures and practices.*

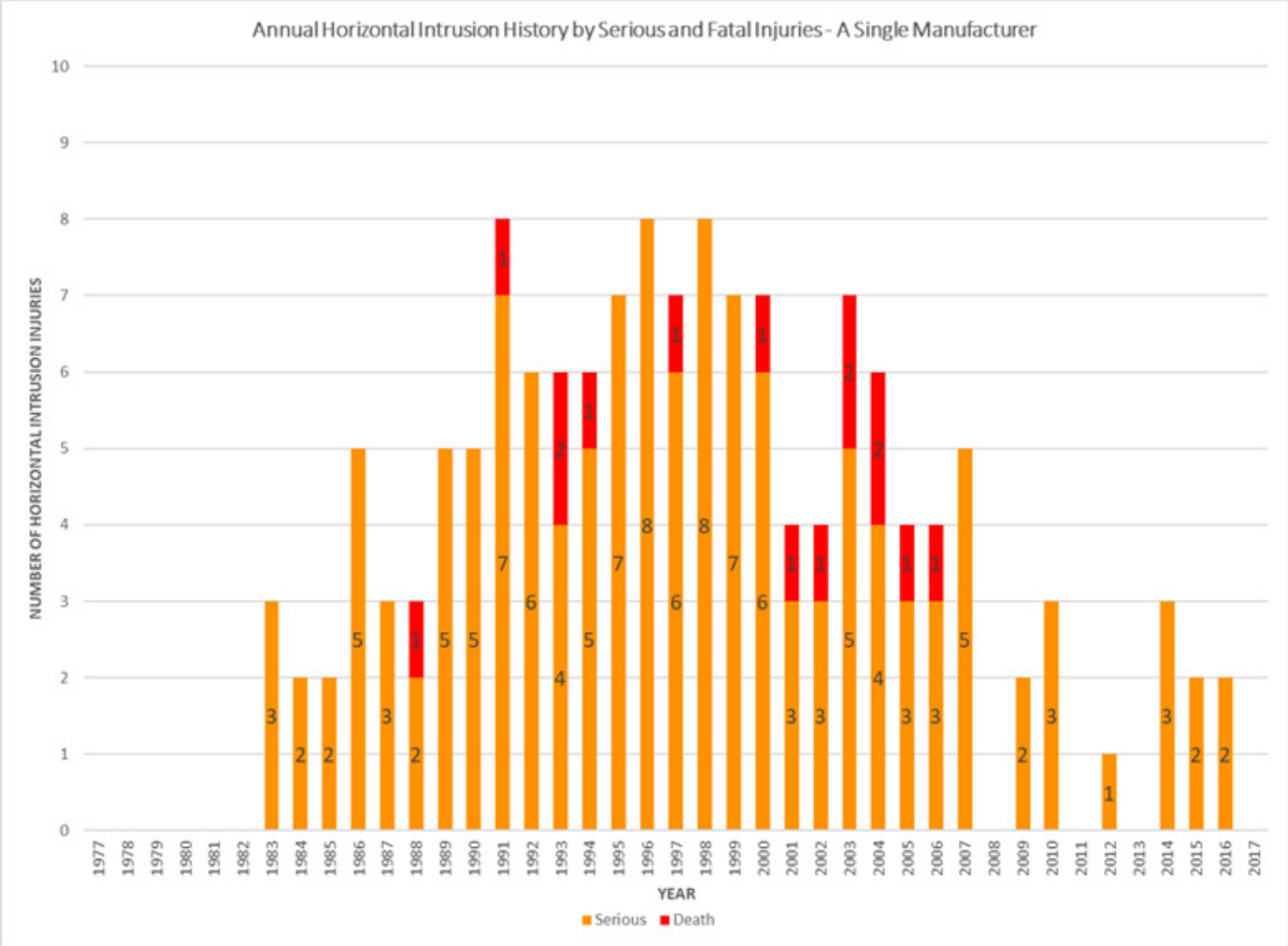

Figure 11
Graph showing annual number horizontal intrusion accidents, categorized by serious and fatal injuries from Manufacturer A's updated database.

It further states, *"Do not choose a lower level of priority until practical applications of the preceding level or levels are exhausted. First and second priorities are more effective because they reduce the risk by design measures that eliminate or adequately control hazards."*

In summary, the recurring theme in safety literature is that when hazard associated with product is recognized, the hazard shall be eliminated or reduced through a hierarchy of design, guard, and warn.

Since the hazard of stand-up forklift collisions cannot be eliminated, the next step in the hierarchy is to guard or incorporate devices to reduce the likelihood and consequences of the underride hazard. Manufacturers have been aware of the hazards associated with horizontal intrusion for decades, have put warnings on their forklifts, and instructed operators about the hazard in the operator's manual. However, manufacturers not equipping third corner posts as a standard feature on forklifts is a violation of well-known and accepted methods to safeguard against hazard of horizontal intrusion.

Although warnings and instructions can reduce the probability of horizontal intrusion incidents from occurring, operators are still getting seriously or fatally injured in horizontal intrusion accidents when there is a lack of effective horizontal intrusion guarding. Warnings and instructions are less effective than physical guards at preventing or mitigating the consequences associated with the incidents, which are usually serious or fatal injuries. In contrast, it is known that rear posts are passive safety devices that can guard an operator from injury when they are involved in an underride incident. The above pattern is further exemplified in Manufacturer A's accident database (previously discussed), where the data shows the rate of combined serious and fatal injuries did not rapidly decrease until after the forklift manufacturer made the third corner post a standard feature on its standup forklifts.

Furthermore, it is foreseeable that operators can unintendedly drive forklifts into racks. Following are examples of literature that state how designers/manufacturers need to consider foreseeable misuse when designing products.

ISO 12100-1 states[10]:

"With regard to foreseeable misuse, the following behavior should be particularly taken into account in the risk assessment — the foreseeable incorrect behaviors resulting from normal carelessness."

"Handbook of System and Product Safety" by Willie Hammer, P.E., 1972[16], states:

"The designer may not only commit errors but be guilty of omissions in failing to incorporate desirable features as safeguards that would have prevented accidents or protected personnel. When a designer cannot eliminate a hazard or the possibility of an accident completely, he must attempt to minimize the possibilities that other personnel will commit errors generating mishaps. In effect, the designer, through foreseeability, must attempt to make the system "idiot-proof," although he knows he will always be subject to the inevitability of Murphy's Law."

"Occupational Safety Management and Engineering" by Willie Hammer, P.E., 1981[15], states:

"Almost every mishap can be traced ultimately to a personnel error. It may not have been an error on the part of the person immediately involved in the mishap, but it may have been one committed by a designer, a worker manufacturing the equipment, a maintenance man, or almost anyone other than the person present when the accident occurred. A mistake by an operator may have no adverse effect with a safely designed piece of equipment. A similar mistake with one that is poorly designed may result in a disaster. It is evident that if a human error apparently caused an accident, other conditions must also have existed which contributed to its possibility."

"Modern safety practice, therefore, is to provide: 1) equipment and procedures that will minimize the possibilities of errors by operators; 2) designs that will eliminate or minimize the possibilities of accidents if an operator does make an error; and 3) designs and safeguards that will prevent injury if an accident does occur."

"Safety Through Design," published by the National Safety Council, 1999[14], states:

"The theme of this book is that it is difficult for engineers to change human nature and therefore, instead of trying to persuade people not to make mistakes, we should accept people as we find them and try to remove opportunities for error by changing the work situation, that is, the plant or equipment design or the method of working. Alternatively, we can mitigate the consequences of error or provide opportunities for recovery."

In summary, the recurring theme in safety literature and standards is designers/manufacturers need to consider reasonably foreseeable human error/misuse in designing their products and prevent/minimize injury if accidents do occur.

In conclusion, since the hazard of horizontal intrusion has been recognized for decades, the first and foremost responsibility of the engineering designer is to guard against the hazard for foreseeable use and misuse. Further, warnings and training are superseded by safe design and guarding in the safeguarding hierarchy; warnings and instruction are an insufficient safeguard to the horizontal intrusion hazard. Therefore, based on the above, it is the authors' opinion that forklift manufacturers need to equip their forklifts with effective horizontal intrusion guards, such as the third corner post, as a standard feature.

Physical Testing of the Rear Posts

The ANSI/ITSDF B56.1 standard outlines impact performance criterion for horizontal intrusion guards. The year 2020 revision of the standard states:

"The means and its mounting shall be strong enough to withstand the impact of a load simulating the collision between a truck carrying a full rated load and traveling at 1.6 km/h (1 mph) and a horizontal rigid barrier simulating a rack beam with a 75 mm (3 in.) vertical dimension.

After impact, there shall be no separation of parts or permanent deflection in excess of 100 mm (3.9 in) in the horizontal plane."

Even though the standard does provide a protocol and impact performance criteria for manufacturers to design rear posts for forklift travel impact speeds of 1 mph, forklifts can impact horizontal rack beams at speeds much higher than the 1 mph impact speed required by the standard. Although the authors of this paper are aware Manufacturer A impact tested their post design at forklift travel speeds of up to 3 mph (nine times the kinetic energy), not every manufacturer tests their third post beyond the requirements of the ANSI standard.

One study published in 2015 evaluated the effectiveness of rear posts in guarding against horizontal intrusion at higher travel impact speeds than what is required by the ANSI/ITSDF B56.1 standard[3]. In the 2015 study, another major manufacturer's (henceforth, will be referred to as "Manufacturer B") forklift equipped with a third corner post and a fourth corner post system was tested. The rear posts had a 1.5-inch by 2.5-inch rectangular tube cross-section with a wall thickness of 0.19 inches. The posts had a length of 41 inches and were made out of mild steel.

Manufacturer B's forklift, while carrying its rated load capacity, collided into a section of typical warehouse racking in a perpendicular manner four separate times at speeds of up to 3.4 mph. The portions of the posts that made contact with the rack beam were approximately 5 to 10 inches from the bottom of the 41-inch-long post.

During the tests, both posts contacted a horizontal beam, with the fourth corner post contacting the beam first because the position of the post on the forklift was a few inches further rearward than the third corner post. The test results showed the maximum permanent deformation of the posts was 0.229 inches — a fraction of the 3.9-inch maximum allowed by the B56.1 standard (a factor of safety of approximately 17 in these type of collisions). Further, the test results showed there was up to 9.5 inches of deformation to the impacted rack beam or significantly more than the deformation to the post (**Figure 12** and **Figure 13**).

The study concluded that the rear posts system from Manufacturer B met and exceeded the B56.1 standard and provided operator protection in the event of a horizontal intrusion incident. Furthermore, based on the minimal deflection of the post and the fact that the rack beam did not significantly intrude into forklift operator compartment, the test results showed the rear corner posts had a significant factor of safety and would have been effective in operator protection at higher collision speeds than the tested 3.4 mph speed.

Case Study: Manufacturer's Testing

A horizontal intrusion incident involving a stand-up forklift and a storage rack that resulted in serious injury was investigated and reconstructed (**Figure 1**, **2**, **3**, and **4**). The horizontal rack beam, which had intruded into the forklift and crushed the operator, was 96 inches long with a C-channel profile that was 3 inches tall, 1.4 inches wide, and ¼ inches thick. The beam was made out of A992 steel. The forklift involved in the incident was not originally equipped with a third corner post but was equipped with the fourth corner extension. However, the third corner post was offered by Manufacturer A as an optional feature when the forklift was originally sold. As part of the incident reconstruction, it was determined that the forklift (with no load) traveled into the rack at a speed of up to 6.1 mph.

Figure 12
Photograph showing the results of the physical testing performed from the 2015 study[3].

As part of the investigation, the manufacturer of the forklift performed testing with a surrogate stand-up forklift that was equipped with a third corner post. Based on the manufacturer's specifications, the third corner post was a 49-inch-long steel tube with a circular cross section profile with an outer diameter of 2.5 inches and a wall thickness of 0.31 inches. The third corner post was made from 1018 carbon steel. The manufacturer performed impact testing with racking systems that were like the one involved in the case. The manufacturer performed its test with an impact speed of approximately 6 mph (**Figure 14** and **Figure 15)**.

The authors were only provided videos of the testing

Figure 13
Photograph showing the results of the physical testing performed from the 2015 study (view showing the operator compartment and the deformed beam)[3].

that was performed by the manufacturer and were not given any written reports or photographs that could be reviewed to quantitatively determine the deflection and deformations observed to the post and the rack system. However, the test videos showed that after the impact the post exhibited minimal to no deformation. The test also showed that the impact caused the rack beam to significantly deform and deflect away from the operator compartment. The testing further showed the bolts that held the beam onto the rack's vertical uprights had sheared off at one end of the beam so the beam acted more like a cantilevered beam instead of a simply supported beam (and allowed the beam to deflect further away from the forklift's occupant compartment). The test also showed the vertical uprights had deformed and deflected significantly.

Therefore, the manufacturer's testing further exemplifies the common trend that when a post-equipped forklift collides with a racking system, there would be minimal to no deformation to the post, there would be significant deformation and deflection of the racking system instead, and the operator compartment space would have been maintained. The results of the analysis can be applied to impacts with similar rack systems and collision configurations.

Furthermore, like the 2015 test, this third corner post system design also exhibited a significant factor of safety and would have been effective in operator protection at

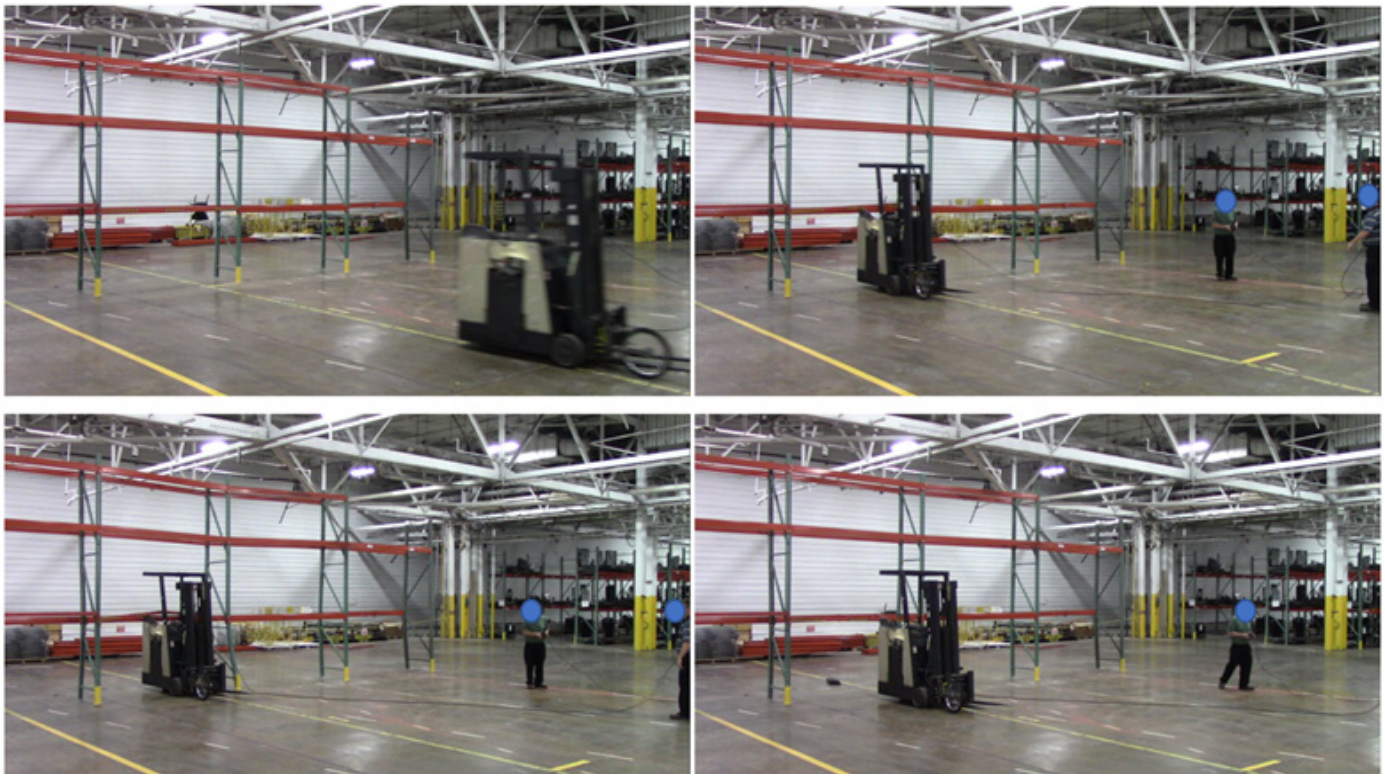

Figure 14
Screenshots from Manufacturer A's testing of a forklift striking a racking system at 6 mph, before impact (top left), at impact (top right), the forklift's maximum intrusion into the rack (bottom left), and the forklift at rest (bottom right).

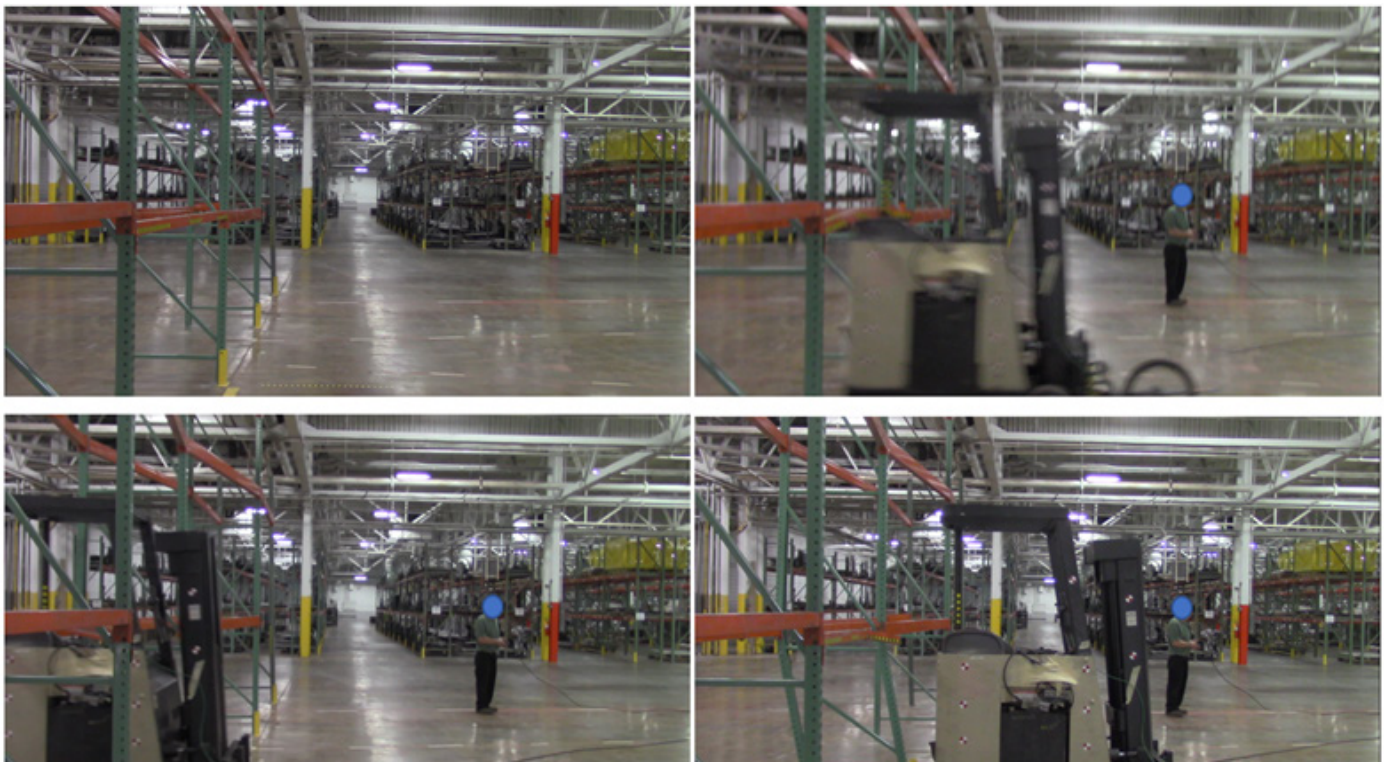

Figure 15
Screenshots from Manufacturer A's testing of a forklift striking a racking system at 6 mph, same test as shown from **Figure 14** but from a side view. Screenshots showing before impact (top left), at impact (top right), the forklift's maximum intrusion into the rack (bottom left), and the forklift at rest (bottom right).

higher collision speeds than the tested 6 mph speed. Future analysis and studies could be performed with different impact configurations that was not presented in this paper, such as impacts with stiffer and more rigid beams, the forklift carrying its full-rated load, higher forklift impact speeds, and different impact points to the rack beam and/or the third corner post.

Fourth Corner Extension and Fourth Corner Post

In the past, some manufacturers chose to forgo equipping third corner post as a standard feature and solely relied on fourth corner extensions for horizontal intrusion protection. Over time, more manufacturers have adopted the third corner post as a standard equipment[9] in addition to the fourth corner extension. However, some manufacturers still choose to solely rely on fourth corner extensions for horizontal intrusion protection.

Although the fourth corner extension does offer some horizontal intrusion protection, these extensions have been shown to have significant deficiencies when compared to a full vertical post. Since these extensions require overlap of the rack beam and the fourth corner for the extensions to be effective in preventing horizontal intrusion of rack beams, these extensions are only effective in certain rack configurations and forklift travel directions. The forklift in the previously discussed case study, was equipped with a fourth corner extension (**Figure 16**). Physical evidence showed the extension did contact the rack beam, and there was an overlap of approximately 4 inches between the rack beam and the fourth corner extension. However, due to the extension's "horseshoe" profile, the rack beam had deformed upward from impact. The beam overrode the extension, and the beam still significantly intruded into the operator compartment, crushing the operator. Therefore, the case study showed these extensions have deficiency in horizontal intrusion protection in certain impact configurations.

Adding a fourth corner post, in some cases, would be more effective than a fourth corner extension in preventing horizontal intrusion injury because the post extends to the overhead guard and provide protection when the horizontal beams intrude toward the fourth corner of the forklift. However, most manufacturers have chosen to not adopt the fourth corner post and some have outright denied customer request for them. Manufacturers justify their position by arguing that since the location of the fourth corner post is much closer to the proximity of the operators' head than a third corner post, the fourth corner post has more associated hazards than a third corner post, such as reduced operator visibility and an increase in the probability of a head or arm injuries. At the time of this paper, there is insufficient data to conclusively determine whether a fourth corner post's safety benefits would outweigh their negative considerations and would therefore make the forklift safer overall. However, there are manufacturers who have chosen to equip their stand-up forklifts with third and fourth corner post as standard features.

Deflection of Racking System vs Post(s)

The referenced physical testing in 2015 and Manufacturer A's testing in the case study have shown that when rear corner post(s) has been designed with stiffness greater than the rack beam, the beam deflects significantly more than the forklift's rear post(s). The rack beam deforming significantly more than the post at impact is to be expected as the post is stiffer because they are typically formed with a stronger and stiffer cross-section (area moment of inertia). The significant deformation to the horizontal beam also aids in maintaining the forklift's occupant space as the significant deformation of the beam starts to wrap around the forklift and prevents intrusion

Figure 16
Stand-up forklift equipped with a horseshoe-shaped fourth corner extension feature (arrow #2).

into the occupant space. Further, the 2015 physical testing and Manufacturer A's testing of rear posts impacting racking systems has shown that as the horizontal beam gets further deflected into the rack, the rack's vertical uprights start to also deflect and/or the bolts fastening the beam to the rack begin to shear off. The bolts shearing off would make the beam cantilevered and no longer simply supported, which would further deflect the beam away from the occupant compartment, improving operator safety.

As previously mentioned, the ANSI/ITDSF B56.1 testing of horizontal intrusion guards requires the guard to be impact tested into a rigid barrier simulating horizontal rack beam with a 3-inch vertical height with a forklift travel speed of 1 mph. Although the B56.1 standard does not define what a "rigid" barrier is, from the authors' experience with inspecting more than two dozen storage rack systems during investigation of forklift underride incidents, the rack systems and beams used in the physical testing in 2015 (and the manufacturer's testing presented in this paper) are consistent with rack systems and beams commonly used in a warehouse.

Requirements of the ANSI/ITSDF B56.1 Standard

Although horizontal intrusion guards for stand-up forklifts have been developed and implemented for decades, the ANSI/ITSDF B56.1, to this day, has not required manufacturers to equip horizontal intrusion guards on stand-up forklifts. Instead, the B56.1 standard still uses suggestive language regarding manufacturer's equipping their stand-up forklifts with horizontal intrusion protection.

The analysis presented in this paper has shown third corner posts are effective guards against horizontal intrusion, and the post increases the overall safety of the forklift. An increasing number of manufacturers have made third corner posts a standard feature on their stand-up forklift[17]. The analyses presented showed stand-up forklifts are safer when they are equipped with standard third corner post than without, because without a third corner post (in certain collision configurations) the operator's body is directly exposed to impact with the rack beams during underride collisions. Furthermore, the accident database from a major forklift manufacturer showed the safety benefits with a third corner post outweigh negative considerations, and the posts increases the overall safety of stand-up forklifts.

Further, the ANSI/ITSDF performance criteria for horizontal intrusion guard have not changed for decades. Forklifts are designed to typically travel well above 1 mph, and rear post systems have been developed for decades by various manufacturers. This paper has shown at least two designs are effective in guarding against horizontal intrusion at impact speeds well above 1 mph. This shows the current design of rear posts are meeting and have exceeded the standard with significant safety margin.

Future evaluations and/or testing could be performed to determine whether the current rear post designs can withstand impacts at above 6 mph. However, based on the testing presented in this paper, the current single and two rear post designs exhibit significant factor of safety when they collide with racking/shelving systems typically seen in storage warehouses. Therefore, the authors expect these rear post designs should be able to withstand and be able to provide operator protection at impact speeds above 6 mph.

Based on the above, it is the authors' opinion that it would be wise for the ANSI/ITSDF committee to revise and update their B56.1 standard, make third corner post a standard feature, and require horizontal intrusion guarding (such as rear posts) to be effective at forklift travel speeds higher than 1 mph.

The authors do not have specific knowledge to why the ANSI/ITSDF committee chose the 3.9-inch of maximum permanent deflection criteria for horizontal intrusion guard testing — because, depending on the shape and size of the forklift's operator compartment, the authors expect survivable operator compartment spacing could still be maintained if a horizontal intrusion guard deflects more than 3.9 inches. Future analysis could be performed to determine whether the 3.9-inch maximum permanent deflection may be too conservative, and the B56.1 standard should be updated to allow more permanent deflection of horizontal intrusion guarding when they are impact tested.

Conclusion

This paper has presented an analysis of Manufacturer A's empirical data of horizontal intrusion incidents before and after they made third corner posts a standard feature on stand-up forklifts, physical testing of Manufacturer A's and Manufacturer B's single and two rear post systems. The analyses presented have all shown that modern rear post systems are effective at preventing intrusion of horizontal rack beams into the operator compartment when the forklift strikes typical warehouse shelving and in the impact configurations presented.

This paper evaluates the deficiency of manufacturers choosing to not make the economically and technologically feasible third corner post system a standard feature on their stand-up forklifts. It is the authors' opinion that by making the third post system an optional feature, forklift manufacturers are violating the safety engineering hierarchy and have failed to guard against the foreseeable consequences associated with horizontal intrusion incidents.

Based on the increased safety benefits of forklifts equipped with third corner posts, it is the authors' opinion that it would be wise for the ANSI/ITSDF committee to revise and update their B56.1 standard and make third corner post a standard feature. In addition, current designs of third corner posts are meeting and have exceeded the standard and have shown to be effective in providing operator protection when forklifts strike shelving/racking systems at up to 6 mph impact speeds. Therefore, the committee should also revise the standard to require horizontal intrusion guards to be effective at impact speeds well above 1 mph.

Once sufficient information and data is available, future evaluations could be performed to determine whether a fourth corner post would increase the overall safety of stand-up forklifts and should also be equipped on stand-up forklifts as a standard feature.

References

1. R. Ziernicki and B. Railsback, "Forensic Engineering Assessment of Safety for Stand-Up Forklifts," Journal of the National Academy of Forensic Engineers, 2008.

2. R. Ziernicki and B. Railsback, "Hazard Analysis and Risk Assessment for the Operators of Stand-up Forklifts", in Proceedings of the 2008 ASME International Mechanical Engineering Congress and Exposition, Boston, Massachusetts, USA, 2008. IMECE2008-66427.

3. R. Ziernicki and B. Railsback, "Forensic Engineering Evaluation and Testing of Horizontal Intrusion Protection Equipment for Stand-Up Forklifts," Journal of the National Academy of Forensic Engineers, 2015.

4. T. Barry, "An Analysis of Stand-Up Forklift Accidents From the 1970's to 2006," in Proceedings of the 2011 ASME International Mechanical Engineering Congress and Exposition, Denver, Colorado, USA, 2011, IMECE2011-63944.

5. "Standup Forklift Under-ride Hazards," Occupational Safety and Health Administration, 2009, SHIB 07-27-2009

6. "Warehouse Forklift Operator Crushed Against Rack Beam," National Institute for Occupational Safety and Health Fatality Assessment and Control Evaluation Program, Report 03IA057, August 24, 2014

7. "ASME/ANSI B56.1-1990 Addenda to ASME/ANSI B56.1-1988 Safety Standard for Low Lift and High Lift Trucks," American Society of Mechanical Engineers/American National Standards Institute, 1990.

8. "Recommended Practices Manual," Industrial Truck Association, 1989.

9. "ASME B56.1-2000 Safety Standard for Low Lift and High Lift Trucks," American Society of Mechanical Engineers, 2000.

10. ISO 12100-1:1992 – "Safety of Machinery – Basic Concepts, general principles of design." International Standards Organization. 1992.

11. D. Ullman, The Mechanical Design Process. McGraw Hill, 1992.

12. W. Christensen. Safety Through Design, National Safety Council, 1999.

13. W. Hammer, Handbook of System and Product Safety. Prentice Hall, 1972.

14. W. Hammer, Occupational Safety Management and Engineering. Prentice Hall, 1981.

15. J. Schell. Letter to W.J. Montwieler of Industrial Truck Association. December 8, 1986.

16. "Reach Truck," Clark Equipment Company, Battle Creek, MI, 1959.

17. "3rd Post Kits for RC3000 RR/RD 5000 & RR/RD 5200 Series Trucks," Crown Equipment Corporation Product Information Bulletin, no. 07-07-01, July 2007.

Evaluation of Two Proximity Warning Devices on a Mobile Elevating Work Platform

By Scott Raszeja, PE (NAFE 906A)

Abstract

Contact between a mobile elevating work platform (MEWP) and an energized overhead powerline (OHPL) is a warned-against event that is associated with damage to property as well as injury or death. The objective of this project was to evaluate the effectiveness of two different proximity warning devices (PWDs) installed on an MEWP operated near OHPLs. The general procedure used was to rotate the MEWP work platform horizontally away from, then toward, the OHPL from each side of the MEWP (at various platform heights), noting the distance between the MEWP and the OHPL when an alarm occurred. PWD2 allowed violation of the simulated OSHA boundary on 74.3% of the total rotations without initiating a warning alarm and was too sensitive to be practical as a startup alarm system. PWD1 did not allow operation of the MEWP within 20 feet of the actual OSHA minimum approach distance. The results of the startup test for PWD1 were nowhere near consistent.

Keywords

Proximity, warning, device, overhead, powerline, contact, mobile elevating work platform, lift, OSHA, safety

Introduction and Background

Hazards[1] are presented when working with cranes, mobile elevating work platforms (MEWPs), telescopic handlers, or similar equipment that operate with articulating/telescopic portions of the equipment above ground level. One hazard is contact with energized overhead power lines (OHPLs). Contact between an MEWP and an OHPL is a warned-against event associated with damage to (or loss of) property as well as personal injury or death.

To account for this hazard, the Occupational Safety and Health Administration (OSHA) dictated the minimum approach distance between equipment and an OHPL[2]. OSHA required a distance of at least 10 feet between equipment and any OHPL energized with a voltage of 50,000V (50kV) or less.

Multiple vendors have marketed proximity warning devices (PWDs) as an effective tool to warn equipment operators when approaching OHPLs. A PWD can be defined as a safety device that provides a warning of proximity to a power line. OSHA defines a proximity alarm as a device that provides a warning of proximity to a power line and has been listed, labeled, or accepted by a Nationally Recognized Testing Laboratory in accordance with 29 CFR 1910.7[3]. OSHA allows the use of PWDs, but not as primary protection from contact with OHPLs. For such a device to be an effective tool in preventing accidental contact with an OHPL, the PWD must consistently and reliably alert the operator when any portion of the equipment has encroached upon a specified distance from an OHPL. As with any warning device, inconsistent or unreliable operation of the alarm will reduce or eliminate the utility of the device, which, in turn, increases the risk of personal injury or death to users or ground personnel.

A great deal of effort has been expended to evaluate PWDs installed on aerial/telescopic cranes. Most PWDs are designed to detect the electric field that surrounds an OHPL. A review of the literature has revealed various issues and complexities inherent in electrical field sensing for OHPL detection. The literature has also revealed various issues with available PWDs. The goal of this project was to evaluate the effectiveness of two different PWDs installed on an MEWP operated in close proximity to OHPLs.

Purpose

The objective of the evaluation was to equip a telescopic boom MEWP with two PWDs. While using the MEWP (as it would typically be used and operated under reasonably foreseeable conditions proximate to overhead

Scott Raszeja, PE, 8197 West Brandon Drive, Littleton, CO 80125, (303) 339-3251, scott@AEIengineers.com

power lines), the author observed and documented performance of the PWDs in consideration of the OSHA-defined boundaries, and identified/documented factors during the above evaluation that influenced the PWDs' operation, accuracy, repeatability, practical utility, and reliability.

Operation of the MEWP occurred at a test site located in a secluded pasture. The PWDs were evaluated as an operational warning device, in which the PWDs warned the MEWP operator when approaching a preset boundary from the OHPLs. The PWDs were also evaluated as a startup device in which the PWDs (on startup) checked the environment for the presence of electromagnetic fields associated with OHPLs and warned the MEWP operator.

Electromagnetic Fields

OHPLs create an electromagnetic field surrounding the conductor. An electromagnetic field consists of both an electric field and a magnetic field.

The magnetic field strength surrounding OHPLs is primarily based upon the electric current moving through the conductors. The electric current can vary over time according to user demand, thus changing the strength of the magnetic field. The variable magnetic field strength becomes problematic for PWD manufacturers and the users of these devices who rely on the detection and quantification of the magnetic field as a method to determine proximity to an OHPL.

The electric field strength surrounding OHPLs is primarily based upon the voltage at which they operate. Power generation companies have become adept at maintaining consistent voltage levels throughout their distribution system. Consistent voltage levels allow PWD manufacturers to design equipment to sense electric field strength and make assumptions that the electric field strength surrounding an OHPL will remain consistent at a point in space over time. However, factors other than voltage can influence the electric field surrounding an OHPL, some of which include grounded objects in the area, phase orientation of the OHPLs, vertical and horizontal orientation of the OHPLs, and proximity to other OHPLs in the area.

Literature Review

The reviewed literature[4,5,6,7,8,9,10] provided an account of PWD evaluations and investigations from 1977 through 2014. The literature was reviewed to get a sense of the prior evaluations with regard to the reliability, repeatability, and general performance of the PWDs. The literature was also reviewed to gain an understanding of the methods used to test the PWDs and lessons learned from such tests. The overall intent of the review was to learn as much as possible from prior evaluations in order to construct the best possible test procedure for the current evaluation. Investigations also highlighted the difficulty inherent with using electric field sensing to accurately and repeatedly warn equipment operators when the equipment was in the vicinity of an OHPL.

PWD Descriptions and Implementation

Two PWDs were evaluated in this study. The first PWD is herein referred to as "PWD1".

PWD1, which was designed to sense magnetic as well as electric field strength surrounding an OHPL, had one sensor unit hardwired to the control module. The sensor unit had both the magnetic field sensor as well as the electric field sensor built into one enclosure. An audible alarm horn was connected to the control module to warn users when OHPLs were detected. PWD1 did not have the capability to create a setpoint.

The second PWD evaluated is herein referred to as "PWD2". Designed to sense the electric field strength surrounding OHPLs, PWD2 allowed for the connection of up to 12 wireless sensors, which communicated wirelessly (via Zigbee radio communication) to the control module. The extent of the effect, if any, of the Zigbee radio on the ability of the wireless sensors to accurately sense the electromagnetic field produced by the OHPLs was unknown and untested. The control module activated a two-tone audible alarm horn based upon the condition sensed. One tone indicated a "warning" condition, while the other indicated a "danger" condition. According to the PWD2 manual, *a warning status means the equipment is getting closer, but has not yet reached the danger zone. A danger status means the equipment has crossed into the danger zone.*

The PWD2 manual describes two modes of operation. As a startup device, the manual states: *Powering up: When power is first applied, the control module will search for sensors. No data will appear while connectivity is in progress (approximately 2 seconds). Once sensors are connected, the control module will go into a maximum setting. If any power lines are in the vicinity, the alarms will sound. The operator must select the reset button to revert the system to the last displayed setpoint.*

PWD2 was also used as an operational device. As an operational device, the manual states: *The operator must*

decide what setpoint is appropriate for each and every job site. To adjust the setpoint, position the equipment at the desired location where an operator would like an alarm state, then depress the "one touch" button. This will change the setpoint to the greatest numerical sensor reading +5 at that position. When adjusting the setpoint, always position the equipment far enough away from the power line to give the operator time to react.

From that point, during normal use, PWD2 should have sounded an audible warning alarm when one or more sensors were within 80% of the setpoint and an audible danger alarm when one of the sensors matched the setpoint.

Test Boundaries and Parameters

The OHPLs present at the test site were energized with less than 50kV. Equipment used in the evaluation was required to maintain a 10-foot minimum approach distance from site OHPLs per OSHA regulations. The PWD2 setpoint was set at a distance of approximately 22 feet from the OHPLs for all tests. This allowed the PWD2 response to be tested at the simulated OSHA boundary (22 feet from the OHPL) as well as up to 10 feet closer to the OHPL (12 feet from the OHPL) while remaining beyond the actual 10-foot minimum approach distance required by OSHA. Once a setpoint location had been created, movement past the setpoint location, without an alarm, was considered a violation of the OSHA boundary.

Given that the actual OSHA minimum approach distance for the OHPLs at the test site was 10 feet from the OHPL, movement of the MEWP 10 feet past the simulated OSHA boundary (setpoint location), without an alarm, constituted simulated contact with the OHPL. The boundaries were selected to allow movement of the MEWP to simulate violation of the minimum approach distance and contact with an OHPL without actually violating the minimum approach distance or contacting an OHPL.

Instrumentation

Two outdoor laser distance meters were used to measure the distance between the MEWP and the OHPL. To verify the accuracy and calibration of the meters, test measurements were verified on two separate occasions prior to the site test by a professional surveying company. Backup measurements during the site test (where appropriate) were performed using a laser scanner with post-processing. A weather station was used to monitor and record ambient temperatures throughout the evaluation.

OSHA Minimum Approach Distance

The sub-transmission voltage present at the test site was approximately 44kV (**Figure 1**, shown in green) and the distribution voltage was approximately 12kV (**Figure 1**, shown in blue). Thus, according to OSHA 1926.1408 Table A, the mandated minimum approach distance was 10 feet. A ground based test boundary was set up 22 feet from the OHPLs. Movement of the MEWPs was allowed beyond the 22-foot barrier, but at no time were the MEWPs or personnel intentionally allowed to come closer than 10 feet to the OHPLs.

Test Site Layout

The test site selected was in a pasture. Four unique station locations were selected for the evaluation (as shown in **Figure 1**) based on availability of level ground as well as proximity to OHPLs. The location of the MEWP at each station is accurate as shown and based upon embedded GPS data with laser scanning. The lateral ground-based distance from directly below the center of the MEWP chassis to directly below the OHPLs is shown for each station.

Test Site Preparation

A site survey was performed. The purpose of the survey was to accurately determine ground-based boundaries from the OHPLs at the site, and to place wooden stakes every 25 feet along those determined boundaries. Colored surveying tape was attached to the stakes for easy visual reference of the boundaries.

Two ground-based danger boundaries were created and marked with red surveying tape. One boundary was placed at 8.7 horizontal feet from the OHPL. This boundary served as the ground-based boundary that denoted the 10-foot minimum approach distance between the MEWP platform and the OHPL when the platform was rotated from a position 5 feet above or below the height of the OHPL.

The second ground-based danger boundary was placed at 10 horizontal feet from the OHPL. It served as the ground-based boundary that denoted the 10-foot minimum approach distance between the MEWP platform and the OHPL when the platform was rotated from a position at the same height as the OHPL. Both ground-based danger boundaries represented actual (opposed to simulated) OSHA boundaries (minimum approach distance). No boundary was required for testing with the MEWP platform 10 feet above or below the OHPL because the platform could not get closer than 10 feet to the OHPL.

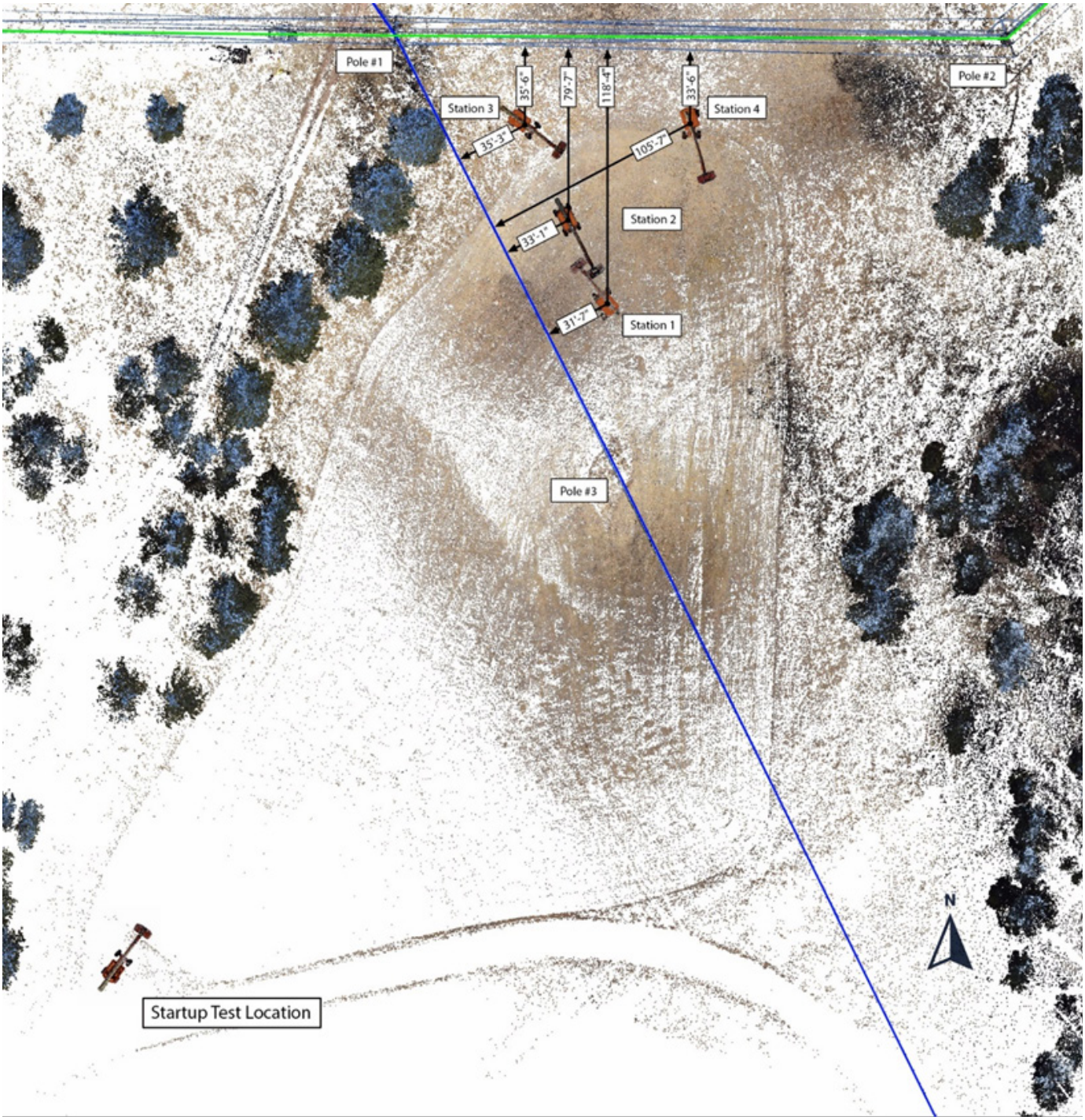

Figure 1
Laser scan point cloud representation of test site with OHPLs, poles, and station locations.

A ground-based test boundary, marked with yellow surveying tape, was created at 22 horizontal feet from the OHPL. It served as the ground-based boundary that denoted the 22-foot limit between the MEWP platform and the OHPL when the platform was rotated from a position at the same height as the OHPL. The 22-foot boundary served as the simulated OSHA boundary (simulated minimum approach distance), as shown in **Figure 2**.

Data Collection and Procedure

For the purposes of this evaluation, the right and left sides of the subject MEWP were defined according to the layout shown in **Figure 2**. Two MEWPs were used to perform the test. The PWD sensors were installed on the subject MEWP. The second MEWP was used to control the movement of the subject MEWP. The subject MEWP was remotely controlled by a qualified operator.

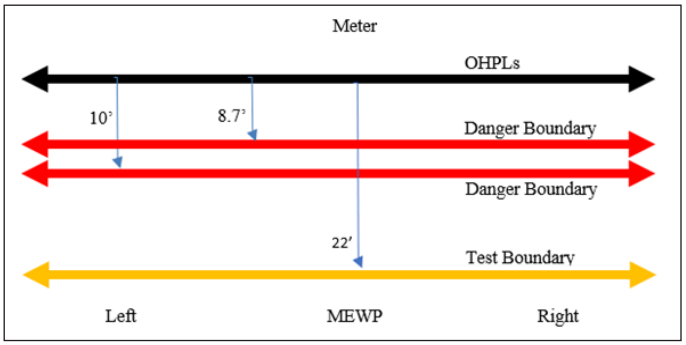

Figure 2
For the purposes of this evaluation, ground-based boundary layout. Location of MEWP and measuring device (meter) relative to the OHPLs.

The purpose of the remote control was to give the operator greater control of the subject MEWP. The subject MEWP was controlled as if the operator was located within the platform of the subject MEWP, while being located safely in the platform of the second MEWP. The setup allowed the operator to rotate the subject MEWP platform toward the OHPLs with greater control and at slower speeds than could be provided with ground-based control of the subject MEWP. The second MEWP was located away from the subject MEWP.

A series of MEWP movements occurred at each of the four stations. A laser scan was performed at each station such that the exact location of the MEWP within the test site was documented. The general procedure used to test PWD2 was to raise the subject MEWP platform to the same height as the OHPL, create a setpoint at the simulated OSHA boundary (22 foot boundary), and then rotate the platform horizontally away from (then back toward) the OHPL from each side of the MEWP, noting the distance between the MEWP and the OHPL when the PWD2 warning/danger alarm sounded.

If a warning alarm sounded, the movement was halted, and a distance measurement was taken. The movement then continued toward the OHPL until a danger alarm sounded, at which point another distance measurement was taken. The horizontal rotation of the MEWP toward the OHPL ceased with the danger alarm or the appropriate (according to platform height) OSHA ground-based danger boundary (actual OSHA minimum approach distance). Spotters were used to halt movement at the appropriate boundary. The procedure was repeated at platform heights relative to OHPL height of +10 feet, +5 feet, -10 feet, and 5 feet.

The procedure was also repeated with the subject MEWP platform at the same height as the OHPL with the second MEWP inserted into the area near the station. The procedure was performed immediately after the rotations with the platform at the same height as the OHPL, and the setpoint was not changed. The purpose of inserting an additional MEWP into the field was to observe the effect, if any, that an additional MEWP near the station would have on the operation of the PWD. For this set of rotations, the subject MEWP was no longer operated by the second MEWP but was instead operated using the ground controls of the subject MEWP.

This general procedure — raising the platform to a specific height and then rotating horizontally away from and back toward the OHPLs from both sides of the subject MEWP — was selected to produce repeatable movements. The subject MEWP had many articulation points, which made it problematic to create repeatable movements at other approach angles. The procedure generally aligns with the procedure developed by NIOSH for PWD testing[9]. Setpoints were created at every height for every station. Setpoints were created on both the right and left sides of the MEWP as noted in the test results. PWD1 did not have the capability to create a setpoint. Thus, PWD1 was merely rotated horizontally away from and then back toward the OHPLs until an alarm sounded.

Measurements between the subject MEWP and the OHPL were always taken between the two closest points. They were obtained with an outdoor laser distance meter, and the MEWP platform/OHPLs were scanned with a laser scanner as often as deemed necessary.

At the time of testing, it was not known how quickly the PWDs could respond to movement of the MEWP and the associated electric field changes. The maximum horizontal swing speed of the subject MEWP was changed to a slower setting to give the PWDs more time to respond to changing electromagnetic fields. The subject MEWP was configured for a maximum horizontal swing speed of 64% of the maximum speed set at the factory.

Both PWDs were also evaluated as a startup device. The goal of the startup device evaluation was to drive the subject MEWP away from the OHPLs in order to deactivate any alarms — then drive the subject MEWP toward the OHPL until an alarm sounded. The distance between the subject MEWP and the OHPL at the time that the alarm sounded was measured. PWD2 automatically starts in the most sensitive detector setting. PWD1 did not have adjustable settings. The PWD1 sensor and the 12 PWD2 wireless sensors were attached to the subject MEWP (as

shown in **Figure 3**).

General Analysis and Discussion

For PWD2, warning rotations were defined as the initial rotations toward the OHPL, in which no alarm had yet sounded. The warning alarm should have occurred when one or more of the sensors were within 80% of the setpoint. Danger rotations were defined as rotations in which the warning alarm had already sounded, measurements were taken, and rotation of the subject MEWP resumed toward the OHPL. The danger alarm should have occurred when one of the sensor readings matched the setpoint.

PWD1 did not allow the operator to select or create a setpoint. PWD1 showed substantial variability in alarm distance from the OHPLs. PWD1 also alarmed far away from the simulated OSHA boundary of 22 feet. Since it did not provide the capability to adjust the sensitivity of the device, PWD1 could not be operated near the simulated OSHA boundary without an alarm. PWD1 did not allow operation of the subject MEWP within 20 feet of the actual OSHA minimum approach distance as it alarmed constantly at even greater distances from the OHPLs. These facts, discovered at Station1, limited PWD1's practicality as a PWD for use with MEWPs. Due to these limitations, it was decided that no further testing of PWD1 would be performed after Station1. However, PWD1 was later evaluated at Station4 to determine how it would respond to the more complex OHPL configuration as opposed to the simple configuration present at Station1.

Graphs

The alarm distance (PWD1 **Figures 4** and **9**) and setpoint deviation (PWD2, **Figures 5** through **8**) graphs produced in the analysis section can be evaluated as follows:

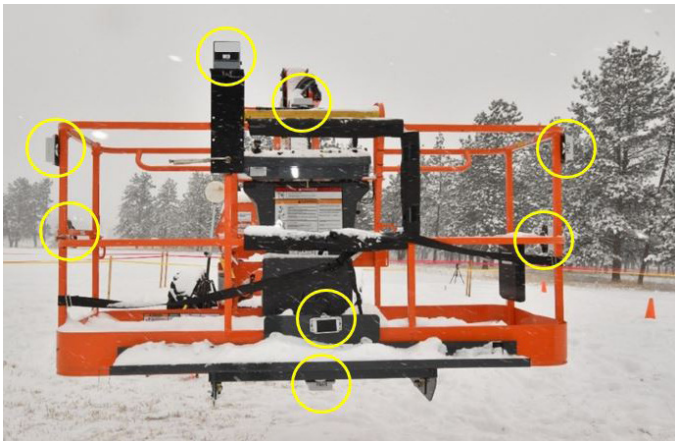

Figure 3
PWD1 and PWD2 sensor locations on MEWP platform and boom. Five PWD2 sensors not shown.

For the PWD1 deviation graphs, the blue line represented the location of the OHPL. Points below the line represented the distance (in feet) that the alarm condition occurred prior to the OHPL. For the PWD2 deviation graphs, the yellow line represented the setpoint (simulated OSHA boundary). Points above the line represented the distance (in feet) that the warning alarm condition occurred past the simulated OSHA boundary. Points below the line represented the distance (in feet) that the warning alarm condition occurred prior to the simulated OSHA boundary. The vertical scales should be noted when each graph is examined.

Station1: Analysis and Discussion

PWD1 alarmed at distances between 30 to 40 feet from the OHPL at the various platform heights. The closest (to the OHPL) alarm occurred at 30.3 feet, and the farthest (from the OHPL) alarm occurred at 39.3 feet. Only the electric field sensor alarmed. No alarms from the magnetic field sensor occurred during any of the rotations. The alarm distances with respect to the OHPL can be seen in **Figure 4**.

Station1A: Analysis and Discussion

The PWD2 setpoints for Station1A were all set on the right side of the subject MEWP. The subject MEWP chassis position for Station1A was the same position that was used for Station1. It should be noted that the "A" in Station1A merely denoted that the test occurred on a different day from the Station1 PWD2 test, which was shut down due to low ambient temperatures.

The subject MEWP was able to operate in ambient conditions below the lowest operating temperature

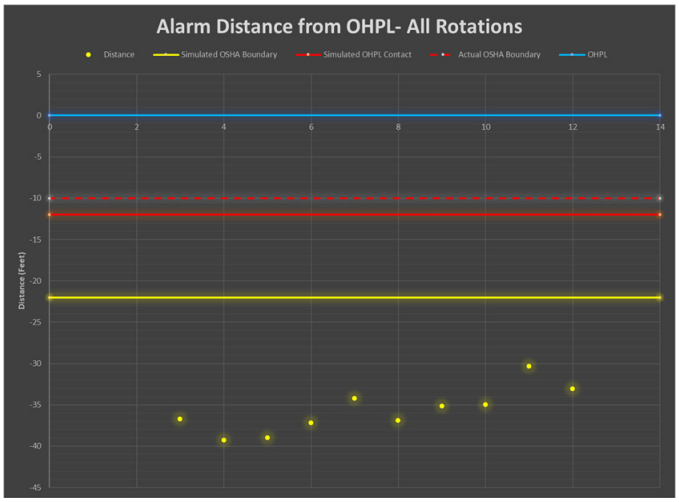

Figure 4
PWD1 alarm distance from OHPL at Station1.

specified in the PWD2 manual, and PWD2 operated erratically at ambient temperatures below its specified range. Operation of PWD2 on an MEWP that was utilized in ambient temperatures below the minimum specified operating temperature of PWD2 would create a dangerous condition in which the operator of the lift may rely on PWD2 to warn of a dangerous condition when the device may not, in fact, be operable. Low ambient temperatures could be experienced at many locations worldwide.

The deviation from the setpoint (simulated OSHA boundary) for all the warning rotations can be seen in **Figure 5**. The warning rotation alarm farthest from the setpoint, prior to the setpoint location, occurred at 4.8 feet. The warning rotation alarm farthest from the setpoint (past the setpoint location) occurred at 12 feet. There was substantial variation in PWD2 responses for the warning rotations. The variation was also substantial for the danger rotations (not shown).

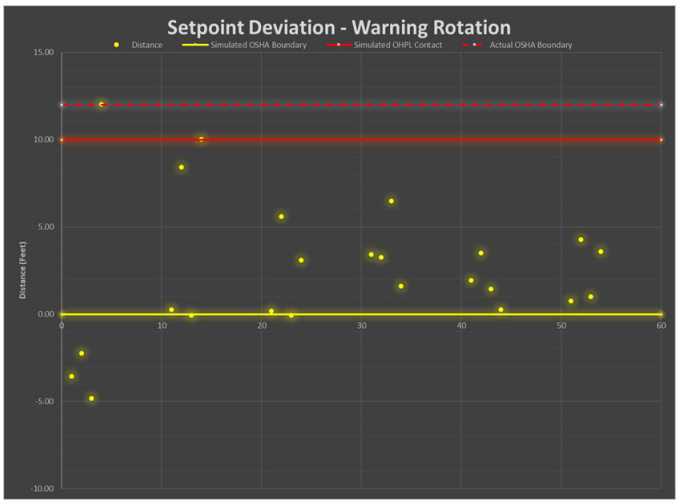

Figure 5
PWD2 deviation from setpoint (warning rotations at Station1A).

Station2: Analysis and Discussion

The PWD2 setpoints for Station2 were all set on the right side of the subject MEWP. The deviation from the setpoint (simulated OSHA boundary) for all the warning rotations can be seen in **Figure 6**. The PWD2 warning rotation alarm farthest from the setpoint, prior to the setpoint location, occurred at 10.6 feet. The warning rotation alarm farthest from the setpoint, past the setpoint location, occurred at 12.7 feet. There was substantial variation in the PWD2 responses for the warning rotations. The variation was also substantial for the danger rotations (not shown).

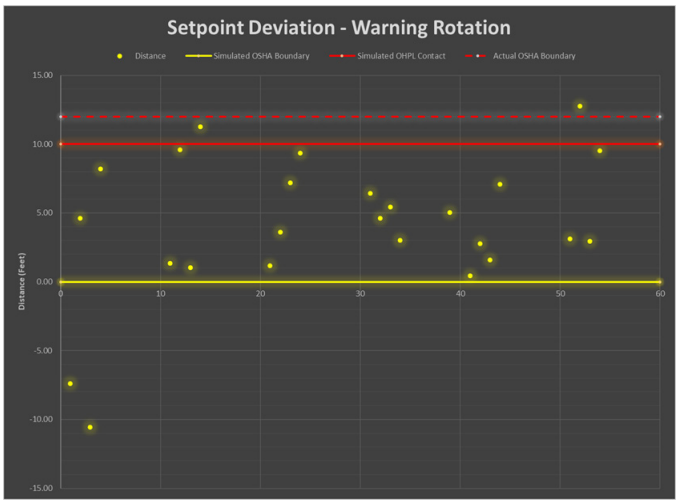

Figure 6
PWD2 deviation from setpoint (warning rotations at Station2).

Station3 Analysis and Discussion

PWD2 setpoints for Station3 were all set on the right side of the subject MEWP. The deviation from the setpoint (simulated OSHA boundary) for all the warning rotations can be seen in **Figure 7**. The PWD2 warning rotation alarm farthest from the setpoint, prior to the setpoint location, occurred at 5.1 feet. The warning rotation alarm farthest from the setpoint, past the setpoint location, occurred at 13.4 feet. There was substantial variation in the PWD2 responses for the warning rotations. The variation was also substantial for the danger rotations (not shown).

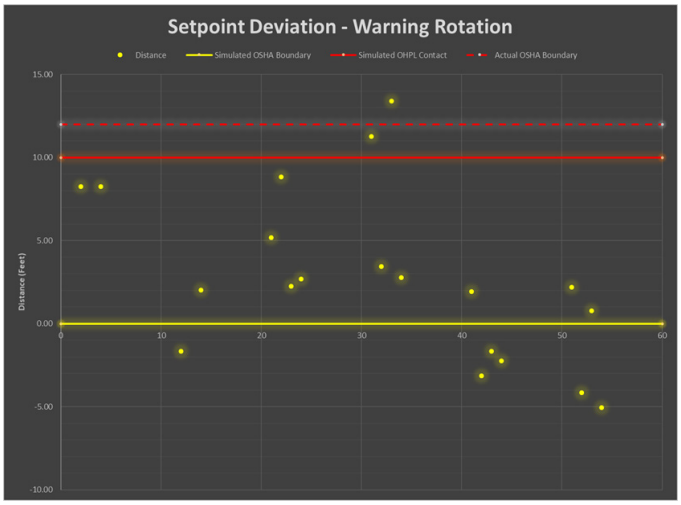

Figure 7
PWD2 deviation from setpoint (warning rotations at Station3).

Station4: Analysis and Discussion

Half of the PWD2 setpoints for Station4 were set on the right side of the subject MEWP; the other half were set on the left side of the subject MEWP. PWD2 deviation from the setpoint (simulated OSHA boundary) for all the warning rotations can be seen in **Figure 8**. The PWD2 warning rotation alarm farthest from the setpoint, prior to

the setpoint location, occurred at 23.2 feet. The warning rotation alarm farthest from the setpoint (past the setpoint location) occurred at 15 feet. There was substantial variation in the PWD2 responses for the warning rotations. The variation was also substantial for the danger rotations (not shown).

The location (right or left side) of a setpoint at a given height negatively affected the response of PWD2. With a right side setpoint, the warning alarm would often sound at a great distance from the simulated OSHA boundary. With a left side setpoint, at the same height, the warning alarm might not occur at all while the subject MEWP achieved simulated OHPL contact. For example, with the platform at OHPL elevation with a right side setpoint on the first left rotation, the PWD2 warning alarm sounded with the platform located 21.7 feet prior to the simulated OSHA boundary. With the platform at OHPL elevation, with a left side setpoint on the first right rotation, the PWD2 warning alarm never sounded even though the MEWP achieved simulated OHPL contact.

PWD1 alarmed at distances between 27 to 66 feet from the OHPL at the various platform heights. The closest (to the OHPL) alarm occurred at 27.3 feet and the farthest (from the OHPL) at 65.6 feet. Only the electric field sensor alarmed. No alarms from the magnetic field sensor occurred during any of the rotations. The alarm distances with respect to the OHPLs can be seen in **Figure 9**.

Other notable issues occurred at every station. For the sake of brevity, only the notable issues at Station2 are listed below:

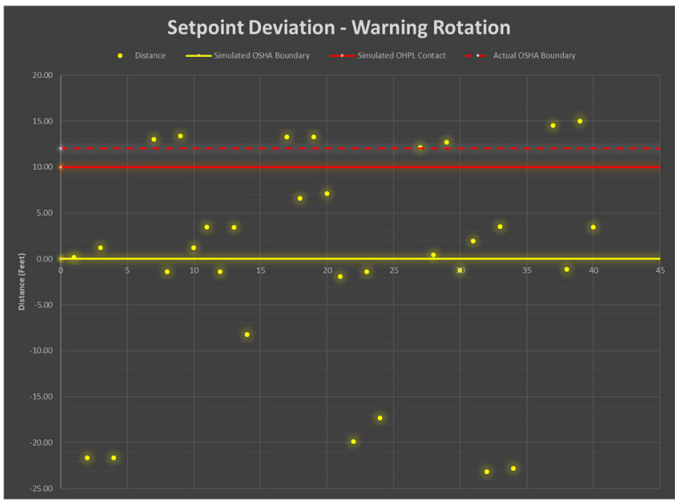

Figure 8
PWD2 deviation from setpoint (warning rotations on Station4).

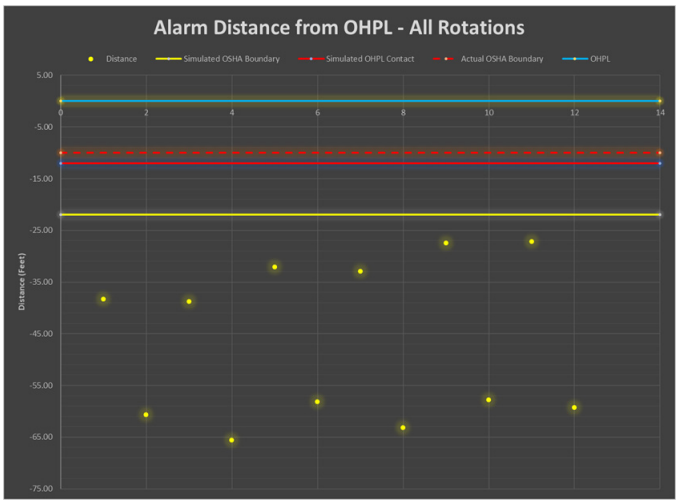

Figure 9
PWD1 alarm distance from OHPLs at Station4.

- There was one danger rotation in which the rotation was stopped by the spotters without the occurrence of a danger alarm, but the danger alarm later activated approximately five minutes into the measurement process with the subject MEWP stationary.

- There was one warning rotation in which the alarmed sensor changed from warning to danger while distance measurements were performed with the subject MEWP stationary.

- There was one rotation in which the warning alarm never sounded. The first alarm to sound was the danger alarm.

- There was one warning rotation in which the warning alarm stopped sounding between the simulated OSHA boundary and the OHPL before sounding again. The control module did not lose communication with the sensors.

- There was one rotation in which the warning alarm toggled on/off as communication between the activated sensor and control module was gained/lost.

- There was one rotation in which the danger alarm toggled on/off as communication between the activated sensor and control module was gained/lost.

Boundary Violations

Boundary violations occurred when the subject MEWP

moved past a boundary without a PWD alarm. For the purposes of this testing, the PWD2 setpoint location functioned as the simulated OSHA boundary (simulated minimum approach distance). Once a setpoint location had been created, movement past that setpoint location (toward the OHPL) was considered a violation of the simulated OSHA boundary. The simulated OSHA boundary was set to approximately 22 feet from the OHPL for all tests.

Given that the actual OSHA mandated boundary (actual minimum approach distance) for the OHPLs at the test site was 10 feet from the OHPL, movement of the MEWP 10 feet past the simulated OSHA boundary constituted simulated contact with the OHPL. Simulated OHPL contact occurred at 10 feet past the setpoint location. Additionally, if a PWD alarm condition had still not occurred — and the spotters did not stop movement of the MEWP precisely at the actual OSHA boundary (10 feet from the OHPL) — an actual OSHA boundary violation occurred. PWD2 boundary violations are shown in **Figure 10**. Only boundary violations that occurred for warning rotations are shown. Boundary violations for danger rotations were more numerous.

Rotation Deviations

A rotation deviation was defined as the difference (in feet) between the alarm distance on one MEWP rotation and the alarm distance on another MEWP rotation. To better understand the nature of the variability of alarm distance experienced during the test, several PWD2 rotation deviations were examined. The comparison was not exhaustive, and other rotation comparisons could be made. Rotation deviations for PWD2 are shown in **Figure 11**.

The following rotations were examined at Station1A, 2, 3, and 4, at each height (for both warning and danger rotations):

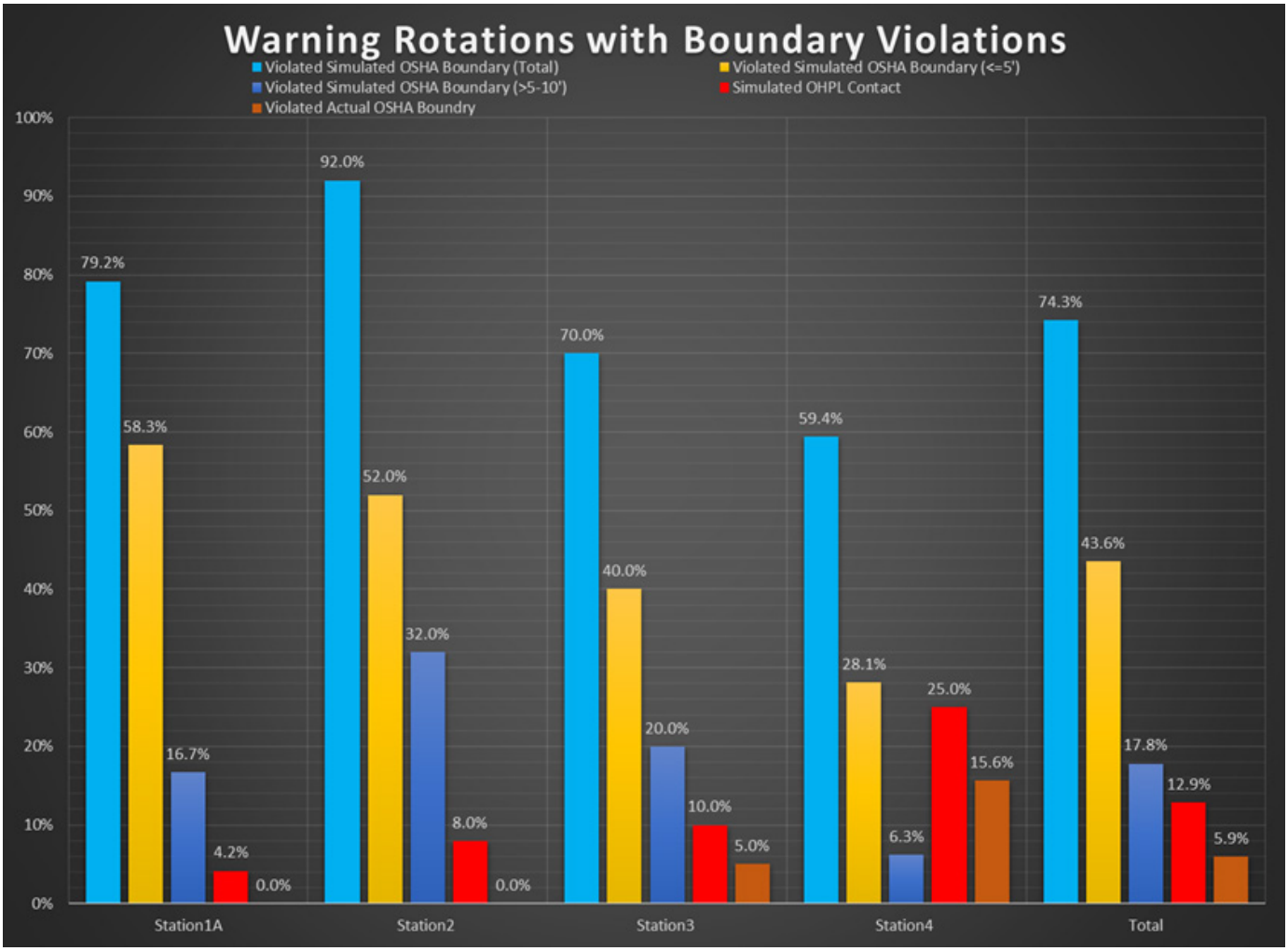

Figure 10
Percentage of PWD2 warning rotations with boundary violations.

1. Right-side rotation versus the subsequent right-side rotation.

2. Left-side rotation versus the subsequent left-side rotation.

3. Right-side rotation versus the subsequent left-side rotation.

Startup Analysis and Discussion

A startup device was defined as a PWD that would warn the user if OHPLs are in the vicinity. PWD1 was evaluated as a startup device. The subject MEWP was driven away from Pole #3, toward the startup test location shown in **Figure 1**. The subject MEWP was driven far enough away from Pole #3 that PWD1 was not in an alarm condition. There were no sensitivity adjustments available with PWD1.

The subject MEWP was driven toward the OHPL on Pole #3 until the PWD1 alarm sounded. In Test Run #1, the subject MEWP was driven to a location directly beneath the OHPL without an alarm. In Test Runs #2 and #3, with the platform raised, the subject MEWP was driven toward the OHPL, and an alarm did sound. However, the alarm sounded between 21 feet and 26 feet (along the ground) from the OHPL. Earlier testing at Station1 (near the same OHPL) revealed that the PWD1 alarm sounded between 30 feet and 40 feet from the OHPL. The results of the startup test for PWD1 were inconsistent. Inconsistent operation is unacceptable for a device that is supposed to warn of a lethal hazard.

PWD2 was evaluated as a startup device. PWD2 was designed to begin operation at startup in its most sensitive setting. The subject MEWP was driven away from Pole #3, toward the startup test location shown in **Figure 1**. The subject MEWP could not be driven far enough

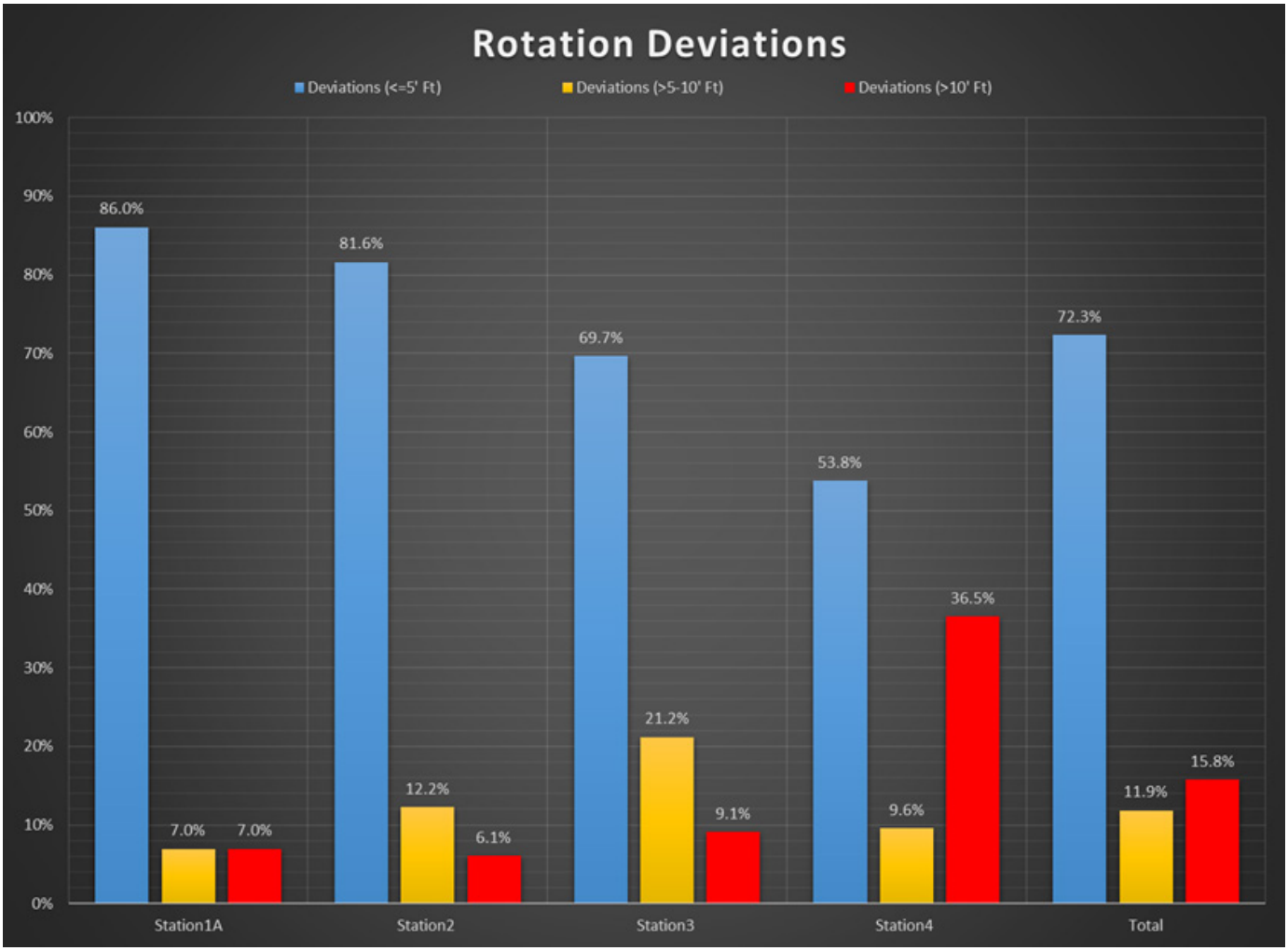

Figure 11
PWD2 rotation deviations.

away from the OHPL to disengage the PWD2 alarm. The subject MEWP was 451 feet (along the ground) from the OHPL and continued to alarm. The PWD2 manual states: *RANGE OF EFFECTIVENESS, Voltage Detection – Between 10 and 200 feet depending on voltage.*

The PWD2 continued to alarm at over twice the distance from the OHPL that was stated as the range of effectiveness. A constant alarm that continuously sounds (even when over 450 feet from an OHPL) would likely cause confusion for the operator. The occurrence of frequent or constant alarms may lead operators to dismiss all alarms as nuisance alarms.

Safety

The following is stated as the intended use[11] of PWD1: *The PWD1 safety system provides overhead power line and above-the-mast illumination. The built-in high voltage, electromagnetic and electrostatic field detection system automatically stops mast extension, providing added protection for the operator and equipment.* The PWD1 manufacturer agreed to allow PWD1 to be evaluated for an expanded intended use on articulating boom lifts.

PWD1 did not provide a means for the operator to select or create a setpoint. PWD1 showed substantial variability in alarm distance from the OHPLs. PWD1 also alarmed far away from the simulated OSHA boundary of 22 feet. Since it did not provide the capability to adjust the sensitivity of the device, PWD1 could not be operated near the simulated OSHA boundary without an alarm. PWD1 did not allow operation of the subject MEWP within 20 feet of the actual OSHA minimum approach distance. These facts limited the PWD1's practicality as a PWD for use with MEWPs.

The following is stated as the intended use of PWD2: *PWD2 is designed to alert equipment operators and other workers to the danger of contact with a live power line. This device will help protect them from injury or death, as well as preventing expensive damage to equipment.*

The PWD2 website further states: *PWD2's proximity detection alarms are designed to warn workers if they are close to power lines. In the event that work must be conducted near a power line (no closer than OSHA minimums, of course), PWD2 proximity alarms can be set to warn of danger when the equipment enters a preset area.*

Death or serious injury are known consequences associated with the hazard of contact between an MEWP and an OHPL. The OSHA minimum approach distance must not be violated in order to protect the operator and personnel in the vicinity of the equipment. The OSHA boundary is rigid, inflexible, and required. Once within the OSHA boundary, the operators and ground personnel are exposed to critical risk and possible injury or death.

The severity of harm incurred from contacting an OHPL is immediate and tragic, almost assuredly resulting in damage to property, personal injury, and/or death. PWD2 allowed violation of the simulated OSHA boundary on 74.3% of the total rotations without initiating a warning alarm. PWD2 allowed violation of the simulated OSHA boundary on 92.0% of the rotations at Station2, without initiating a warning alarm. PWD2 allowed simulated OHPL contact on 12.9% of the total rotations without initiating a warning alarm. PWD2 allowed simulated OHPL contact on 25.0% of the rotations at Station4, without initiating a warning alarm.

The International Electrotechnical Commission (IEC) is the world's leading organization for the preparation and publication of International Standards for all electrical, electronic, and related technologies[12]. IEC International standards serve as the basis for risk and quality management and are used in testing and certification to verify that manufacturer promises are kept[13]. The Organization for Standardization (ISO) is an independent, non-governmental international organization with a membership of 165 national standards bodies. Through its members, it brings together experts to share knowledge and develop voluntary, consensus-based, market relevant International Standards that support innovation and provide solutions to global challenges[14]. The following excerpts presented in this section, shown in italics, have been extracted from GUIDE ISO/IEC GUIDE 51:2014(E), "Safety aspects — Guidelines for their inclusion in standards."

The term "safe"[15] is often understood by the general public as the state of being protected from all hazards. However, this is a misunderstanding: "safe" is rather the state of being protected from recognized hazards that are likely to cause harm. Some level of risk[16] is inherent in products or systems.

Tolerable risk[17] can be determined by:

- *the current values of society;*
- *the search for an optimal balance between the ideal of absolute safety and what is achievable;*

- *the demands to be met by a product or system;*
- *factors such as suitability for purpose and cost effectiveness.*

The following procedure should be used to reduce risks to a tolerable level:

a. identify the likely users for the product or system, including vulnerable consumers and others affected by the product.

b. identify the intended use, and assess the reasonably foreseeable misuse, of the product or system;

c. identify each hazard (including reasonably foreseeable hazardous situations and events) arising in the stages and conditions for the use of the product or system, including installation, operation, maintenance, repair and destruction/disposal;

d. estimate and evaluate the risk to the affected user group arising from the hazard(s) identified: consideration should be given to products or systems used by different user groups; evaluation can also be made by comparison with similar products or systems;

e. if the risk is not tolerable, reduce the risk until it becomes tolerable.

All products and systems include hazards and, therefore, some level of residual risk. However, the risk associated with those hazards should be reduced to a tolerable level.

Industries and standards committees, such as the American Society of Mechanical Engineers, have held reservations regarding the concept of detrimental reliance (when a party is induced to rely on another's promise or commitment resulting in a detrimental outcome to the party) or false sense of security (a feeling of being safer than one really is): *If cage-type boom guards, insulating links, or proximity warning devices are used on cranes, such devices shall not be a substitute for the requirements of this section, even if such devices are required by law or regulation. Electrical hazards are complex, invisible, and lethal. To lessen the potential of false security, instructions related to the devices and hazards shall be reviewed with the crane operator, crew, and load-handling personnel. Instructions shall include information about the electrical hazard(s) involved, operating conditions for the devices, limitations of such devices, and testing requirements prescribed by the device manufacturer*[18].

Reliance on a safety device that does not function consistently and reliably would amplify the existing hazard by instilling a false sense of security in the operators of the equipment who rely upon the safety device in place of alternative operating procedures to reduce the risk.

Inconsistent operation of a safety device that alarms at distances well beyond the OSHA minimum approach distance would result in many "false" alarms. The occurrence of frequent false alarms may lead operators to dismiss all alarms as nuisance alarms.

Given the fact that PWD2 allowed violation of the simulated OSHA boundary on 74.3% of the total rotations (without a warning alarm) — and that simulated OHPL contact occurred on 12.9% of the rotations (without a warning alarm) — the risk associated with use of PWD2 was not reduced to a tolerable risk for the intended use. Having not reduced the risk to a tolerable risk, PWD2 is not safe for the intended use.

Conclusions

The results of the evaluation indicate the following:

1. PWD1 is not practical for use as a PWD on an MEWP that is operated in close proximity to OHPLs.

2. PWD1 does not produce repeatable or reliable alarms when used as an operator warning device on an MEWP operated in close proximity to OHPLs.

3. The results of the startup test for the PWD1 were inconsistent. This is unacceptable for a device that is supposed to warn of a lethal hazard.

4. PWD2 did not produce repeatable or reliable alarms when used as an operator warning device on an MEWP operated in close proximity to OHPLs.

5. The PWD2 manufacturer stated: *PWD2's proximity detection alarms are designed to warn workers if they are close to power lines. In the event that work must be conducted near a power*

line (no closer than OSHA minimums, of course), PWD2 proximity alarms can be set to warn of danger when the equipment enters a preset area. The results of this evaluation indicated that PWD2 allowed violation of the simulated OSHA boundary, without a warning alarm, on 74.3% of the total rotations.

6. The PWD2 manufacturer stated: *This device will help protect them from injury or death, as well as preventing expensive damage to equipment.* The results of this evaluation indicated simulated OHPL contact, without a warning alarm, on 12.9% of the rotations. Injury or death, along with damage to equipment, would likely occur from MEWP contact with an OHPL.

7. The risk in use of PWD2 was not reduced to a tolerable risk.

8. PWD2 is not safe for its intended use as marketed/sold by the manufacturer.

9. PWD2 was too sensitive to be practical as a start-up alarm system on an MEWP operated in proximity to OHPLs.

PWDs are commercially available products. Owners and users of MEWPs may elect to purchase, install, and operate PWDs. Based upon the results of the testing and analysis outlined in this paper, owners and users that intend to equip MEWPs with a PWD should be fully aware of the limitations associated with such devices and have that device certified in writing by the vendor of that product, by a qualified engineer, or by the appropriate certifying entity, to be safe for use in all foreseeable environments, conditions, and applications.

References

1. Safety aspects – Guidelines for their inclusion in standards, Guide ISO/IEC Guide 51, 2014(E). Hazard. A potential source of harm.

2. United States Department of Labor Occupational Safety and Health Administration, "1926.1408 – Powerline Safety (up to 350kV) – equipment operations". OSHA.gov. https://www.osha.gov/laws-regs/regulations/standardnumber/1926/1926.1408 [accessed June 16, 2021].

3. United States Department of Labor Occupational Safety and Health Administration, "1926.1401 – Definitions". https://www.osha.gov/laws-regs/regulations/standardnumber/1926/1926.1401 [accessed January 13, 2022].

4. G.S. Allin, J.T. Wilson, and R.E. Zibolski, "A Practical Review of High Voltage Safety Devices for Mobile Cranes," Society of Automotive Engineers, Warrendale, PA, 1977.

5. Bureau of Mines, United States Department of the Interior, Alternative Power-Line Proximity-Warning Techniques. 1982.

6. Bureau of Mines, United States Department of the Interior, Evaluation of Proximity Warning Devices. Southwest Research Institute, San Antonio, TX, 1980.

7. Bureau of Mines, United States Department of the Interior, Evaluation of Proximity Warning Devices, Phase III, Volume 1, Southwest Research Institute, San Antonio, TX, 1982.

8. Mining Enforcement and Safety Administration, United States Department of the Interior, Field Evaluation of a Proximity Alarm Device. Pittsburg, PA.

9. Department of Health and Human Services, Centers for Disease Control and Prevention, National Institute for Occupational Safety and Health, Pittsburgh Research Laboratory, A Performance Evaluation of Two Overhead Power Line Proximity Warning Devices. Pittsburgh, PA, 2008.

10. D. Andres, G. Stevick, "Overhead powerline early warning devices for cranes, lifts and other aerial mobile equipment," Berkeley Engineering and Research, Inc., May 2014.

11. Safety aspects – Guidelines for their inclusion in standards, Guide ISO/IEC Guide 51, 2014(E). Intended use. Use in accordance with information provided with a product or system, or, in the absence of such information, by generally understood patterns of usage.

12. IEC, "Who We Are," https://www.iec.ch/who-we-are [accessed January 13, 2022].

13. IEC, “What We Do,” https://www.iec.ch/what-we-do [accessed January 13, 2022].

14. ISO, “About Us,” https://www.iso.org/about-us.html [accessed January 13, 2022].

15. Safety aspects – Guidelines for their inclusion in standards, Guide ISO/IEC Guide 51, 2014(E). Safe. Freedom from risk which is not tolerable.

16. Safety aspects – Guidelines for their inclusion in standards, Guide ISO/IEC Guide 51, 2014(E). Risk. a combination of the probability of occurrence of harm and the severity of that harm.

17. Safety aspects – Guidelines for their inclusion in standards, Guide ISO/IEC Guide 51, 2014(E). Tolerable Risk. The level of risk that is accepted in a given context based on the current values of society.

18. Mobile and Locomotive Cranes: Safety Standard for Cableways, Cranes, Derricks, Hoists, Hooks, Jacks, and Slings, ASME/ANSI B30.5, 2018, Section 5-3.4.5.1(g) Crane Operation in the Vicinity of Electric Power Lines.

Meteorology and Physics Analysis of Rail Car Fatality

By Drew Peake, PE, DFE (NAFE 460F) and Muhammad Salman, PhD

Abstract

When borax gets wet, it clumps. In this case, 76,000 pounds of previously wetted borax clumped on the inside of a rail car. The unbalanced load caused the rail car to fall on a yard worker, killing him. Tracking meteorological conditions in transit from Turkey to a port in Deleware, truck transit to a warehouse, handling at the warehouse, and rail transit to an interim transfer station was key to developing the origin and cause for the rail car derailing. There was evidence that clumping had rendered the product unusable by the end-user. However, this event occurred at the interim transfer station where the rail car product was transferred to trucks. This paper describes the process of determining how and where the borax absorbed moisture and shows physics that determined derailing was the result of an unbalanced load. This demonstrates the cause and effect of this event.

Keywords

Borax, shipping, ocean transport, rail transport, truck transport, center of gravity, lean angle, turning moments, suspension stiffness, forensic engineering

Introduction and Background

At approximately 10:15 a.m. on September 4, 2013, a rail car left the track and fell on a rail yard transfer station worker, killing him. The event occurred at a private transfer station in middle Georgia. Rail car NS 253219 was built in May 1970 with a load capacity of 223,300 pounds and an expected life of 50 years. (It will be shown that rail creep was caused by a buildup of 76,420 pounds of borax caked on the side of an otherwise empty car.)

The rail car was transporting bulk borax that clumps when wet. The borax had become wet either during transport from overseas, during transfer, storage, or overland transport. Operations and coincident meteorological conditions (primarily precipitation and humidity) were important to validate the assumption of borax caked on the side of the rail car. Engineering calculations were necessary to verify that the uneven distribution of product resulted in the derailment.

Material

Borax is anhydrous sodium tetraborate ($Na_2B_4O_7$; mol wt. 202), sodium tetraborate pentahydrate ($Na_2B_4O_7$ * 5 H_2O; mol wt. 292), or sodium tetraborate decahydrate ($Na_2B_4O_7$ * 10 H_2O; mol wt. 382). When exposed to water, anhydrous sodium tetraborate hydrates and begins to clump as it hydrates. To prevent clumping, temperatures greater than 85°F and relative humidity greater than 45% should be avoided. Borax occurred naturally in seasonal lakes that evaporated and left deposits millions of years ago[2]. This paper tracks borax mined in Turkey, transported overseas to Delaware, handling and storage near the seaport, and overland transport to a middle-Georgia transfer station.

Six primary steps are required to refine raw ore into refined borates:

1. In the first step of refining, crushed ore is dissolved through steam addition and agitation. Insoluble rocks, sand, and other solids are removed using screens;

2. Next, the saturated borax solution is pumped into large settling tanks called “thickeners” where remaining fine particles settle to the bottom of the tank, leaving a clear, hot borax solution on top;

3. Crystals of borax pentahydrate and borax decahydrate form as this hot solution is cooled in the crystallizers;

Drew Peake, 3111 Vandiver Drive, Marietta, GA 30066, (678) 521-4647, dpeake@peakeeng.com

4. The newly formed borax crystals pour out onto special fabric filters where they are also washed to ensure purity. Water is drawn away from the crystals by a vacuum underneath the filter;

5. After this washing, the crystals are transferred to the dryers. These large rotating dryers use hot air to dry the borate crystals;

6. Dry borate crystals exit the dryer and drop onto a conveyor belt. The refining process is complete. The refined borates travel by conveyor to covered hopper cars for transport to the seaport[3].

Transfer Operation

The borax was mined in the Emet[2] region of Turkey. It was refined at the mine, stored in weather-protected bins until loaded into covered hopper rail cars. Transported hundreds of kilometers over land to seaports, the borax is loaded onto bulk container ships by a conveyor, and moved from the rail cars to the ship conveyors that feed hoppers that direct the material into cargo holds.

The average monthly relative humidity in Istanbul, Turkey (port of embarkation) in March (estimated time the ship was loaded) was 55%. These calculations were developed using maximum daily temperature (MXT), minimum daily temperature (MNT), and the average daily dew point (DP) for September 2013 at Sabiha Gocken Airport in Istanbul[4]. Average temperature was estimated by taking the average of the average MXT and MNT.

This statistic was used with the average DP to estimate the average daily relative humidity. The mine operators understood the moisture impact[1] on borax and maintained climate control conditions after drying and during rail shipment to the seaport. Given typically covered hopper loading methods, that prior operation near Emet was the first uncontrolled climate. Moisture may not have significantly affected the borax during the short time on the loading conveyor.

The borax was shipped to Delaware where it was received by a warehousing company. The product was unloaded on April 16 and 17, 2013 by a crane-mounted grab that drops the mineral into a hopper. The hopper opened and loaded trucks with the loose product. The trucks were then covered with a screen and driven to the warehouse where the borax was delivered to an uncovered way station.

Borax was exposed to humidity while unloading from the ship and during transport to the warehouse yard. The daily average relative humidity on April 16 and 17 was 76% and 71%, respectively[5]. There, the borax was screened to get out any lumps or foreign material. After screening, the warehousing company transferred the product to another warehouse a few blocks away. The warehouse was covered, but not climate controlled. From there, it was loaded on rail cars using a conveyor belt.

The warehousing company was advised by email from the product owner that borax would clump if it got wet — and that it should be stored in a climate-controlled warehouse. At each transfer after delivery to the trucks, borax was exposed to atmospheric moisture. As the borax was being loaded into the rail cars for shipment, loading was stopped for two days because light precipitation started late on August 12 and continued the next day. Loading was started on August 12 and completed on August 14, 2013. There was only a trace of rain on August 12. However, on August 13, there was 3.10 inches of rain. There was no rain on August 14. The load was then shipped by rail to a middle Georgia transfer station. The relative humidity on August 12 was 73% and 58% on August 14[4].

Quantifying the Amount of Material

Two companies worked in concert to transfer borax from rail cars to trucks for delivery to the end-user. A local railroad company moved the cars into and out of the transfer station. Transfer station workers unloaded the rail cars and loaded the product into trucks. Borax flowed out of the hopper cars when opened from the bottom. A mechanical unloader moved the material from the bottom of the rail car to load trucks. The hopper chutes were equipped with shakers that helped free the product so it would flow more easily into the enclosed conveyor that lifted the load to drop into trucks. The shaker was not operational on the unloader that was used to transfer the borax. The transfer station workers used hammers to aid the flow of material into the conveyor.

Transfer station workers were in the process of unloading the subject rail car when the locomotive came on that track to move cars. The free product had flowed out onto the conveyors and loaded in trucks. As the cars sat on the track, they appeared stable, although one of three cars was leaning. Unloading was stopped, and the unloader was removed from under the rail car so the locomotive could move cars.

After unloading was completed, 76,000 pounds of

borax remained in one rail car (clumped on one side). The weight of borax remaining in the rail car was determined by weigh scale measurements before and after unloading. There were three cars coupled together. When stationary, static friction held the wheels on the rails. Once the locomotive moved the cars, the drop in friction from static levels to dynamic levels facilitated wheel climb, releasing the wheels. The last rail car (NS 253219) immediately fell, pulling the other two cars with it. Witnesses observed borax clinging to the side of the rail car.

The timeline for these transfers — from unloading to the transfer station — was documented. A timeline for mining, processing, and transport to the Turkish seaport was not available.

Workers' Roles

The railroad had three employees on site: the engineer, conductor, and flagman. The engineer operates the locomotive. The conductor oversees the train and gives instructions to the crew on what needs to be accomplished and how. The flagman walks down and checks the train for chocks that are put under the wheel sometimes (for anything hanging off a car), checks hoses, and identifies any safety appliance that is defective on the car. The flagman's primary responsibility was to observe the train's right of way.

There were two transfer station workers at the time. When the locomotive pulled onto the yard, they were unloading the rail car. When the locomotive pulled the cars, one of these workers was walking along the side of the track. At the first movement, the rail car derailed and landed on that worker, killing him.

The transfer station workers did not notice the lean of the rail car from their vantage point near the base of one side. The flagman was responsible for a general inspection to assure the car was safe to pull.

Rail Car Derailment Calculations

There were two main factors that caused the derailing accident. The main factor of rail car derailment was the shifting of the mass center due to the unbalanced weight of borax (caked on one side); the other one was friction. Static friction held the car upright until the locomotive moved forward slowly at a speed of 4 to 5 miles/hr (kinetic friction). The wheels on the light side rode up on the rail, and the car derailed when the wheel lip left the rail (as shown in **Figure 1**).

Center of Gravity Calculation

The specific density of borax is 1.73 grams/cubic centimeter (gm/cc^3).[6] After converting and increasing the specific density to 76,420 pounds, the volume of borax is 20.3 m^3. The center of gravity (CoG) was calculated in two pieces: one with an empty car; the other with the borax caked-on the left-hand side. The length (L) of the hopper car is 65 ft.[7]

H = 15.5 ft [7]

Borax Volume = 20.3 = L x W x H

W = 0.2168 m, CoG of borax from the left edge of the car is located at l_2 = W/2 = 0.1084 m and Y = H/2 = 2.3628 m (as shown in **Figure 2**).

Moments Calculation

F_1 = Borax Weight = 76,420 lb = 339,314 N

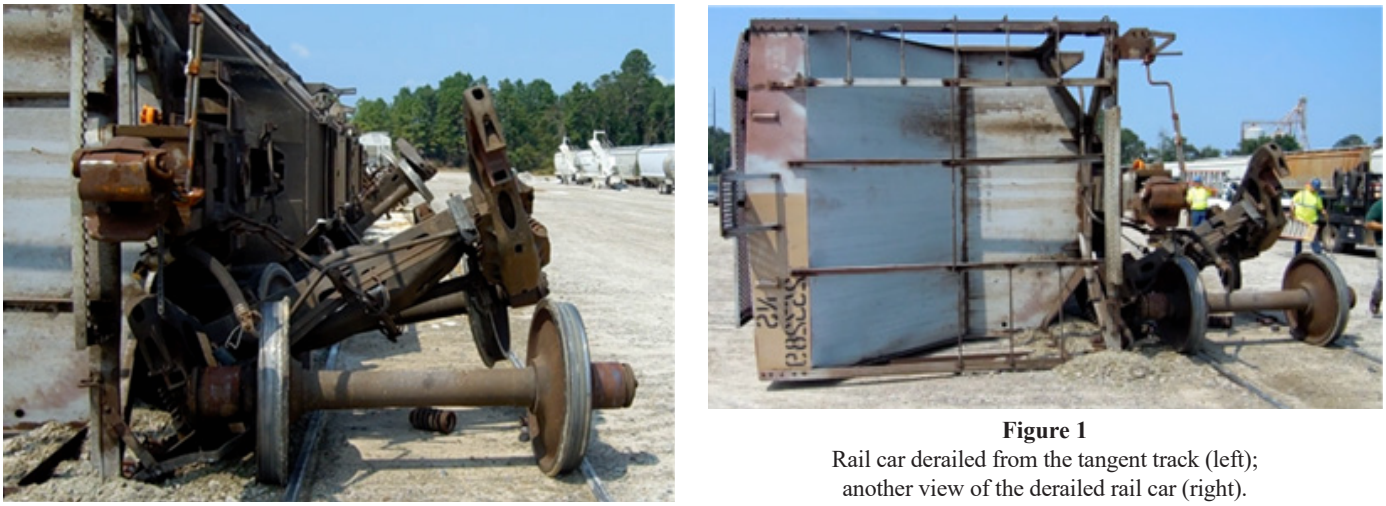

Figure 1
Rail car derailed from the tangent track (left); another view of the derailed rail car (right).

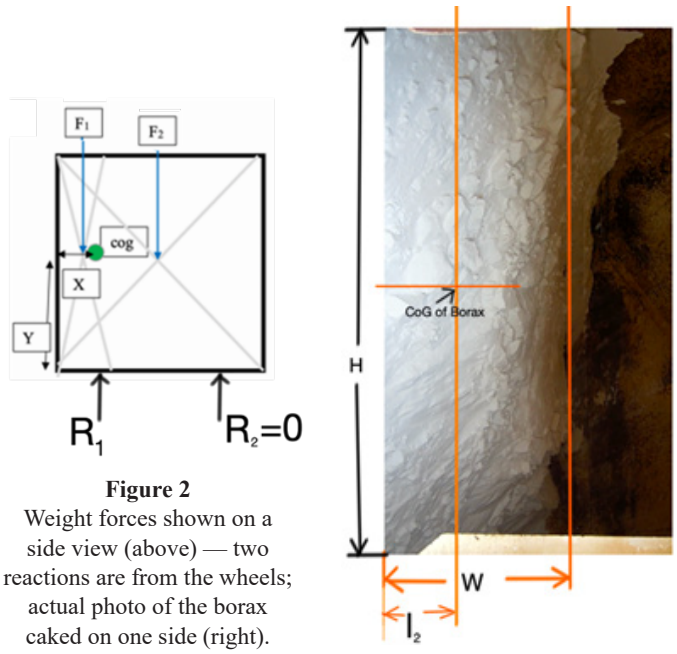

Figure 2
Weight forces shown on a side view (above) — two reactions are from the wheels; actual photo of the borax caked on one side (right).

F_2 = Empty Rail Car Weight = 62,700 lb = 278,396 N

Gauge Length = 1.435 m

Total Car Width = 3.23 m; l_1 = ½ (car width) = 1.615 m; $l_2 = 0.1804\ m$

a = ½ (gauge length) = 0. 7175; $b = l_1 - a - l_2 = 0.79\ m$ (as shown in **Figure 3**).

$M_{R1} = F_1 (b) - F_2 (a) = 339414 * 0.79 - 278396 * 0.7175 = 68088$ N-m

Maximum Load to Avoid Tipping Over-Calculation

The condition for the moments about to tip the rail car

$M = F_2 * a - F_1 * b = 0$

$F_1 = F_2 * a/b = 253130$ N

Borax; $F_1 = 339414$ N

Extra load that caused the tip over = 339414-253130 = 86284 N = 19047 lb

Lean Angle Calculation

The lean angle is the threshold angle beyond which it will tip over (as shown in **Figure 4**). It is calculated from the left side of the rail car, which is 26.3˚.

$\Phi = \tan^{-1}(1.925/0.95) = 63.7^{\circ}$

Lean angle, $\theta = 90 - \Phi = 26.3^{\circ}$

The pivot point of the rail car is the location of wheel-to-rail contact. The tipping angle was found to be 26.3˚. The rail car was pulled in place by the railroad locomotive while it was fully loaded. It was emptied by transfer station workers using an unloader placed under the car at the drop chute. The unloader conveyed borax up to drop in the dump trucks. Unloaders had shakers to help loose material in the rail car, so it fell freely into the unloader. The shaker on this device was not working.

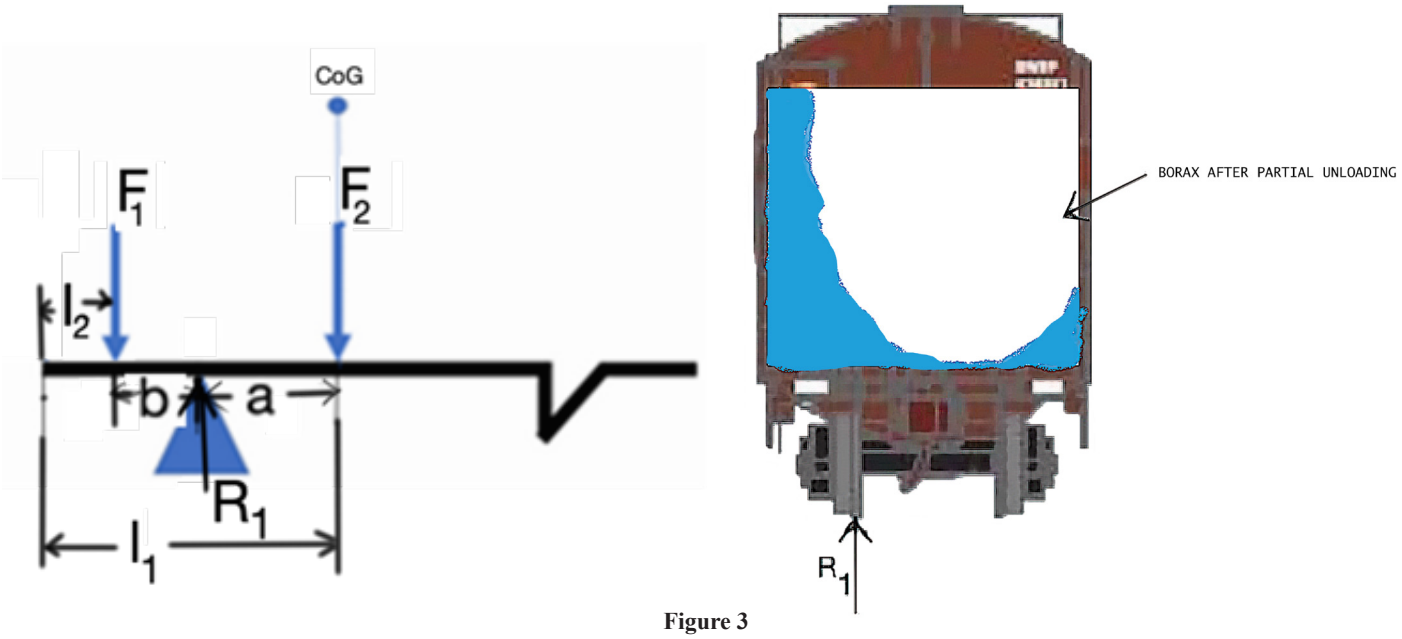

Figure 3
Moments calculations with moment arms.

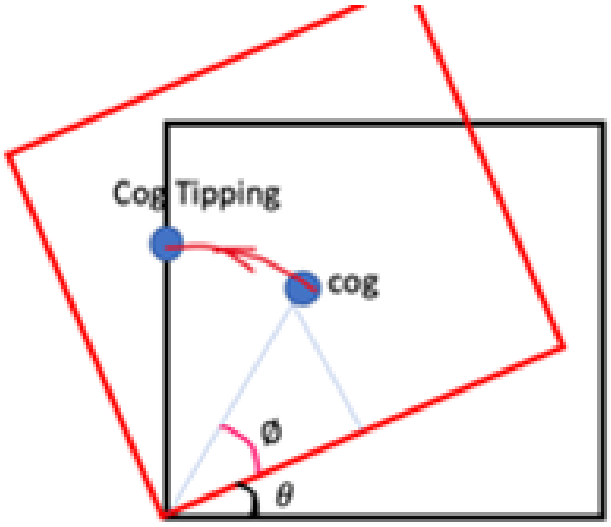

Figure 4
Lean angle calculations.

Conclusion

Anhydrous borax absorbed moisture from the ambient relative humidity, which caused the borax to clump and adhere to the side of the rail car. This caused an unstable situation. With the limited information available to the yard workers, they could not have known the rail car was not empty — and, from their perspective, could not see the rail car was leaning.

The flagman was responsible for ensuring the work crews and equipment were clear and the train was unobstructed to travel. The uneven load was not apparent to the flagman or other workers in the rail yard. Once the train began to move, the static friction forces no longer restrained the borax car wheels, and the car tipped over. The origin of this event was lack of climate control in the warehouse that resulted in borax clumping to unbalance the load. The cause was the train beginning to move resulting in loss of static friction.

References

1. 20 Mule Team Borax, Borate Caking: Understanding and Prevention, Boron, California, 2021.

2. C. Helvaci and R. Alonso, "Borate Deposits in Turkey and Argentina; A Summary and Geological Comparison," Turkish Journal of Earth Sciences, vol. 9, pp. 1-27, 2000.

3. P. Withers, "Economic Geology of Death Valley,"Boston University, 2000. [Online]. Available: http://sirius.bu.edu/withers/pppp/pdf/dvminerals2000.pdf. [Accessed 30 January 2022].

4. H. Diamond, "Climate Science Program Manger at NOAA's Air Resources Laboratory," College Park, 2021.

5. National Environmental Satelite, Data, and Information Service, "Local Climatological Data, Daily Summary Wilmington New Castle Co Airport, DE," National Center for Environmental Information, Asheville, 2013.

6. Taylor & Francis Group, CRC Handbook of Chemistry and Physics, D. R. H. W. M. Lide, Ed., Boca Raton: CRC Press, 2009-2010 at page 4-134.

7. "https://www.csx.com/index.cfm/customers/resources/equipment/railroad-equipment/," [Online].

Forensic Investigations of Propane-Related Food Truck Incidents

By John L. Schumacher, PE (NAFE 1052S), Charles R. Brown III, Zachary J. Jason, PE (NAFE 1053S), and Dennis E. Shelp, PE (NAFE 1058S)

Abstract

The proliferation of propane-fueled food trucks and concession trailers over the last decade has led to a fast-growing industry. As with many nascent industries, accidents accompany the surge in growth, and the food truck industry is no exception. Numerous propane-related fires, flash fires, and explosions have resulted in property damage, business interruption, injury, and death. Conducting a proper investigation of a food truck incident is essential in determining the origin/cause and ultimately assigning liability and preventing recurrences. This paper discusses the food truck industry as well as the design, construction, and layout of the trucks. It provides an overview of the gas systems installed in the vehicles — from the cylinder or tank to the appliances, properties of propane, and relevant codes and standards applicable to food trucks that utilize propane. Finally, an outline of the proper methodology to use when investigating a food truck incident is provided, and a food truck explosion case study is presented.

Keywords

Food truck, concession trailer, design, layout, codes, standards, fire, flash fire, explosion, propane, gas system, appliances, accident investigation, methodology, BLEVE, forensic engineering

Introduction

Food trucks and concession trailers (hereafter collectively referred to as "food trucks") are mobile commercial kitchens. As such, they have similar cooking equipment and systems to those found in restaurants. However, they also have unique components like engines and on-board generators. The potential incidents that can occur with a mobile kitchen are like those historically encountered in a commercial restaurant kitchen. Examples include fires (electric, solid-fuel, cooking, self-heating, etc.), carbon monoxide poisoning (appliance, generator, etc.), and flash fires/explosions (gas leak). While it is acknowledged there are many different types of incidents that can occur with food trucks, this paper will focus on propane-related fires, flash fires, and explosions.

The Industry

The mobile food industry is nothing new, considering it has been a part of U.S. history in many different configurations for years. Some historical examples include pushcarts in New York City (circa 1691), chuckwagons and railway dining cars in the 1800s, field kitchens for military personnel in the early 1900s, ice cream trucks in the 1950s, and present-day mobile food trucks and carts[1]. Recent statistics indicate that more than 26,000 food truck businesses exist in the U.S. market, employing more than 32,000 people. In addition, the food truck business has been prospering, showing a revenue growth rate of 7.5% since 2016[2].

Amid the Covid-19 pandemic, many food trucks and carts experienced a depletion of foot traffic in their regular operating business districts. This caused operators to become innovative and change their focus to essential businesses, residential neighborhoods, and, in some instances, hospitals and factories[2]. As Covid-19 restrictions ease, gatherings such as the one shown in **Figure 1** will return, thereby reinforcing the need for safe design, construction, and operation of food trucks/mobile cooking operations.

Food Trucks

Although there are many different mobile commercial kitchens driving down the road and/or parked on streets and in parking lots on any given day, most trucks have a similar design, construction, layout, and gas system installed in them.

John L. Schumacher, PE, 8197 West Brandon Drive, Littleton, CO 80125, (303) 756-2900, john@AEIengineers.com

© Miker/Shutterstock.com

Figure 1
Example of tightly packed food trucks at a food truck fair in Minneapolis in 2012[3].

A. Design and Construction

Food trucks and trailers are found in many configurations and designs, including repurposed portable trailers, converted and repurposed trucks, and newly constructed trucks/trailers. In many circumstances, the construction of the food truck was performed by well-trained professionals, displaying pride, craftsmanship, and purpose in their product.

Many of the trucks have the functionality and configuration of an actual mobile commercial kitchen, utilizing stainless steel surfaces and purposeful safety components. It is not uncommon for these units to come with design drawings and operators' manuals that encompass safety and training requirements/recommendations. Other food trucks are often repurposed bread trucks or homemade conversion units that incorporate large quantities of aluminum diamond plate walls and display minimum efforts with regard to craftsmanship, safety, and code compliance.

B. Layout

An example of the typical layout of a food truck is illustrated in **Figure 2**. Components common to most food trucks include: the cylinder housing; generator and external power hookup; air conditioner; service counter and window; preparation area(s); sink(s); refrigerator and freezer; cooking line; hood and restaurant hood fire suppression system; and cab.

C. Gas Systems

Food truck gas systems generally contain a tank or cylinder(s), hoses, regulator(s), gas piping, manifolds, appliance shutoff valves, flexible connectors, appliances, and automatic fuel shutoff valve. The system starts with the container storing the propane (either a motor vehicle tank or portable cylinder). The motor vehicle tanks are designed, fabricated, tested, and marked or stamped in accordance with the regulations of the American Society of Mechanical Engineers (ASME) Code, Section VIII, Rules for the Construction of Unfired Pressure Vessels[5].

The motor vehicle tank will contain a metal nameplate, indicating the manufacturer, serial number, year of manufacture, maximum allowable working pressure (MAWP), tank capacity (in gallons), and year of manufacture, among other things. The appurtenances on a motor vehicle tank include the vapor shutoff valve, fixed maximum liquid level gauge (also known as a spitter valve), float gauge, filler valve (which incorporates an overfilling prevention device or OPD), and pressure relief valve. The fixed maximum

Figure 2
Images of the typical interior layout of a food truck (www.United-Food-Truck.com)[4].

liquid level gauge is used to fill the tank by volume. Typical motor vehicle tanks used on trucks have a capacity ranging from 30 gallons to 60 gallons, and they are most often mounted to the underside of the truck frame.

By far, portable cylinders are the most common container used on food trucks. These are designed, fabricated, tested, and marked or stamped in accordance with the United States Department of Transportation (DOT)[6]. Cylinders manufactured prior to 1967 may have been fabricated to the requirements of the Interstate Commerce Commission (ICC) Rules for Construction of Unfired Pressure Vessels[7].

The manufacturer, serial number, year of manufacturer, DOT cylinder specification (e.g., details of cylinder construction), water capacity (in pounds), and tare weight (in pounds) are stamped into the cylinder collar. All cylinders (whether DOT or ICC) are typically required to be requalified within 12 years after the date of manufacture. Three methods are used to requalify cylinders, each of which have different periods until the next requalification time: volumetric expansion (12 years); proof pressure (seven years); and external visual inspection (five years).

The collar will have stamped into it the retester identification number (RIN or entity that performed the requalification), requalification method used (S for proof pressure or E for external visual inspection), and requalification date. Alternatively, a sticker containing the same information may be found affixed to the collar instead of stamping. Unless a cylinder is correctly requalified, DOT rules do not allow it to be filled or transported.

The appurtenances on a cylinder include the vapor shutoff valve, fixed maximum liquid level gauge, and pressure relief valve. Cylinders with capacities of 4 pounds to 40 pounds should also be equipped with an OPD. The tare weight and water capacity weight stamped into the collar are used to fill the cylinder by weight (i.e., using a scale), and the fixed maximum liquid level gauge is used to fill the cylinder by volume. Typical sizes of cylinders used on trucks include 20-pound, 33-pound, 40-pound, and 100-pound. Cylinders can be mounted in open air configurations on the back of a truck or (in the case of food trailers) mounted on the tongue. On some food trucks, the propane cylinders are contained in compartments built into the side or attached to the rear of the vehicle.

The pressure relief valve protects the tank/cylinder from rupturing due to excessive internal pressure. Two possible causes of excessive internal pressure include external heat from a fire, heat-producing appliance, or sunlight (i.e., high vapor pressure) or a liquid-full condition associated with an overfill (i.e., hydrostatic pressure).

Since the vapor pressure inside the container is too high for use by the gas appliances inside the truck, system regulation is required to reduce the pressure to a usable level. For propane appliances, this is approximately 13 inches water column (in. wc) or approximately ½ pound per square inch gauge (PSIG).

Regulation is accomplished through a regulator, either a single integral twin-stage regulator or the combination of two regulators, a first stage and a second stage (i.e., a two-stage system). An integral twin-stage regulator is comprised of two stages in one device. The container pressure is reduced to 13 in. wc. Some integral twin stage regulator models, referred to as "automatic changeover regulators," are connected between two cylinders and designed to automatically switch from the active cylinder (determined by the position of the changeover lever on the regulator) to the reserve cylinder when pressure decreases to a level indicative of the primary cylinder going empty. The changeover regulator is installed near the two cylinders on the outside of the truck.

A true two-stage system uses two separate regulators to decrease gas supply pressure going into the food truck to 13 in. wc. The first-stage regulator connected to the cylinder or tank decreases the pressure to 10 PSIG, and the second-stage regulator (typically found some distance downstream from the cylinder/tank) drops the pressure from 10 PSIG to a usable pressure of 13 in. wc. The two regulators can be connected using a hose, black iron pipe, or copper tubing. Both regulators are installed on the exterior of the truck. If, under the rare situation the second stage regulator is installed inside the food truck, the regulator vent opening should be piped to the outside of the truck, as the vent serves as the discharge port for the regulator's built-in internal relief valve, which protects the appliances from the potential damaging effects of high gas pressure should the regulator malfunction.

From the final point of system pressure regulation (i.e., the outlet of the integral twin-stage regulator or second-stage regulator), black iron, copper, and/or non-metallic tubing or hose is used to provide gas to the interior of the food truck. Typically, the first device encountered inside the truck is the automatic fuel shutoff valve, which is part of the restaurant hood fire suppression system. The automatic fuel shutoff valve is designed to close automatically in the

case of a fire on the cooking line or by manual operation via a pull station. When activated, the shutoff valve closes, thereby preventing propane fuel flowing to the cooking line and removing it as a potential fuel source for the fire.

A gas manifold with individual appliance shutoff valves is usually located downstream of the automatic fuel shutoff valve. The shutoff valve and manifold are connected using lines constructed of black iron pipe, copper tubing, or corrugated stainless steel tubing (CSST). The lines provide gas to the appliances. Valves connected to the manifold, which is normally constructed out of black iron, are used to isolate (i.e., stop the flow of gas to) individual appliances. The appliances can be connected to the manifold using steel flexible gas connectors or copper tubing.

Common appliances found on food truck cooking lines include commercial fryers, cook-top ranges, griddles, charbroilers, ovens, warming tables, and/or salamanders. These individual appliances may have their own gas valves, which provide additional gas pressure regulation and temperature control. The reader is encouraged to obtain the manufacturer's information for the specific appliances found in the food truck of interest.

Propane Properties

Propane is a viable fuel source because it burns readily and can be liquified at relatively low pressures, making for easy bulk transport. The specific gravity of propane liquid at 60°F is 0.504 (about 50% lighter than water), which equates to a density of 4.2 pounds/gallon. The specific gravity of propane vapor at 60°F is 1.50 (about 50% heavier than air), which equates to a density of 0.115 pounds/ft^3. Thus, propane gas is often described as being heavier than air, and it tends to sink[8].

From the two densities, the expansion of one gallon of liquid to vapor at atmospheric pressure can be determined. One gallon of liquid propane will generate approximately 36.4 ft^3 of vapor/gas at sea level atmospheric pressure or 14.7 pounds per square inch absolute (PSIA). The flammable range for propane is 2.15% to 9.60% by volume in air, and the heating value is 2500 Btu/ft^3 of gas. As a comparison, natural gas has a flammable range of 5% to 15% and a heating value of 1,000 Btu/ft^3.

The propane stored in a container is present in two distinct phases in equilibrium with one another — a liquid phase and a vapor phase in the headspace (e.g., ullage). **Figure 3** shows the saturated vapor pressure versus liquid temperature relationship for pure propane; the pressure of the vapor in the headspace is determined by the liquid temperature, and the liquid temperature is typically driven by the ambient temperature and radiant sun exposure[9]. As the liquid temperature increases, there is an accompanying increase in pressure. Conversely, as the liquid temperature decreases, there is an accompanying decrease in pressure. As long as there is a vapor space above the liquid, the vapor pressure-temperature relationship depicted in **Figure 3** will be followed. Under normal operating conditions, the vapor pressure inside a container will not reach the set point of a tank or cylinder relief valve (312 PSIG for ASME tanks and 375 PSIG for DOT cylinders, respectively). However, if heat from an outside source (e.g., operating appliance, generator, external fire, etc.) impinges on a tank or cylinder, the liquid temperature and consequently pressure can potentially increase sufficiently to cause the relief valve to function.

Liquid propane in a container expands with an increase in temperature, thereby decreasing the headspace volume. Cylinders and tanks are typically only filled to 80% to prevent them from becoming liquid-full due to anticipated atmospheric temperature changes — the concern being, if a container was to become liquid-full, the pressure generated by the incompressible liquid propane is significant enough to cause rupture if not relieved. Additionally, if pressures reach the set point of the relief valve (and the relief valve opens), then the release of vapor or liquid propane could pose a fire/explosion risk in the presence of an ignition source.

Codes and Standards

Prior to 2017, there were references published in

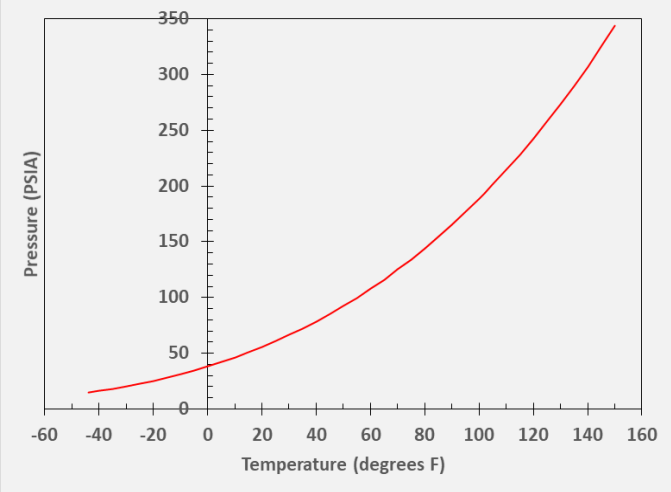

Figure 3
Saturated vapor pressure versus temperature relationship for pure propane.

multiple codes for the design, construction, and operation of food trucks, including the following examples:

- National Fire Protection Association (NFPA) 1, *Fire Code*, for licensing, emergency equipment access, public seating requirements, and portable power supply placement[10].

- NFPA 58, *Liquefied Petroleum Gas Code*, for cylinder and tank requirements, documented leak test requirements on gas connections, closure of gas supply valves when not in use, accessible gas supply valves, upright and secured propane containers, and appropriately installed flexible gas connectors[8].

- NFPA 70, *National Electrical Code*, for the appropriate installation of electrical systems[11].

- NFPA 96, *Standard for Ventilation Control and Fire Protection of Commercial Cooking Operations*, for refueling operations, location of portable power sources, gas detection system installation, proper appliance operation and ventilation, and approved fire extinguishing systems[12].

The dearth of specific and centralized code requirements for mobile kitchen construction and operation has caused many jurisdictions to create their own regulations. Jurisdictions are adopting excerpts from NFPA 58, NFPA 96, and NFPA 1192, *Standard on Recreational Vehicles*[13]. NFPA 1192 regulates recreational vehicles that contain cooking appliances. However, the scope of this standard is not applicable to mobile kitchens that contain commercial appliances, ventilation systems, and fire prevention systems. Some jurisdictions (like the state of Indiana) have chosen to not inspect a food truck because it is a vehicle, while others (like the city of Chicago) have adopted specific requirements, such as always having an employee present on the vehicle who is trained by the fire department in handling and exchanging propane tanks.

In June 2017, the NFPA 96 Technical Committee added a normative annex section on mobile and temporary cooking operations. This annex section consolidated extracts from the requirements of NFPA 1, NFPA 58, and NFPA 70 as well as applicable chapters from NFPA 96 in an effort to provide the user with common requirements. While this annex section is written in mandatory language, it is not enforceable, unless adopted by the local jurisdiction[14]. In 2018, NFPA 1 added Section 50.7, a new enforceable section that is applicable to Mobile and Temporary Cooking Operations[15]. These two additions to the current NFPA codes added clarity to the requirements for jurisdictional authorities and food truck builders — whether commercial or homemade.

In 2020, NFPA compiled a Food Truck Safety Fact Sheet that references Code sections for each applicable requirement[16]. The compilation of this resource added clarity and guidance for the Authority Having Jurisdictions (AHJs), commercial truck builders, and the homemade food truck builders.

In 2021, a proposal was submitted to the NFPA 58 Technical Committee to compile Mobile and Temporary Cooking Operations requirements within NFPA 58. At the time of publication of this paper, the proposal is currently under review.

Several jurisdictions have adopted the NFPA family of codes, while others have adopted the International family of codes. The current consolidation of excerpts from the NFPA codes found in NFPA 1 and NFPA 96 may not be readily available or enforceable in jurisdictions that have adopted the International code family. One specific code that is common by reference to the International and NFPA code families is NFPA 58, the *Liquefied Petroleum Gas Code.* A new proposed chapter has been submitted to the NFPA 58 Technical Committee for review. This proposed new chapter has consolidated the code references similar to NFPA 1 and NFPA 96. This new proposal, if adopted, can potentially become an important avenue of information that adds consistency for jurisdictions and truck builders toward the safety in the food truck industry. The need to reference different code books to fully understand the design, construction, and operational requirements pertaining to the various components of a food truck will remain a necessity for truck builders and jurisdictional authorities.

Accident Investigation Methodology

The investigation of a food truck incident is similar to that of a structure fire, flash fire, or explosion investigation where a propane system may be involved. The ultimate goal of the investigation is to determine where the incident originated, what caused the incident, and, where applicable, assign responsibility. The general process entails: A) pre-investigation activities, such as reviewing public entity reports and witness statements; B) examining and documenting the truck and surrounding location, explosion/fire damage, and gas system; C) examining and documenting the gas system components and layout; D) testing

the gas system for leaks and obtaining propane samples; E) analyzing the fill history and weather data; and F) researching the applicable codes and regulations. These steps are discussed in more detail in the sections that follow. It should be noted, however, that the sections below are not intended to be a definitive guide on conducting these investigations. Instead, they should be viewed as a starting point for an investigator to understand the basic concepts and methodology involved.

A. Pre-Investigation

Although not exhaustive, **Figure 4** is a detailed list of items an investigator should consider collecting, identifying, and gathering prior to and/or during the initial documentation phase of the investigation. Many of these items are similar to those collected during a typical fire or explosion investigation, but the list also includes data specific to food truck/propane incidents.

B. Overall Documentation: Truck and Surrounding Location

As with any fire or explosion scene, the investigator should document the overall condition of the scene in a systematic fashion, typically starting from areas of least damage and progressing to the areas of greatest damage. In incidents involving food trucks, that typically entails a thorough examination of the area immediately surrounding the food truck, the exterior of the truck, the interior cooking spaces, and the driver's compartment.

Investigators should conduct a thorough canvas of the immediate area to identify and collect any surveillance

Item	Details
Witness Statements, Interviews, and Media	Social media — GoFundMe, Twitter, Facebook, Instagram, Snapchat, etc.
	Electronic media (videos and photography) per local news media and/or witnesses
	Surveillance videos
Public Entity Reports and Data	National Fire Information Reporting System (NFIRS) incident reports
	State and local public authority investigation reports — police department, fire department, sheriff's department, Department of Transportation, Bureau of Alcohol, Tobacco, and Firearms, Occupational Safety and Health Administration, LP gas inspector
	Medical records — EMT/emergency room notes and reports
	Interviews/statements provided by first responders
	Post-incident testing conducted by the gas utility and/or public agencies (including leak testing of the subject gas system)
Subject Food Truck Data/History	Owner's name and contact information
	Purchased new vs. converted/remodeled
	Chassis manufacturer — make, model, year, VIN
	Kitchen design and build company
	Design drawings
	Service, maintenance, and inspection records — truck, gas system, and restaurant hood system
	Pre- and post-incident photographs (food truck, design/build company web sites, social media, etc.)
	Recent modifications/changes and operating history
Historical Weather Records	The day of the incident and weeks prior to the incident
Propane Fill Records	Most recent prior to the incident and as many as possible preceding the most recent

Figure 4
Pre-investigation guide checklist.

media. This includes surveillance footage captured by adjacent food trucks, businesses, and residential security/doorbell cameras. For systems that are not cloud-based (e.g., systems using a digital video recorder or DVR, the footage should be preserved immediately post-incident to ensure it is not overwritten or lost.

A detailed examination of the subject food truck is critical. Investigators should specifically document and photograph the overall condition of both the driver's and kitchen compartments. Specific attention should be given to the fuel-gas system, appliances, hood and restaurant hood fire suppression system, generator, engine compartment, electrical system, and any other safety systems.

Further, the overall scene documentation of both the food truck and surrounding area should include any relevant explosion, overpressure, and thermal damage. Specifically, explosion damage to the truck, propane tank/cylinders, gas piping and appliances, nearby structures, and vehicles (as well as thermal damage to the inside and outside of the truck, occupants, customers, pedestrians, and passengers in vehicles) should all be documented and photographed.

A detailed survey/laser mapping of any debris fields should be considered to memorialize the position of evidence relative to original locations. Investigators should prepare both comprehensive scene diagrams and detailed diagrams of the subject food truck. **Figure 5** is a list of data investigators should attempt to include on the respective diagrams.

C. Gas System Components and Layout

In the event of an explosion or suspected fuel-gas related incident, a detailed examination and thorough testing of the fuel gas system are necessary. In particular, the investigator should document the information and/or components in the system, as listed in **Figure 6**.

D. Leak Testing and Propane Samples

When possible, a leak test of the fuel-gas system using propane, nitrogen, or air should be performed in situ to verify system integrity and quantify any potential leaks that may exist. System integrity testing of the fuel-gas system is typically divided into two parts. The first is the gas distribution system, which includes supply regulators, piping/tubing, and flexible connectors that connect to the appliances. The second is testing/examination of the respective appliances, including their individual regulators and associated gas controls/safety valves. Supply

Item	Details
Overall Scene Diagram	Location of subject truck relative to surrounding structures and/or other permanent landmarks
	Overlay diagram with satellite/drone imagery
	Clearances to adjacent buildings, structures, vehicles, food trucks, public seating areas, and any combustible materials
	Location/position of fire/explosion debris and other critical evidence relative to the incident
	Surveillance video camera locations
Food Truck Diagram	Location/routing of fuel-gas system (propane tank/cylinders, gas piping, hoses, regulators, manifolds, shutoff valves, flexible connectors, etc.)
	Appliances and cooking line (manufacturer data tags, date codes, position of control knobs/settings, location, etc.)
	Position of valves, switches, and other pertinent controls
	Fire suppression and kitchen hood system (automatic fuel shutoff valve position and cable, nozzle location and aim, location and condition of fusible links and cables, overall cleanliness of system, expellant cartridge condition, cylinder charge level, evidence of system deployment, etc.)
	Fire extinguishers (type, service/inspection tag, fill level, pin position)
	Electrical system (switches, receptacles, breakers, fuses, controls)
	Ventilation/HVAC systems, size and location of windows, doors, and any openings

Figure 5
Truck and surrounding location checklist.

Item	Details
Cylinder(s)	Collar information (date, water capacity, tare weight), requalification stamp, visual condition, ICC vs. DOT, cylinder valve (make, model, date), position of cylinder valve, weight
Tank	Nameplate and appurtenances information (auto-stop fill valve, fixed maximum liquid level gauge, float gauge, pressure relief valve, and vapor valve), position of vapor valve, volume of fuel in tank
Tank/cylinder installation	Shielded by enclosure or direct sunlight impingement, isolated from the interior, nearby heat sources (e.g., generator, appliance, truck engine exhaust, etc.)
Regulator or regulators	Type (integral twin stage, integral twin stage with automatic change-over, two stage system), date codes, model numbers, serial numbers, vent condition and point of discharge, installation orientation and location
Gas piping/hoses from tank/cylinders to automatic fuel shutoff valve and manifold	Type, size, lengths, etc.
Automatic fuel shutoff valve	Confirm existence, document state (i.e., open or closed), location in gas system
Manifold and valves	Valve positions and associated appliances
Gas piping to appliances	Type, size, lengths, etc.
Appliances	Type, nameplate data (usage rates Btu/h, model and serial numbers), location, knob and valve positions, power switch (on or off), plugged in or not, settings
Accessory cylinders	Location (inside or outside food truck), type (one pound, 20-pound, etc.), condition (separate or connected to a portable heater), position of cylinder valve, heater settings, hose connected between heater and cylinder, weight of cylinders

Figure 6
Gas system components and layout checklist.

regulators should be tested and checked for proper operation, including measuring both lockup (i.e., pressure output under "no flow" conditions) and flow pressures under various loads. Investigators should document any condition that would cause the regulator(s) to malfunction.

If leaks are discovered during the system integrity testing, the location of the leaks should be identified and the size of each quantified using flowmeters and pressure gauges/manometers. This quantitative data can be of particular importance for conducting future consumption analysis and energy calculations — and for overall causation theory determination.

E. Fill History and Weather Data

Determine when and where the food truck propane cylinders/tank were filled, and document the findings as listed in **Figure 7**.

Item	Details
Dispensing station	Pump and scales
Fill method	Weight, volume, weight/volume, company procedures, training
Dispenser operation	Confirm the accuracy of the dispenser pump and scale
Fill ticket	Obtain and review the fill ticket for the subject truck containers and compare the size of the containers to the amount of propane dispensed
Ambient temperature	At the time of the fill, between fill and accident, at time of accident

Figure 7
Fill history and weather data checklist.

F. Regulations

A review of the codes and standards applicable to the incident is an important step in the overall investigation. This review can identify construction or operational practices that may have contributed to the incident.

Case Study

An explosion and subsequent fireball erupted from a food truck while it was parked and operating on a street in an eastern U.S. city. At the time of the incident, the owner was at the rear of the food truck near the door between the two propane cylinders, a second individual was inside the food truck seasoning chicken, and a third was in the front of the food truck next to a fourth individual. A fifth individual was sitting in a chair on the sidewalk outside the food truck, and two others were driving by in a vehicle. The owner and the third individual died, 13 others (including the two individuals in the front of the food truck, the individual in the chair, and the two individuals in the vehicle) were injured, and the food truck and nearby items were damaged.

A joint investigation into the cause of the explosion (that spanned approximately four years) was conducted by several public entities and other potentially interested parties. The truck and other artifacts had been collected and moved from their post-incident locations by the public entities prior to these writers being engaged to investigate the accident. As such, the public entity reports and photographs had to be relied upon for some of the analysis. Further, the Federal DOT significantly limited access to the cylinders, rubber hoses, changeover regulator, and copper tubing from the food truck gas system. The authors were not given the opportunity to examine those artifacts and had to rely on the photographs taken by others. Presented below is a summary of the investigation and ultimate findings.

A. Pre-Investigation

The owner purchased a used food truck (first food truck) on Craigslist. The owner acquired the truck about 1.5 years prior to operating it for approximately six months. The first food truck had only one 100-pound propane cylinder that fueled the gas appliances.

Two years after purchasing the first food truck, the owner purchased an empty, used truck on Craigslist (the food truck subsequently involved in the explosion). The owner of the truck then contracted a separate entity to design and build a kitchen inside the truck. The owner started operating the subject food truck seven days a week at the location where the incident occurred — approximately two months prior to the explosion (see **Figure 8**).

Figure 8
Location where the food truck was being operated at the time of the incident (see red box; street and business names redacted). North is at the top of the image.

The subject food truck came with two propane cylinders. A nearby dispenser would not fill them for an undetermined reason. Consequently, the truck was initially operated using only the single cylinder until a customer gave the owner a second cylinder about a week and a half later. Both were filled at the nearby dispenser the day the owner was given the second cylinder. From that point forward, both cylinders were used on the food truck. The left cylinder was the one brought over from the first food truck, and the right cylinder was the one given to the owner by the customer. The cylinders were routinely filled at the nearby dispenser and sometimes at a second dispensing location.

A customer complained to the owner about an odor of propane around the end of the first month of operation, and the valve on the cylinder from the first food truck was reportedly replaced by the entity that designed/built the kitchen. Odor complaints ceased after the valve was replaced.

The last documented fill of the two propane cylinders occurred in the morning two days prior to the incident at the nearby dispenser. No fill ticket or receipt was available detailing the total gallons added to the two cylinders. After the cylinders were filled, the owner installed them on the food truck and operated the truck. There was conflicting testimony as to whether the food truck was operated the day prior to the accident. However, when in operation over the three-day period leading up to the incident, only the right cylinder was in use.

In the early evening on the day of the incident, the left cylinder ruptured, and the propane vapor was subsequently ignited, resulting in a large fireball. A security camera at a nearby business captured the explosion. **Figure 9** shows

Figure 9
Images of the explosion taken from the video captured by a nearby security camera.

Figure 10
Images of the rear of the food truck post-incident. The left cabinet and cylinder were missing.

Figure 11
Pre-incident images of the rear of the food truck and the left and right propane cylinder cabinets.

images taken from the video (approximately 25 frames per second) at different times. The first sign of the white cloud associated with propane is visible in Frame 1. The white cloud increases in size in Frames 2 through 7. Ignition is first observed in Frame 8, and the fireball expands in Frames 9 through 11. Smoke without fire is seen in Frame 12.

B. Overall Documentation

Figure 10 shows the back of the food truck post-incident; the left cabinet and cylinder were both missing, but the right cylinder was still intact (and in place) inside the right cabinet. The right cylinder valve was closed after the incident by the fire department. As a comparison, pre-incident images of the food truck are illustrated in **Figure 11**.

Various pieces of the back of the food truck were identified in the debris field, which was dispersed rearward away from the back of the truck. **Figure 12** shows the

Artifact Description	Approx. Distance (ft)
Diamond plate bumper cover	0
Flexible tubing, ~24 inches in length	32
Left cylinder cabinet remnants	42
Lid of left cylinder cabinet	56
Section of copper tubing and tee fitting	66
Left cylinder cabinet remnants and changeover regulator	84
Left cylinder	105
Door of left cylinder cabinet	120
Padlock	122

Figure 12
As-found location of artifacts in the debris field as measured from the rear of the food truck.

Figure 13
The front (left), driver (middle), and passenger (right) sides of the food truck.

distance each artifact was found as measured from the rear of the food truck. The diamond plate bumper cover was found underneath the rear bumper. The cover over the portable tent structure to the right or south of the food truck was consumed by the fireball.

The post-incident appearance of the food truck is illustrated in **Figure 13**. The windshield was missing from its frame. The truck was equipped with a generator located inside a cabinet near the back on the driver's side. Metal on the front and rear sides of the generator cabinet were pushed to the front. The exterior diamond plate on the rear of the truck, which formed the back wall of the left cabinet, had a dent or impact mark about 2 feet 10 inches above the bumper. Reconstruction of the left cabinet, which was framed using square metal tubing covered with diamond plate, is shown in **Figure 14**. The exterior diamond plate on the rear wall of the truck enclosed the back of the cylinder cabinet. The cabinet exhibited signs of forces from the inside acting in an outward direction.

C. Gas System Components and Layout

The subject food truck was equipped with six propane-fired appliances fueled by the two 100-pound propane cylinders. The left and right cylinders were originally located inside of bottomless diamond plate metal cabinets — one on either side of the rear door above the bumper cover/step, as illustrated in **Figure 11**.

The following observations were made with regard to the left cylinder (see **Figure 15**):

1. The cylinder had ruptured;

2. There was no evidence of cylinder failure related to corrosion or fatigue;

3. Based on the model number, the cylinder valve was not manufactured with a relief valve and was meant to be used with a separate relief valve;

4. There was no separate relief valve;

5. A plug was threaded into the gauge tap opposite the POL (Prest-O-Lite) connection;

6. The cylinder valve did not have a fixed maximum liquid level gauge; and

7. The cylinder valve was in the closed position.

The following observations were made relative to the right cylinder (see right image in **Figure 10**):

1. The cylinder was intact;

2. The cylinder valve had a relief valve;

3. The cylinder valve did not have a fixed maximum liquid level gauge; and

4. The cylinder valve was in the closed position. It was learned through discovery that the fire department closed the valve after the incident.

The information displayed on each cylinder and cylinder valve is delineated in **Figure 16**. The left and right cylinders were manufactured in November 1948 and September 1985, respectively, and were qualified for service for 12 years past their dates of manufacture. The left cylinder required requalification in November 1960. However, the cylinder was never requalified. The right cylinder was requalified in February 1995 (i.e., 2 95 in 2 95s) and was good for seven years or until February 2004 (the "s" in the requalification stamping "2 95s" signifies it was requalified using the hydrostatic pressure proof

Figure 14
Reconstruction of the left cabinet.

test). The cylinder was never requalified after February of 1995.

The "W.C. 239" indicates each cylinder could hold a total of 239 pounds of water or 28.7 gallons at a temperature of 60°F when 100% full. Therefore, if properly filled with propane to 80%, each cylinder would hold 22.9 gallons.

Rubber hoses had been used to connect the cylinder service valves and the two inlets to a low-pressure two-stage automatic changeover regulator. The regulator was housed in the left cabinet above the cylinder, and the ⅜-inch hose from the right cylinder was routed to the regulator through the bumper cover via notches below the cabinets. Three-eighths-inch copper tubing was connected between the outlet of the regulator and a ½-inch steel tee. The tee was attached to a ½-inch 90-degree elbow near the bottom of the left cabinet via a ½-inch short nipple. The 90-degree elbow was connected to a ½-inch steel line that penetrated the rear wall and supplied gas to five appliances on the left side of the food truck. The other end of the tee supplied gas to the only appliance on the right side of the truck via ¼-inch copper tubing that penetrated the rear wall of the food truck inside the right cylinder cabinet. Like the rubber hoses, the ¼-inch copper line was routed to the right-side appliance through the bumper cover.

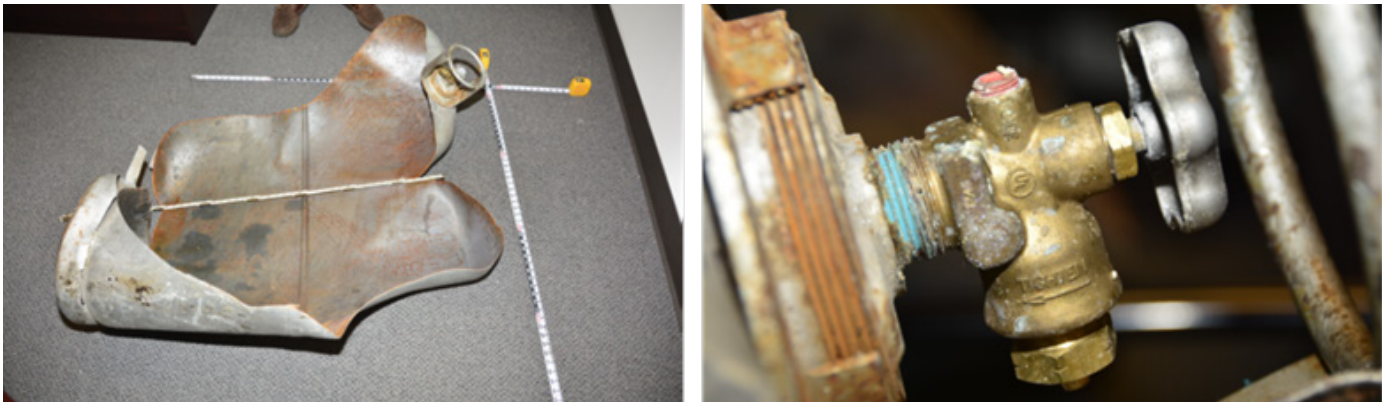

Figure 15
Left cylinder. The cylinder was ruptured, and the cylinder valve had no relief valve or fixed maximum liquid level gauge.

Cylinder	Cylinder Information	Valve Information
Left	PST, D-3090, ICC-4BA240-717, W.C. 239#, 11-48	3329, 5112
Right	J536298, DOT 4BW240, W.C. 239, T.W. 74, D.T. 9.0, 9-85, 2 95s, B154	3250A

Figure 16
Cylinder and cylinder valve information.

As shown in **Figure 17** prior to the incident, the five gas-fired appliances on the left side of the food truck (from rear-to-front) consisted of a deep fat fryer (1), flat-top griddle (2), charbroiler (3), vertical broiler (4), and range (5). A refrigerator and freezer were adjacent to and forward of the range. An exhaust hood and fan were installed above the five appliances. The exhaust hood did not have a restaurant hood fire suppression system or automatic fuel shutoff valve. A steam table (6) was located on the right side at the rear.

Propane gas was supplied to the five appliances on the left side via a ½-inch steel line. The steel line was located against the left wall below the appliances, and branched off to feed two manifolds, both of which were below the metal counter supporting the flat top griddle, charbroiler, and vertical broiler, as depicted in the top image of **Figure 18**. The first manifold was just forward of the deep fat fryer and below the flat-top griddle, as seen in the bottom left image of **Figure 18**. The manifold, which consisted of two appliance shutoff valves and three ½-inch flexible gas connectors, provided gas to the deep fat fryer (1, driver's side line), charbroiler (3, middle line), and flat top griddle (2, passenger's side line). The deep fat fryer did not have an appliance shutoff valve. The second manifold was just to the rear of the range, as shown in the bottom right image of **Figure 18**. The manifold, which consisted of two appliance shutoff valves and two ½-inch flexible connectors, provided gas to the vertical broiler (4, horizontal line) and range (5, vertical line). Propane gas was supplied to the steam table safety valve through ¼-inch copper tubing. The steam table did not have an appliance shutoff valve.

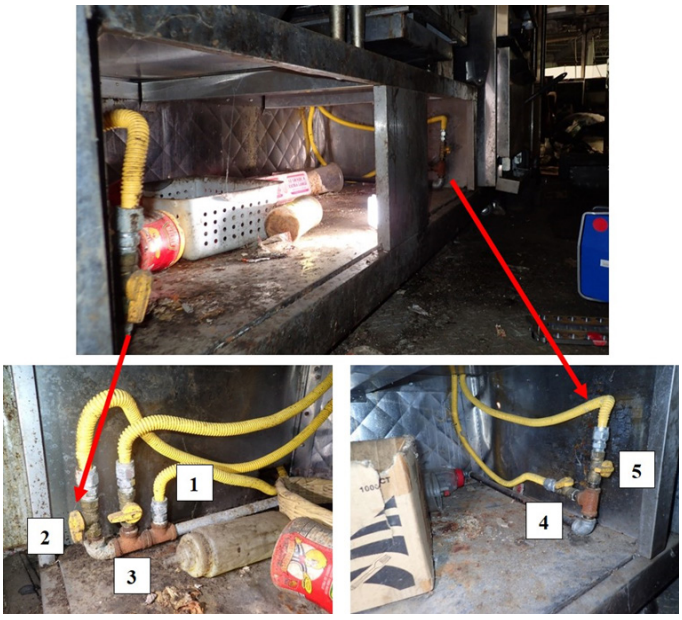

Figure 18
The images show the as-found positions of the manifold valves after the incident.

All the gas system components (rubber hoses, regulator, and copper tubing) between the cylinders and where the piping connected to or penetrated into the rear of the food truck were accounted for during the investigation. No relief valve external to the left cylinder was noted. Several fractures and separations were observed in the rubber hoses, regulator, and copper tubing.

The four manifold valves supplying gas to the appliances on the left side were found in the following positions (see **Figure 18**): flat top griddle (2) open, charbroiler (3) closed, vertical broiler (4) closed, and range (5) closed.

Figure 17
Six gas appliances inside the food truck.

The five appliances on the left side and the one appliance on the right side of the food truck after the explosion are shown in **Figure 19**. The appliance information and as-found valve positions for each appliance are detailed in **Figure 20** (the valves for each appliance were assigned a number). For example, the left valve on the griddle was labeled as "2L," the left rear valve on the cooktop of the range was labeled "5LR," and the oven control was labeled "5O."

D. Leak Testing

The food truck gas system was leak tested using a setup consisting of a nitrogen cylinder, cylinder regulator with a pressure gauge (P_1), flow meters (F), a regulator, and manometers upstream (P_2) and downstream (P_3) of the bank of flow meters. The leak test setup was connected to the elbow to test the gas piping and appliances on the left side, and then to the ¼-inch copper tubing to test the steam table on the right side. The results of the leak tests are summarized in **Figure 21**.

Some flow was measured through the standing pilots of a few of the appliances, but no leaks were detected in the gas system.

E. Fill History and Weather Data

The cylinders were filled 10 separate times at the two dispensers. **Figure 22** summarizes the time of fill, gallons added, and final percent full for each fill. Both cylinders were filled during the two 50-gallon fills and one 49.1-gallon fill. As can be seen in the third column of the table in **Figure 22**, the cylinders were historically overfilled (i.e., filled beyond 80%). The final percent full calculation assumed the cylinders were empty prior to filling (the start volumes during each fill were unknown), the 49.1 gallons and 50 gallons were divided equally into the two cylinders, and the cylinders had capacities of 28.7 gallons when completely 100% full.

Figure 19
Post-explosion images of the six gas appliances inside the food truck, which included a deep fat fryer (1), griddle (2), charbroiler, (3), vertical broiler (4), range (5), and steam table (6).

Appliance	Information	Valve Positions
Deep fat fryer (1)	Gross input 90,000 BTU/hr, gas type prop	Control valve knob ON, safety OFF, thermostat set at 400°F
Flat top griddle (2)	Input 20,000 BTU/hr, 5.9kW	Left valve (2L) ON and right valve (2R) OFF, standing pilots
Charbroiler (3)	Input 30,000 BTU/hr, 8.8kW	Left valve (3L) and right valve (3R) OFF, standing pilots
Vertical broiler (4)	Gas LP, 20,000 BTU/hr	Rotisserie switch OFF, thermostat valve PARTIALLY OPEN
Range (5)	Oven 35,000 BTU/hr, oven top 32,000 BTU/hr	Left front (5LF), left rear (5LR), right front (5RF), right rear (5RR), and oven (5O) valves OFF, oven safety OFF, standing pilots
Steam table (6)	Not available	Thermostat valve handle vertical or OFF, safety OFF

Figure 20
Appliance information and as-found valve positions for each appliance.

Video from a security camera at the dispenser where the cylinders were filled two days prior to the incident showed the scale was not used to fill the cylinders (i.e., the cylinders were not filled by weight). The ambient temperature at the time of filling was about 77°F, and the ambient temperature when the incident occurred was about 90°F.

P_1 (PSIG)	P_2 ("WC)	P_3 ("WC)	F (CFH)	Comment
~10	14.3	14.3	0	Test setup connected to the elbow, 14.3 in. WC on water manometer as a check, pressure holding with valve downstream of second stage regulator and valve at outlet of test rig closed
60	14.3	14.3	0	Increased P_1 into service regulator
55	14.0	13.5	10	5-50 CFH FM,[a] as-found condition
55	12.0	11.2	9.5	Adjusted second stage regulator so that P_3 ~ 11" WC per the protocol
55	12.0	11.3	9.5	Closed valve 3L (charbroiler)
60	12.5	12.5	NM[b]	Closed valve 2L (flat top griddle)
60	12.5	12.0	0.2	0.1-1.0 CFH FM
60	12.5	12.5	NM	Closed manual valve 2
60	12.5	12.5	NM	0.05-0.5 CFH FM
60	12.5	12.5	NM	Opened manual valve 3, 5-50 CFH FM
60	12.5	12.5	NM	0.05-0.5 CFH FM
55	11.8	11.4	16.5	Rotated 3R CCW 90° so knob vertical, 5-50 CFH FM
60	12.5	12.5	NM	Closed valve 3R (charbroiler) and manual valve 3, opened manual valve 4
60	12.5	12.5	NM	0.05-0.5 CFH FM
55	12.4	11.5	>0.5	Closed manual valve 4, opened manual valve 5
60	12.4	11.5	1.5	0.05-5.0 CFH FM
60	12.5	12.5	NM	Test setup 2 connected to the 1/4-inch tubing to warming table on the right side of the truck, as-found condition of steam table (6), 0.5-5.0 CFH FM
60	12.5	12.5	NM	0.05-0.5 CFH FM
				a = flow meter, b = not measurable

Figure 21
Results of the leak tests.

Days Prior to Incident	Gallons	Percent Full
108	27.7	97
83	25	87
78	26	91
74	25	87
66	25	87
47	50	87
25	50	87
17	25	87
12	49.1	86
2	No record	-

Figure 22
Summary of the time of fill, total gallons added to the cylinder(s), and final percent full for each fill.

F. Regulations

Based on the requirements of NFPA 58: 1) the left and right 100-pound cylinders were out of requalification by 66 years and 19 years, respectively; 2) the left cylinder should have been equipped with a pressure relief valve, either as part of the cylinder valve or as a separate add-on appurtenance; and 3) the left and right cylinders should have had fixed maximum liquid level gauges so they could be accurately filled to 80% by volume[8].

G. Analysis and Findings

The main goal of an explosion origin and cause investigation is to scientifically determine the origin, point of origin, first fuel ignited, oxidizer, ignition source, and cause of the incident. Related to the origin, the security video and still images taken from the video (**Figure 9**) clearly show the explosion and subsequent fireball originating proximate to the rear of the food truck. More specifically, they show the first appearance of a white cloud consistent with the release of liquid propane near the left cylinder cabinet, the white cloud significantly increasing in size, the appearance of projectiles from the left side of the truck, ignition of the propane vapors, expansion of the fireball, and complete consumption of the propane vapors. In addition to the video and images, the following observations support the point of origin of the explosion originating at the left cylinder:

- Physical damage to and displacement of the left cabinet, rear door, and bumper cover.
- Damage to the wall behind the left cylinder cabinet.
- Appearance (i.e., ruptured/split open) and displacement of the left cylinder.
- Damage to and displacement of the propane regulator, hoses, tubing, and fittings.
- Damage to the generator cabinet walls.
- Relative lack of damage to the right cylinder cabinet and right cylinder.

The explosion with the left cylinder can be classified as mechanical, which is defined as, "A mechanical explosion is the rupture of a closed container, cylinder, tank, boiler, or similar storage vessel resulting in the release of pressurized gas or vapor. The pressure within the confining container, structure, or vessel is not due to a chemical reaction or change in chemical composition of the substances in the container[17]."

Once the mechanical explosion occurred, the contents of the left propane cylinder were released. The white cloud observed in the video and still images after rupture of the cylinder and prior to ignition is likely a combination of moisture (e.g., water vapor or humidity) in the air condensing as the liquid propane near the moisture vaporizes and an aerosol of liquid propane droplets. The propane vapors were the first fuel ignited after the left cylinder ruptured. As in most fuel-air combustion events, the oxidizer was the oxygen in the air (20.9% v/v) that mixed with the flammable propane vapors. The exact ignition source for the combustion event was not determined, but there were many competent ignition sources on the food truck including, but not limited to, open flames from standing pilots and burners, hot surfaces, and contacts/switches in electrical equipment.

Ultimately, the incident was caused by rupturing of the left cylinder. The cylinder ruptured because the internal pressure exceeded the strength of the cylindrical vessel. The cause of the excessive internal pressure merits further discussion.

As previously noted, cylinders are required to have a fixed maximum liquid level gauge (bleeder valve or spitter valve) if they are to be filled by volume, and they are required to have a relief valve. The bleeder valve is used to correctly fill a cylinder to 80% when filling by volume. It provides the filler with a visual cue (i.e., the release of white liquid) when the liquid level inside the cylinder reaches 80%. The 20% vapor space is necessary to allow for expansion of the liquid as the ambient temperature and ultimately liquid temperature increase. This prevents a cylinder from reaching a liquid-full condition from expected ambient temperature changes.

To demonstrate the magnitude of the temperature change required to cause a properly filled cylinder to become liquid-full, consider a cylinder properly filled with propane initially at 75°F would need to be heated to about 175°F (a differential of approximately 100°F) to make it liquid-full, which is not a realistic situation under normal ambient conditions. As the initial fill level of a cylinder increases, the temperature change needed to reach the liquid-full state decreases. For the same cylinder initially filled to 95% with 75°F propane, a temperature change of only about 27°F (final liquid temperature of about 102°F) is required to make it liquid full[8].

The left cylinder had a water capacity (W.C.) equal to 239 pounds, which means it had a total volume of 28.7 gallons and could be correctly filled with 100 pounds or 22.9 gallons (80% of 28.7 gallons) of propane at 60°F. The left cylinder did not have a fixed maximum liquid level gauge as part of its cylinder valve, nor was one provided separately as an add-on appurtenance. Under this condition, it would be difficult to properly fill it to only 80% without weighing the cylinder to determine the amount of propane to add — that is to say, determining the amount of propane to put in the left cylinder without weighing it would amount to guessing.

The vapor pressure inside a cylinder under typical ambient temperature conditions is not high enough to cause failure. As an example, the vapor pressure of commercial grade propane inside a cylinder with liquid at 105°F and 130°F is 218 PSIG and 300 PSIG, respectively[8]. Based on historical weather data, the ambient temperature at the time of the incident was about 90°F. If the liquid propane temperature was between 105°F and 130°F because of solar gain and/or external heating sources (e.g., food truck appliances and/or generator), the pressure inside the cylinder should only have reached between 218 PSIG and 300 PSIG.

The left cylinder had a service pressure of 240 PSIG, as indicated by the "240" in ICC-4BA240-717 stamping. The cylinder was likely manufactured with a safety factor of about four, which means it would not fail until about 960 PSIG or significantly above the expected vapor pressure inside the cylinder. On the other hand, as previously discussed, the pressures that can be generated by an incompressible fluid like propane in a liquid-full condition are significant[18].

Figure 23, which was created using NIST Reference Fluid Thermodynamic and Transport Properties Database (REFPROP), illustrates the pressure versus temperature relationship for pure propane under two different scenarios[9]. The solid red line in **Figure 23** depicts the scenario where a cylinder is filled to 80% at 75°F, allowing 20% vapor headspace. The liquid propane is allowed to expand into the headspace of the cylinder and maintain the saturated vapor pressure versus temperature relationship. On the other hand, the dashed blue line in **Figure 23** depicts the scenario where a cylinder is filled to 95% at 75°F, leaving only 5% vapor headspace. The propane is allowed to expand until the 5% vapor headspace becomes occupied by the liquid, which occurs at about 102°F (a temperature differential of 27°F). At that point, the pressure inside the cylinder rapidly increases with an increase in temperature due to the hydrostatic condition (Note: This assumes constant volume — i.e., no expansion of the cylinder).

In the unusual situations where the vapor pressure is abnormally high (e.g., in a fire condition) or the cylinder becomes liquid full (e.g., overfill), the relief valve is designed to release the excess pressure at a specified setting, typically 375 PSIG, or well below the failure point of the vessel. However, the left cylinder did not have a pressure relief valve, either as part of the cylinder valve or as a separate add-on appurtenance. The lack of bleeder and relief valves on the left cylinder contributed to the incident, as outlined in the following causation scenario:

1. The cylinder was filled without the use of a fixed maximum liquid level gauge or a scale.

2. The cylinder was overfilled.

3. The temperature of the liquid propane inside the cylinder increased due to an increase in the ambient temperature, solar radiation, and/or external heating sources, which caused the cylinder to become liquid-full.

4. The internal pressure increased to the point of vessel failure because the cylinder was not equipped with a pressure relief valve.

5. Once the cylinder began to fail, the sudden reduction to ambient pressure resulted in rapid flashing of the liquid propane to vapor, splitting open of the cylinder, and projecting the cylinder across

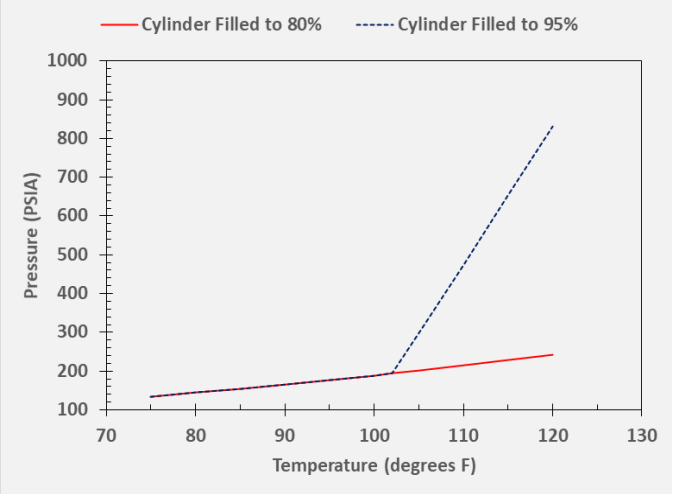

Figure 23
Pressure versus temperature relationship for pure propane under two different scenarios.

and down the street.

Item 5 in the causation scenario is often associated with the term BLEVE, which is an acronym for boiling-liquid-expanding-vapor explosion and is a subset of mechanical explosions. There are many definitions for BLEVE such as, "A BLEVE is an explosion resulting from the failure of a vessel containing a liquid at a temperature significantly above its boiling point at normal atmospheric pressure[19]." In this case, the normal boiling point for propane is -44°F.

Most theories related to BLEVEs consider the superheat limit temperature when defining a BLEVE[19]. For propane, the superheat limit is generally regarded to be 127°F (53°C). If the liquid propane in a cylinder is at or above the superheat limit temperature and the pressure is suddenly reduced to atmospheric, the bulk of the liquid will rapidly and violently flash to vapor, creating a blast wave[19]. The temperature of the liquid propane in the left cylinder may not have achieved or exceeded the superheat limit temperature, and the mechanical explosion may not have technically been a BLEVE. However, the end result was more or less the same. As stated in Guidelines for Evaluating the Characteristics of Vapor Cloud Explosions, Flash Fires, and BLEVEs by the CCPS[19]:

A theory that adequately explains all BLEVE phenomena has not yet been developed. Reid's (1979, 1980) theory seems to be a good approach to explain the strong blast waves that may be generated. But even when a liquid's temperature is below the superheat limit, the liquid may "flash" within seconds after depressurization, resulting in a blast wave, a fireball, and fragmentation.

Neither the right or left 100-pound propane cylinders should have been filled by the dispenser for the following reasons:

1. The left and right cylinders were 66 years and 19 years past their requalification dates, respectively.

2. The left cylinder did not have a spitter valve, eliminating the ability to accurately fill the cylinder by volume.

3. The left cylinder did not have a relief valve to protect it from the possibility of overpressurization.

4. The right cylinder did not have a spitter valve, eliminating the ability to accurately fill the cylinder by volume.

Even though the cylinders should not have been filled for the above listed reasons, the cylinders could have been properly filled using the weight method using a scale. The dispenser, however, did not fill these cylinders using the weight method. Ultimately, it was determined that the left cylinder was overfilled, and the overfill was the proximate cause of the explosion.

Conclusions

Correctly and scientifically investigating an incident is essential in determining root cause and ultimately preventing recurrence. Following the systematic approach outlined in this paper (and illustrated in the case study) will give the investigator the best chance of success for determining the cause of an accident, which will advance industry safety.

As the food truck industry continues to grow, the expectation is accidents associated with food trucks utilizing propane systems will continue to occur on a similar or more frequent basis. Educating the food truck designers, builders, and owners on propane use and handling, developing food truck-specific codes and standards, and consistently implementing and enforcing those codes and standards will help decrease the frequency of accidents.

References

1. R. Myrick, "mobile-cusine.com," [Online]. Available: https://mobile-cuisine.com/business/history-of-american-food-trucks/. [Accessed 18 September 2019].

2. "Food Trucks in the US-Market Research Report," 23 September 2020. [Online]. Available: http//:ibisworld.com. [Accessed 27 May 2021].

3. Shutterstock, [Online] Available https://www.shutterstock.com/image-photo/minneapolis-august-5-large-crowd-attends-109409474. [Purchased 21 December 2022].

4. United Food Truck, "Deluxe Kitchen Combination 18' Food Truck Simple Layout," [Online]. Available united-food-truck.com/deluxe-kitchen-combination/. [Accessed 09 September 2021].

5. "Rules for the Construction of Unfired Pressure Vessels," Section VIII, ASME, Boiler and

Pressure Vessel Code, 2021.

6. Title 49, Code of Federal Regulations, 178 Subpart C, "Specifications of Cylinders."

7. Interstate Commerce Commission (ICC) Rules for Construction of Unfired Pressure Vessels, U.S. Department of Transportation, Washington, DC.

8. National Fire Protection Association, NFPA 58, Liquefied Petroleum Gas Code, 2020 Edition, Baltimore: National Fire Protection Association, 2019.

9. NIST Reference Fluid Thermodynamic and Transport Properties Database (REFPROP), Version 10. Available: https://www.nist.gov.

10. National Fire Protection Association, NFPA 1, Fire Code, "Food Truck Fact Sheet," November 2020. [Online]. Available: http//nfpa.org. [Accessed 27 May 2021].

11. NFPA 70, National Electrical Code, 2020 Edition, "Food Truck Fact Sheet," November 2020. [Online]. Available: http//:nfpa.org. [Accessed 27 May 2021].

12. NFPA 96, Standard for Ventilation Control and Fire Protection of Commercial Cooking Operations, 2017 Edition, "Food Truck Fact Sheet,"November 2020. [Online]. Available: http//nfpa.org. [Accessed 27 May 2021].

13. NFPA 1192, Standard on Recreational Vehicles, 2021 Edition, Quincy: National Fire Protection Association, 2020.

14. National Fire Protection Association, in NFPA 96, Standard for Ventiliation Control and Fire Protection of Commercial Cooking Operations Handbook, Baltimore, 2017, pp. 130-133, Annex B.

15. National Fire Protection Association, "Food Truck Fact Sheet," November 2020. [Online]. Available: http//:nfpa.org. [Accessed 27 May 2021].

16. National Fire Protection Association, NFPA 1, 2018 Fire Code, Section 50.7, Published November, 2017. [Online]. Available: http//:nfpa.org. [Accessed 27 May 2021].

17. National Fire Protection Association, NFPA 921, Guide for Fire and Explosion Investigations, Quincy: National Fire Protection Association, 2020.

18. N. de Nevers, Propane Overfilling Fires, Salt Lake City: University of Utah, 1990.

19. Center for Chemical Process Safety of the American Institute of Chemical Engineers, Guidelines for Evaluating the Characteristics of Vapor Cloud Explosions, Flash Fires, and BLEVEs, New York: American Institute of Chemical Engineers, 2010.

Failure Analysis of Cylinder Used In a Car Flipper Device

By Faisal Khan, PEng (NAFE 1026M) and Altaf Gafoor, PEng (NAFE 1185A)

Abstract

A car flipping device is a special effects aid used to flip cars in the production of movies and television shows. The device uses a pivoting arm that moves under the stroke of a cylinder powered by compressed nitrogen. In a trial run of the device, the cylinder's piston broke through the cylinder cap. A kinematic analysis developed a parametric mathematical model of the motion of the cylinder arm and piston, which formed the basis for a finite difference analysis to determine the speed of the cylinder's piston at the end of its stroke. Metallurgical testing was conducted on the broken cylinder to determine the stress-strain characteristics, impact resistance, and Scanning Electron Microscopy (SEM) used to examine the fracture surface. The analysis determined that the kinetic energy of the piston was adequate to cause yielding of the cylinder but not rupture. Continued usage degraded the impact resistance available until rupture occurred.

Keywords

Cylinder cap, kinematics, finite difference, fracture, impact energy, metallurgical analysis, numerical methods, pneumatic piston travel speed, forensic engineering

Introduction and Background

The production of movies and television shows often use practical special effects to enhance story telling. One such effect involves the flipping of cars using proprietary devices typically fabricated by visual effects studios. The subject of this paper is the methodology used to analyze the failure of such a device.

Figure 1 shows the general construction of the car flipper. As illustrated, the device has a steel arm that is free to rotate in the vertical plane about a hinge fixed to its base. The rotation of the car flipper's arm is controlled by a cylinder and piston that is energized using compressed nitrogen fed from an actuator. As the actuator pressure is released into the cylinder, the piston and rod extend, which causes the car flipper arm to rotate while ejecting load on the arm.

The car flipper was being tested to confirm the desired car flipping effect could be achieved. The test methodology placed the device under loading from a prop car and was fed by a compressed gas actuator. Three tests in total were conducted: the first at 1,500 psi (10.3 MPa) actuator pressure and the second and third at 3,000 psi (20.6 MPa). During the third test, the piston and rod broke through the end cap of the cylinder, maintaining sufficient velocity to remain a projectile for approximately 118.5 feet (36.1 m).

Figure 2 is a photograph of the car flipper after failure showing the location of the ruptured end cap, and **Figure 3** provides a closer view of the rupture. **Figure 4** and

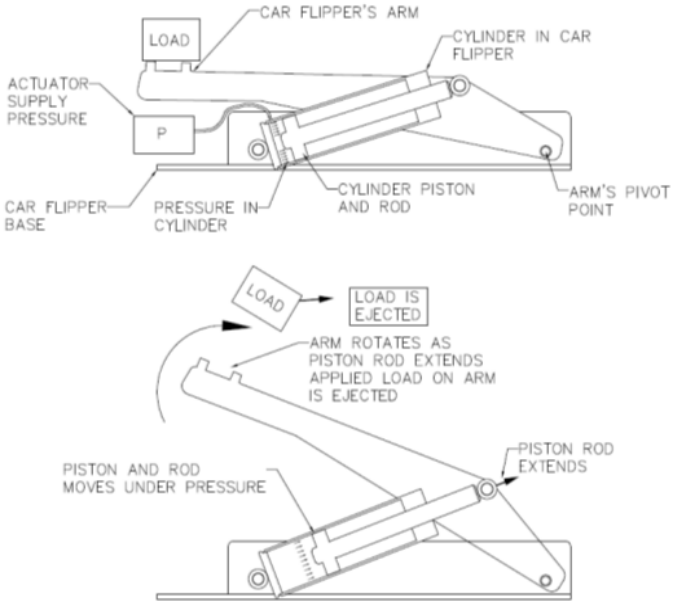

Figure 1
General construction and operation of car flipper.

Faisal Khan, PEng, 505 University Ave., 19th Fl., Toronto, ON M7A 1T7, (416) 518-7597, Faisal.Khan2@ontario.ca

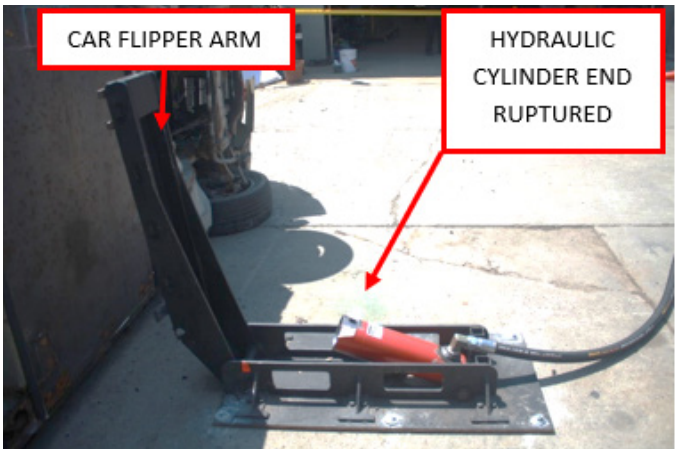

Figure 2
Close of car flipper after failure.

Figure 3
Cylinder end where cap was severed.

Figure 5 show the piston head and piston rod after the failure. As shown, the piston head did not show any significant deformation, and the piston rod was generally straight.

The design of the cylinder did not have a damping mechanism to attenuate the impact of the piston head and piston rod. The kinetic energy of the piston head and piston rod was absorbed by impact with the cylinder end cap. The hypothesis tested in this investigation was whether the piston and rod were moving with sufficient velocity such that their kinetic energy was adequate to result in a rupture of the cylinder as shown in **Figure 6**. The piston rod also

Figure 4
Inside of piston head after incident.

Figure 5
Piston rod after incident.

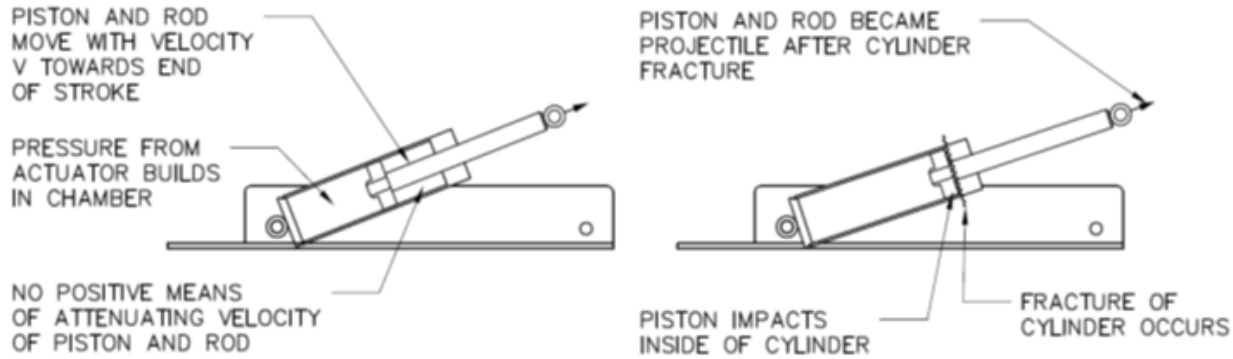

Figure 6
Impact of piston and rod on cylinder end cap. (Note: There was no positive connection — just a C-type clamp around the pin. The pin broke through the frame at its point of supports.)

broke the connection where it was secured to the car flipper's arm.

To evaluate the veracity of the hypotheses, the investigation was broken down into five components as follows:

- Component 1 utilized kinematic principles to formulate a mathematical model of the car flipper's movement.
- Component 2 derived the forces acting on the piston.
- Component 3 applied the finite difference method to estimate the velocity of the piston as it progressed through its stroke.
- Component 4 was metallurgical testing, which provided material properties and identified features of interest on the fracture surface using SEM in addition to estimating the energy required for yielding and rupture of the cylinder.
- Component 5 reviewed the manufacturer's specifications for the cylinder to ascertain the general applicability of the cylinder in the car flipper application.

Mathematical Model of Car Flipper's Movement

The first component of the investigation analyzed the spatial relationship between the movement of the car flipper's arm, the piston, and the car to be flipped with respect to fixed reference points on the car flipper. **Figure 7** shows the general arrangement and variables used to establish these relationships.

The car flipper in its application fits the definition of a mechanism[1] with points and A and C identified as the fixed reference points. The distances AC, CB, and BD (a_3) are constant, whereas the distance AB varies as the piston undergoes a displacement x_i. Points E and O are reference points that are necessary to account for the rotation of the car in response to the action of the car flipper's arm. The distances CO (a_4) and OE (a_1) are also constants. The net torque resulting from the application of the car flipper's arm pushing on the chassis of the car and resisted by the weight of the car induces an angular acceleration that contributes to the flipping of the car.

The effect of angular acceleration and angular momentum is beyond the scope of this analysis. Due to the rotational inertia gained from the car flipper, the resistance induced on the car flipper arm would decrease. Hence, the analysis conducted would produce a lower bounds estimate of the speed of the piston due to the increase in resistance to piston motion.

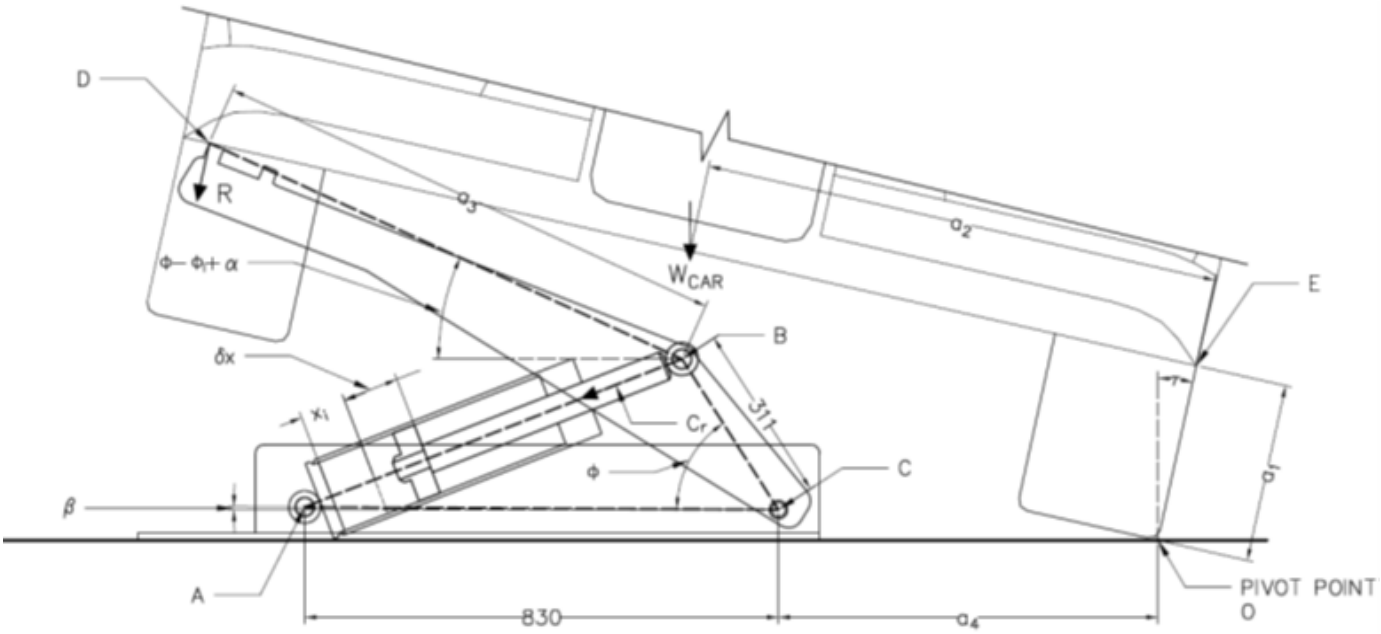

Figure 7
Geometry of car flipper adopted for mathematical model (all unis in millimeters).

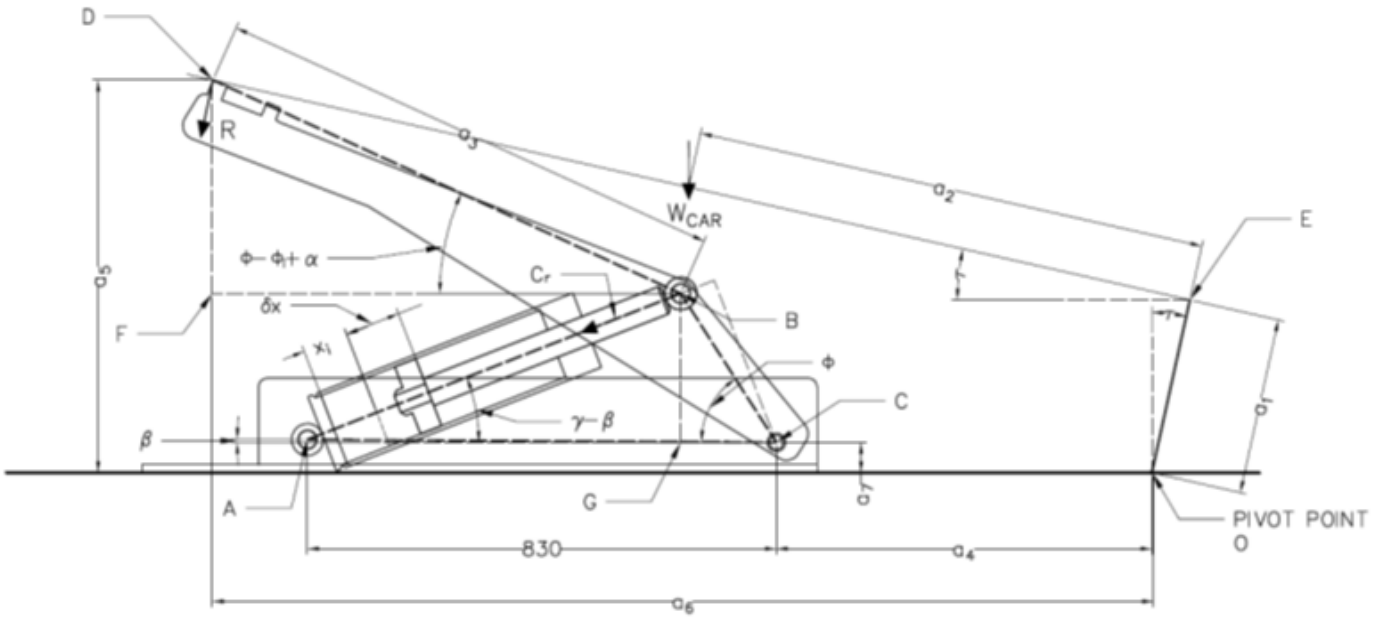

Figure 8
Identification of variables used to describe motion of car flipper's arm.

$$\tau = arcos\left(\frac{a_1}{S}\right) - U \qquad \text{EQ. 1}$$

Where,

$$S = \sqrt{a_5^2 + a_6^2}$$

$$U = \arctan\frac{a_6}{a_5}$$

$$a_5 = a_3 \sin(\emptyset - \emptyset_i + \alpha) + BC\sin(\emptyset + \beta) + a_7$$

$$a_6 = a_3 \cos(\emptyset - \emptyset_i + \alpha) + BC\cos(\emptyset + \beta) + a_4$$

$$\gamma = arcsin\left[\frac{BC}{AB_{initial} + \delta x}\sin\emptyset\right] \qquad \text{EQ. 2}$$

Where,

$AB_{initial}$ – initial length of arm AB

BC – length between points B and C, remains constant throughout event

φ – general inclination of arm CB with respect to horizontal

γ – angle BAC

EQ. 3

$$\phi = arcos\left(\frac{AC^2 + CB^2 - (AB_{initial} + \delta x)^2}{2(AC)(CB)}\right)$$

Figure 8 shows the variables used to describe the motion of the car flipper's arm as the piston extends. From this figure, the following key relationships are derived:

$$R = \frac{(a_2\cos\tau - a_1\sin\tau)}{(a_5\sin\tau + a_6\cos\tau)}W \qquad \text{EQ. 4}$$

Figure 8 also shows the reaction (R) due to the weight of the car (W), acting on the car flipper's arm. This relationship was determined to be:

EQ. 5

$$C_r = \frac{R_V[a_3\cos(\phi - \phi_i + \alpha) + BC\cos(\phi + \beta)] + R_H[a_3\sin(\phi - \phi_i + \alpha) + BC\sin(\phi + \beta)]}{830\sin(\gamma - \beta)}$$

The reaction (R) provides resistance to the motion of the piston C_r. This relationship was determined to be:

Where,

$$R_H = R\sin\tau$$

$$R_V = R\cos\tau$$

Determination of Forces on Piston

Figure 9 shows the position of the piston as it transitions from a general position x to x+δx. In **Figure 9(a)**, the piston is at a linear displacement x from its initial position. At this position, the piston is acted upon by the following pressures and forces, resulting in a velocity v_x and acceleration a_x:

- Pressure in supply line $P_{ch,x}$

- Pressure of air in cylinder $P_{cp,x}$
- Resistance on piston rod caused by car's weight $C_{r,x}$
- Air resistance to the motion of the cylinder $P_{a,x}$. (Note: This is due to the air resistance from the motion of the piston. The term $P_{cp,x}$ is due to the pressure of the air being compressed in the cylinder by its motion. The analysis is isothermal.)
- Weight component of piston's weight mg sin $(\gamma-\beta)_x$

The resulting acceleration at the general position, x, in **Figure 9(a)** is given by:

EQ. 6

$$a_x = \frac{(P_{ch,x} - P_{cp,x} - P_{a,x})A - C_{r,x} - mg\sin(\gamma-\beta)_x}{m}$$

Similarly, the resulting acceleration at the position x+δx, in **Figure 9(b)** is given by:

EQ. 7

$$a_{x+\delta x} = \frac{(P_{ch,x+\delta x} - P_{cp,x+\delta x} - P_{a,x+\delta x})A - C_{r,x+\delta x} - mg\sin(\gamma-\beta)_{x+\delta x}}{m}$$

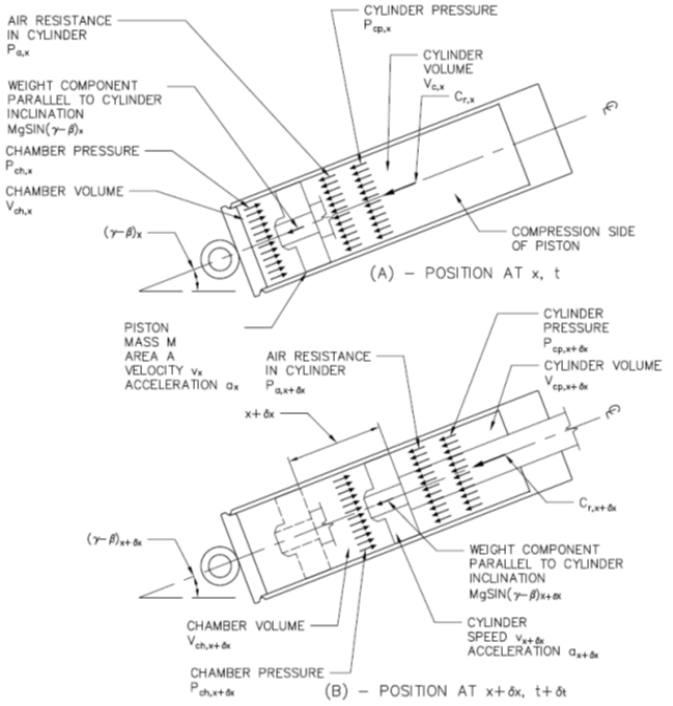

Figure 9
Forces on piston as it moves from x to x +δx.

Equations 6 and 7 provide estimates of the acceleration across a small distance δx that occurs over a small time step δt. If the time step δt is sufficiently small, then the distance step δx will also be small and:

$$\lim_{\partial x \to 0} a_{x+\partial x} \to a_x$$

Therefore, discretizing the movement of the piston in this manner allows for the application of linear equations of motion across each time and distance step. The change in velocity across each time step can be approximated using equations of motion under constant acceleration for the given step, giving: EQ. 8

$$\partial v_x = \left[\frac{(P_{ch,x} - P_{cp,x} - P_{a,x})A - C_{r,x} - mg\sin(\gamma-\beta)_x}{m}\right]\partial t$$

The conditions at t=0 and x=0 are known. Thus, Equation 8 can be applied at the initial conditions to determine the change in velocity over the time step δt. At the end of this time step, the velocity is known, and the distance moved by the piston δx can also be calculated. In this manner, the problem is spatially and temporally discretized, allowing for the continuous application of Equation 8 to evaluate the velocity and distance at further time steps.

The pressure from the actuator is released into the expansion side of the cylinder (supply chamber), which is at atmospheric pressure. The difference in pressure between the nitrogen supply and the supply chamber pressure results in a flow of mass from the actuator to the supply chamber. **Figure 10** shows the general arrangement of the actuator pressure feeding into the supply chamber. The complete isothermal equation for steady flow[2] was adopted for each time step to approximate the mass flow of gas between the supply pressure and the chamber pressure. This equation is given as:

EQ. 9

$$w^2 = \left[\frac{\rho_s A^2}{\left(\frac{fl}{D} + 2ln\left(\frac{P_s}{P_{ch}}\right)\right)}\right]\left[\frac{P_s^2 - P_{ch}^2}{P_s}\right]$$

Where,

w - mass flow rate in kilograms per second per (kg/s)

ρ_s - density of nitrogen at supply in kilograms per cubic meter (kg/m^3)

P_s - absolute supply pressure in pascals (N/m^2)

P_{ch} - absolute chamber pressure in pascals (N/m^2)

L - length of supply line in meters (m)

A - area of supply line in square meters (m^2)

D - diameter of supply line in meters (m)

f - friction factor, dimensionless

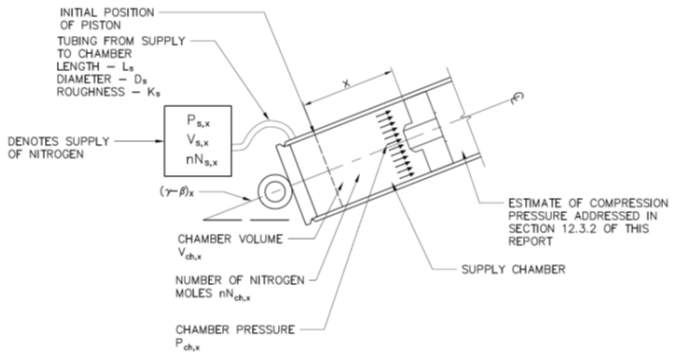

Figure 10
Supply pressure and chamber pressure.

The friction factor was calculated using the Colebroke-White equation[3] and requires the calculation of the Reynold's Number. Equation 11 requires estimates of the friction factor, which is also a function of the flow-rate. Therefore the calculation of the mass flow rate cannot be done independently of the friction factor or Reynold's Number. This problem was solved using an iteration in which a trial friction factor was assumed and the mass flow rate calculated. Based on this trial flow rate, the flow velocity and Reynold's Number was re-calculated, and using the Newton-Raphson method[4], the friction factor was calculated using the Colebrole-White equation. The mass flow rate was recalculated. If the difference between this calculated value and the initial value was outside the range +/- 0.00001, the entire iteration was repeated. This methodology was programmed using Visual Basic in Microsoft Excel.

The behavior of nitrogen approximates to an ideal gas[5] in the range of pressures and temperature (up to 3,000 psi and 305 kelvin) under consideration in this analysis. Applying the ideal gas equation, the number of moles of nitrogen entering the supply chamber was calculated as shown in Equation 10.

EQ. 10

$$\delta nN = \frac{w\delta t}{mMn}$$

Where,

δnN - change in the number of moles of nitrogen

w - mass flow rate (kg/s)

mMn - molecular mass of nitrogen (kg/moles)

The volume of the supply chamber increases as the piston moves, and the change in volume (δV) can be calculated based on the distance moved by the piston for a given time step. The volume of the nitrogen in the supply actuator does not change. Therefore, there will be a reduction of pressure in the supply actuator because there is a loss of nitrogen mass. Equations 11 and 12 estimate the pressure in supply chamber and nitrogen supply actuator at the end of each time step.

EQ. 11

$$P_{ch,x+\delta x} = \frac{(nN_{ch,x} + \delta nN)RT}{V_{ch,x} + \delta V}$$

EQ. 12

$$P_{s,x+\delta x} = \frac{(nN_{s,x} - \delta nN)RT}{V_s}$$

Where,

$P_{s,x+\delta x}$ - Pressure in nitrogen supply and end of time step (Pa)

$nN_{s,x}$ - Number of moles of nitrogen in supply at beginning of time step

δnN - Change in the number of moles of nitrogen

V_s - Volume of nitrogen supply

R - Universal gas constant, taken as 8.314 J/kg/K

T - Temperature, taken as 305 Kelvin

The density of nitrogen in the supply actuator and supply chamber of the cylinder also changes. These values were calculated using Equations 13 and 14 based on the change in nitrogen concentration in the supply chamber and supply actuator as well as the change in volume in the supply chamber.

In the nitrogen supply,

EQ. 13

$$\rho_{s,x+\delta x} = \frac{mM_n P_{s,x+\delta x}}{RT}$$

And in the chamber as,

EQ. 14

$$\rho_{ch,x+\delta x} = \frac{mM_n P_{ch,x+\delta x}}{RT}$$

The behavior of air on the compression side of the cylinder was also analyzed to determine the resistance to

cylinder motion developed by the compressed air. **Figure 11** illustrates the behavior of the cylinder on its compression side and the supply side

As the piston moves, the volume available within the cylinder decreases. This decrease is equal to $A_{cyl}\delta x$ and causes the pressure within the cylinder to increase. Initially, the air in the cylinder is at atmospheric pressure. However, due to the movement of the piston, the pressure increases along with the density of air. (Note: The duration of the event is so short that temperature change would have minimal effect.)

Considering a general position where the pressure is $P_{c,x}$ and density is $\rho_{c,x}$, the presence of the opening on the compression side of the cylinder will be assumed to function as an orifice with area A_{esc} and coefficient of discharge C_d. The nature of the gas flow was checked as either sub-critical, critical, or super-critical — and appropriate estimates of the escaping air velocity calculated using ISO Standard 4126-1, 2004. Using this methodology allows for an estimate of the mass flow rate of the air exiting the compression side of the cylinder. The pressure and density of the air on the compression side of the cylinder is estimated at the end of each time step as follows:

EQ. 15

$$P_{c,x+\delta x} = \frac{(n_{a,x} - \delta n_a)RT}{V_{c,x} - A_{cyl}\partial x}$$

EQ. 16

$$\rho_{c,x+\delta x} = \frac{mM_a P_{c,x+\delta x}}{RT}$$

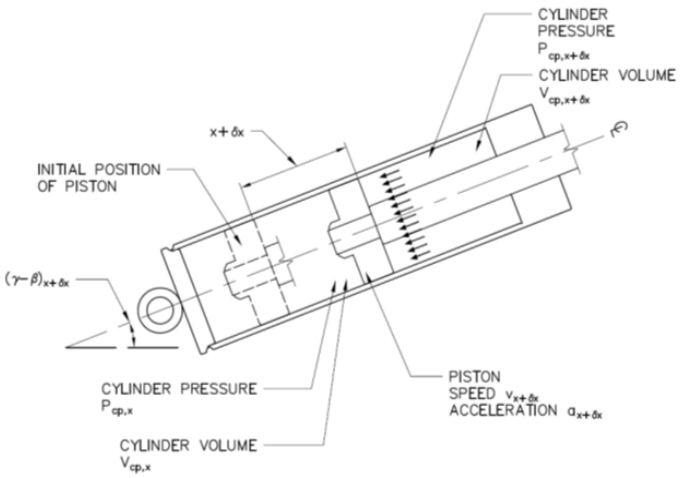

Figure 11
Pressure and volume on compression side of cylinder.

Where,

$P_{c,x+\delta x}$	-	pressure on compression side of cylinder at end of time step
$\rho_{c,x+\delta x}$	-	air density on compression side of cylinder at end of time step
$n_{a,x}$	-	number of moles of air in compression side of cylinder at start ot time step
δna	-	change in moles of air on compression side of cylinder over time step
mMa	-	Molecular mass of air, taken as 0.02891 kg/mol
A_{cyl}	-	area of cylinder

The resistance to the motion of the piston by the presence of air on the compression side of the cylinder can be estimated using the following expression:

$$F_{air,cyl} = C_{d,air}\frac{1}{2}A_{cyl}\rho_{c,x}v^2$$

The drag coefficient is assumed to be unity to maximize the effect of air resistance, reducing the above expression to:

EQ. 17

$$F_{air,cyl} = \frac{1}{2}A_{cyl}\rho_{c,x}v_x^2$$

Note: This variable was not measured in the cylinder and is considered to be small in comparison with the applied pressures.

Using the mathematical model of the geometry outlined in Equations 1 through 3, the reaction of the car's weight on the car flipper's arm and the resistance to the motion of the piston due to the car's weight, C_r can be calculated using Equations 4 and 5 for each position of the piston considered. Finally, the weight component of the piston acting to resist motion was considered as shown in Equation 18.

EQ. 18

$$W_p = m_p g \sin(\gamma - \beta)$$

Applying the Finite Difference Method

It is clear that the motion of the piston is continuous and that the velocity and acceleration can be determined by differentiation of the displacement time relationship. However, as the expressions derived to describe the geometry and forces on the piston do not allow for an analytical solution, the finite difference method replaces derivatives with discrete approximations[6]. In this regard, over a discrete time step, the change in velocity and displacement of the piston can be calculated.

The initial geometry of the car flipper and supply

actuator was known in addition to the dimensions of the cylinder. Starting at the initial conditions, the forces acting on the cylinder were calculated. Hence, the net force could be determined. The acceleration across the time step was calculated and the velocity and displacement estimated based on the calculated time step acceleration. The analysis relied on a forward pass method as only the initial conditions were known, and the accuracy of the results were limited to a first order analysis. In such an analysis, the error in the calculation was proportional to the time step chosen. For this reason, it was important to choose a very small time step that also satisfied convergence of results.

To determine the time step necessary to achieve this, several trials were run using varying time steps. To accommodate the numerous calculations required for the solution of the velocity-time relationship and to confirm convergence of the chosen time step, the analysis was coded using Visual Basic in the Microsoft Excel Environment. The velocity time relationship for various time steps using an actuator pressure of 3,000 psi is shown in **Figure 12**. As shown in this graphic, there is convergence of the results as the time step decreases — and at a time step of 0.0001 seconds, convergence is maximized.

The analysis was conducted for actuator pressures of 1,500 psi and 3,000 psi, the results of which are presented in **Figures 13** and **Figure 14**. As shown in these graphics, the velocity of the piston at the end of its stroke was approximately 14m/s under an actuator pressure of 1,500 psi and approximately 23m/s under an actuator pressure of 3,000 psi. Deceleration is due to the decrease in pressure on the supply side of the cylinder as the volume expands due to piston movement. Graphs of pressure on the supply side and compression side were added for the various actuator pressures.

Figures 15 and **16** show the pressure on the compression side of the cylinder for 1,500 psi and 3,000 psi actuator pressure.

Metallurgical Testing

The properties of the material from which the failed cylinder was fabricated was determined by destructive testing of the cylinder's material. Two samples were tested from which the yield strength and ultimate tensile strength were determined and compared with the grade of steel specified by the manufacturer (Grade 1020 CW, ASTM A519 Steel). The material was found to be consistent with

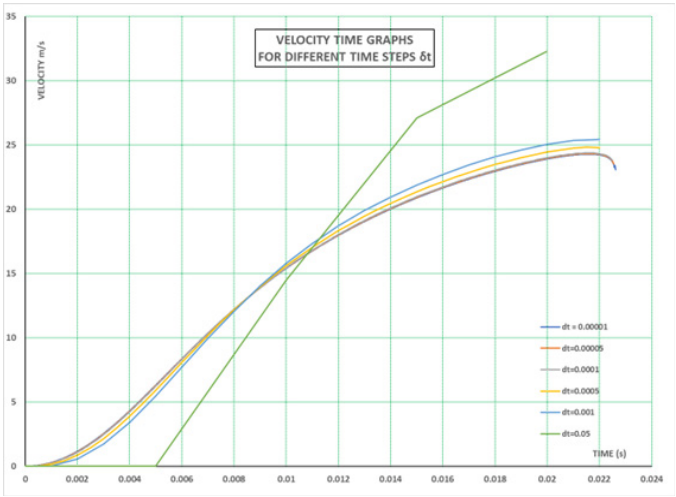

Figure 12
Velocity time relationship using various time steps and 3,000 psi actuator pressure.

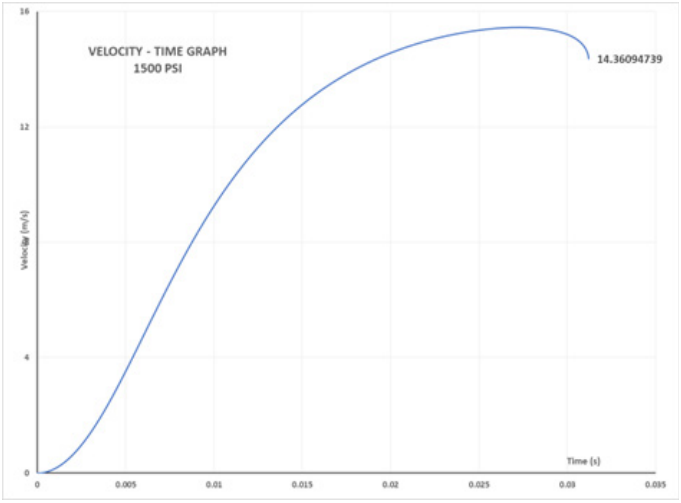

Figure 13
Velocity — time graph for 1,500 psi actuator pressure.

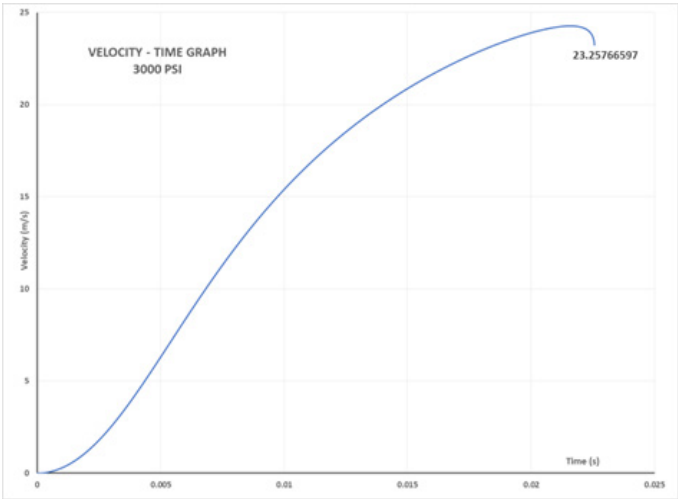

Figure 14
Velocity — time graph for 3,000 psi actuator pressure.

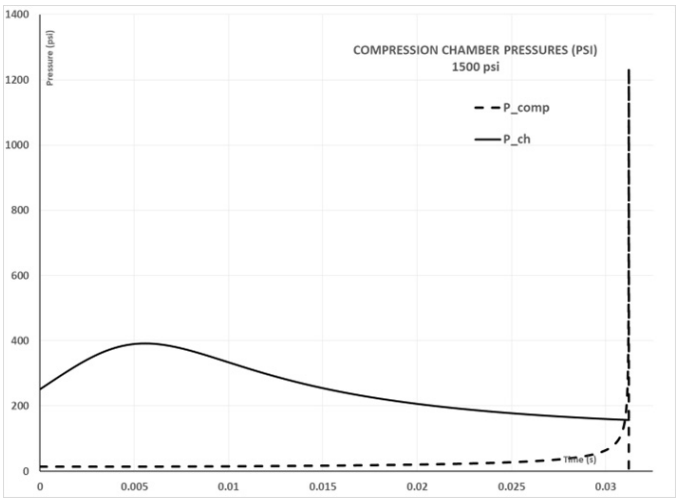

Figure 15
Compression and supply pressure in cylinder at 1,500 psi actuator pressure.

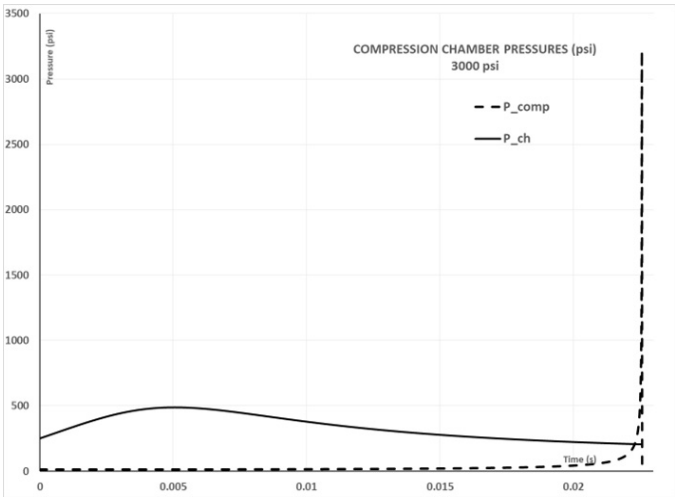

Figure 16
Compression and supply pressure in cylinder at 3,000 psi actuator pressure.

the grade of steel specified by the manufacturer.

Figure 17 shows a cross-section of the cylinder. The plane of fracture was located at the cylinder's end cap. The cylinder end cap was threaded onto the cylinder body, resulting in a smaller thickness than the cylinder wall. The equivalent spring method[7] was used to estimate the energy required for yielding and rupture of Member 2, taking into account the deformation in Member 1. Examinations of the piston did not reveal any significant deformation.

The stress-strain graphs of the cylinder material was obtained from testing and used in conjunction with the equivalent spring method to calculate the amount of energy required to cause rupture. The stress-strain curves are shown in **Figure 18**.

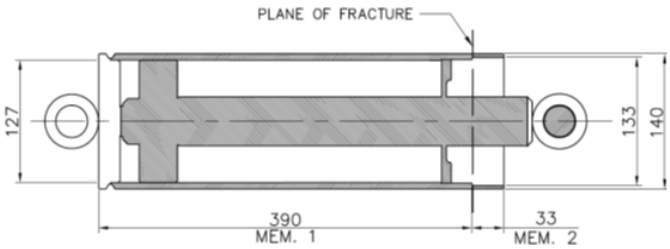

Figure 17
Cross-section of cylinder showing member identification.

The expression developed for this calculation is shown below:

$$E = Al\int_0^{\varepsilon} \sigma\,\delta\varepsilon \qquad \text{EQ. 19}$$

Where,

E	-	Rupture energy
A	-	Cross-sectional area of member
l	-	length of member
$\int_0^{\varepsilon} \sigma\,\delta\varepsilon$	-	area under stress-strain graph

The cylinder was analyzed as two discrete sections: the thicker body (wall thickness of 6.5 mm) and the thinner end cap (wall thickness 3.5 mm) connected in series. Two samples were tested to obtain the stress-strain graph. It was found that the energy required for rupture of the

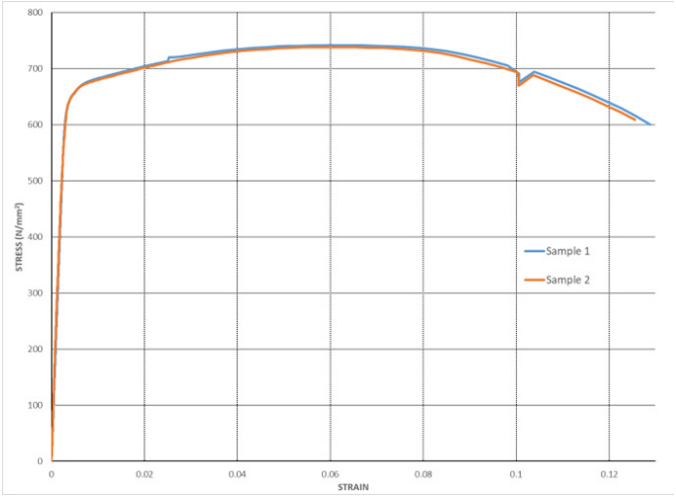

Figure 18
Stress-strain graphs from testing.

thinner end cap was between 4500 Nm to 7000 Nm. For this reason, the impact force was considered to be the same in each member, but the stresses differed due to wall thickness, as did the strain.

The limiting force is the rupture force in the thinner member, which was calculated using the ultimate stress from testing and found to be approximately 1100kN. The stress in the thicker member at this force was found to be below the material's yield stress, and the stress-strain relationship was linear. The energy absorbed by the thicker member, determined using Equation 19, was found to be approximately 360Nm. Thus, the total energy required to be imparted into the cylinder from impact ranged between 4860Nm and 7360Nm and was the minimum kinetic energy required by the piston for rupture. The piston velocity for this to occur was estimated to be 37.1m/s. This analysis was also done for yielding, and the speed required was found to be 8m/s.

Referring to **Figure 13** and **Figure 14**, the velocity at the end of the piston's stroke was approximately 14m/s under an actuator pressure of 1,500 psi and approximately 23m/s under an actuator pressure of 3,000 psi. These velocities were less than the 37 m/s required to result in rupture but greater than the 8m/s required to result in yielding. Therefore, yielding likely occurred in Member 2 on the first trial run at 1,500 psi. The further application of an actuator pressure of 3,000 psi likely resulted in further permanent deformation of the cylinder. The final application of 3,000 psi actuator pressure would have been adequate to result in rupture of the cylinder adjacent to the threaded section holding the cap in place, due to the continued plastic deformation on previous trials.

The results of the SEM examination and impact testing (laboratory tests on samples using Charpy V-notch tests per ASTM E23-18 in the longitudinal direction of the cylinder cap) supported the preceding discussion. As shown in **Figure 19**, significant portions of the fracture surface showed cleavage facets that indicated a brittle process[8]. This loss of ductility was likely due to high strain rates associated with impact load.

The examination was done on the fracture surface of the end cap. The orientation of the end cap was on the annulus of the wall thickness. Impact tests conducted at samples near the fracture surface in the longitudinal direction returned results (ranging between 3 to 5 Joules) that were approximately 80% of expected values for carbon steel at 20°C[9]. Failure occurred when stresses were repeatedly between yield and ultimate. Impact testing showed 20% of expected value. Referencing **Figure 19**, impact loading was investigated by considering the minimum velocity required to develop the kinetic energy required for yielding and rupture. Brittle failure occurred because the initial operation of the car flipper was such that the kinetic energy was more than enough to cause yielding, but not rupture. Each time the device was run, the end cap plastically deformed until its ability to absorb further impact was so diminished that rupture occurred below ultimate stress values.

There was also some evidence of accompanying ductile fracture near the inner and outer diameters of the end cap, as shown in **Figure 20**. There was no evidence of striations, beach marks, or corrosion damage observed in the SEM examination.

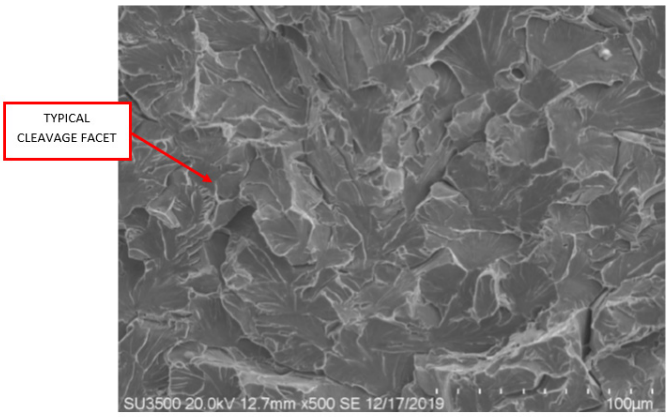

Figure 19
Cleavage facets on majority of fracture surface.

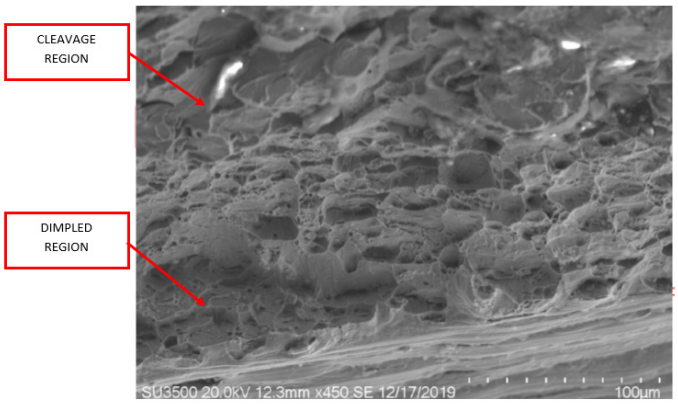

Figure 20
Dimpling near inner diameter.

Review of Manufacturer's Specifications

The manufacturer of the cylinder was contacted regarding the general suitability of the cylinder to the function in the car flipper application. The manufacturer confirmed that the cylinder was intended to be used in a double acting application using hydraulic oil over a working range of 0 to 3,000 psi. The manufacturer further confirmed that the allowable piston speed is 0.168 m/s, and — if used in a pneumatic application — the working pressures reduce to 87 to 116 psi. Therefore, the use of the cylinder in a single-acting application using compressed nitrogen at 3,000 psi was outside the manufacturer's specifications. Furthermore, the velocity of the piston exceeded manufacturer's specifications.

Conclusions

- The cylinder was not used in a double-acting application and utilized compressed nitrogen at pressures far greater than the manufacturer's specifications.
- The finite difference analysis demonstrated that the likely piston speed exceeded the manufacturer's specifications.
- The velocity of the piston ranged between 14 m/s at a supply pressure 1,500 psi (10.3 MPa) and 23 m/s at a supply pressure of 3,000 psi (20.6 MPa).
- The movement of the piston and rod was arrested at the end of the piston's stroke by impact with the cylinder. The piston was stopped by impact with the end cap.
- In the area of impact between the piston and the cylinder, the cylinder's wall thickness was reduced to accommodate threads for the securement of the cylinder's end cap. The fracture surface occurred in this area of reduced wall thickness in the cylinder.
- The range of speeds of the piston exceeded the ability of the cylinder to absorb the impact energy without yielding.
- The continued use of the car flipper at an actuator pressure of 1,500 psi (10.3 MPa) followed by an additional attempt at an actuator pressure of 3,000 psi (20.6 MPa) successively reduced the ability of the cylinder to absorb the energy of the impacts.
- On the final operation of the car flipper, at an actuator pressure of 3,000 psi (10.3 MPa), the cylinder could no longer absorb the kinetic energy of the piston/rod, and rupture of the cylinder occurred.

References

1. J. McCarthy, An Introduction to Theoretical Kinematics, Cambridge: MIT Press, 1990, p. Chapter 1.
2. Crane, Flow of Fluids Technical Paper 410M, New York: Crane Company, 1982, p. Chapter 1.
3. M. R. Lindeburg, PE Civil Reference Manual, Sixteenth Edition, Belmont: Professional Publications Inc., 2018, p. Chapter 17.
4. S. C. R. Chapra, Numerical Methods for Engineers, Sixth Edition, New York: McGraw-Hill Companies Inc., 2010, p. Chapter 6.
5. R. Mortimer, Physical Chemistry Third Edition, London: Elsevier Academic Press, 2008, p. Chapter 1.
6. R. LeVeque, Finite Difference Methods for Ordinary and Partial Differential Equations, Seattle: Society of Industrial and Applied Mathematics, 2007, p. Chapter 1.
7. R. Hibbler, Mechanics of Materials, 6th Edition, New Jersey: Prentice Hall, 2004, p. Chapter 14.
8. A. Liu, Mechanics and Mechanisms of Failure: An Introduction, Ohio: ASM International, 2005, p. Chapter 2.
9. ASM International, Steel Castings Handbook, 6th Edition, ASM International, 1995, p. Chapter 23.
10. ISO, Safety devices for protection against excessive pressure Part 1 - Safety Valves, ISO, 2004, p. Chapter 8.

Forensic Engineering Investigation of Factors Contributing to the Explosion of an International Natural Gas Pipeline

By Jahan Rasty, PhD, PE (NAFE 768S), Olin Parker, and Mathew Mills, PE (NAFE 1199C)

Abstract

Following the explosion of a natural gas pipeline that resulted in extensive property damage, personal injury, and loss of life, a forensic engineering investigation was performed to determine factors that significantly contributed to the failure. Metallurgical analysis of the failure region resulted in the conclusion that the pipeline rupture was caused by hydrogen embrittlement acting on hard spots created during manufacturing. The next phase of this investigation involved root cause analysis of factors contributing to the pipeline rupture as well as evaluation of missed risk-reduction opportunities of the nondestructive analyses employed. It was ultimately determined that hydrogen embrittlement, caused by improper operation and maintenance procedures, resulted in an overabundance of hydrogen from excessive cathodic protection. Additionally, excessive operating pressure exceeded the resulting degraded ultimate capacity of the pipeline, which then manifested in the rupture of the natural gas pipeline and the ensuing explosion. It is recommended that operators exercise due diligence by considering the age of a pipeline when determining appropriate operating, monitoring, and maintenance procedures.

Keywords

Pipeline, hydrogen embrittlement, hard spot, cathodic protection, operating pressure, maintenance, natural gas pipeline, pipeline inspection, forensic engineering

Background

Gas transmission pipelines play a critical role in national economies and are an essential part of the world's infrastructure. As such, it is essential to properly operate, maintain, and monitor them to prevent gas distribution interruptions due to pipeline failures.

According to the Pipeline and Hazardous Materials Safety Administration (PHMSA), more than 12,794 pipeline failures were recorded between 2002 and 2021 in the United States, resulting in 276 fatalities, 1,147 injuries, and $10.1 billion in damages[1]. Failures can be classified as leaks or ruptures. While either can result in fire or explosion, leaks represent the bulk of pipeline failure and typically result in less damage; ruptures are significantly more costly and catastrophic. Of all reported pipeline failures, 24.1% result in fires, and 12.3% result in explosions[2].

As shown in **Figure 1**, the 1950s and 1960s saw the installation of a large number of natural gas pipelines in the United States. As of this paper's publication date, the average pipeline in the United States is approximately 47 years old, as per the analysis of PHMSA data. As such, engineers and technical operators should be mindful of the detrimental effects of age-related degradation and environmental factors that adversely affect the operation of the world's energy infrastructure.

The Present Case

An incident occurred involving a section of a vintage natural gas pipeline in the United States that unexpectedly ruptured, resulting in one fatality, destruction of 30 acres of the surrounding area, hospitalization of six people, and the evacuation of more than 75 residents (**Figure 2** and **Figure 3**). The families of those affected filed suit against the owners of the pipeline, pursuing legal theories of recovery based on negligence and gross negligence.

Following a thorough investigation, it was determined that significant factors synthesized to create the perfect

Jahan Rasty, PhD, PE, 805 Boston Ave., Lubbock, TX 79409-9831, (806) 834-6571, jahan.rasty@ttu.edu

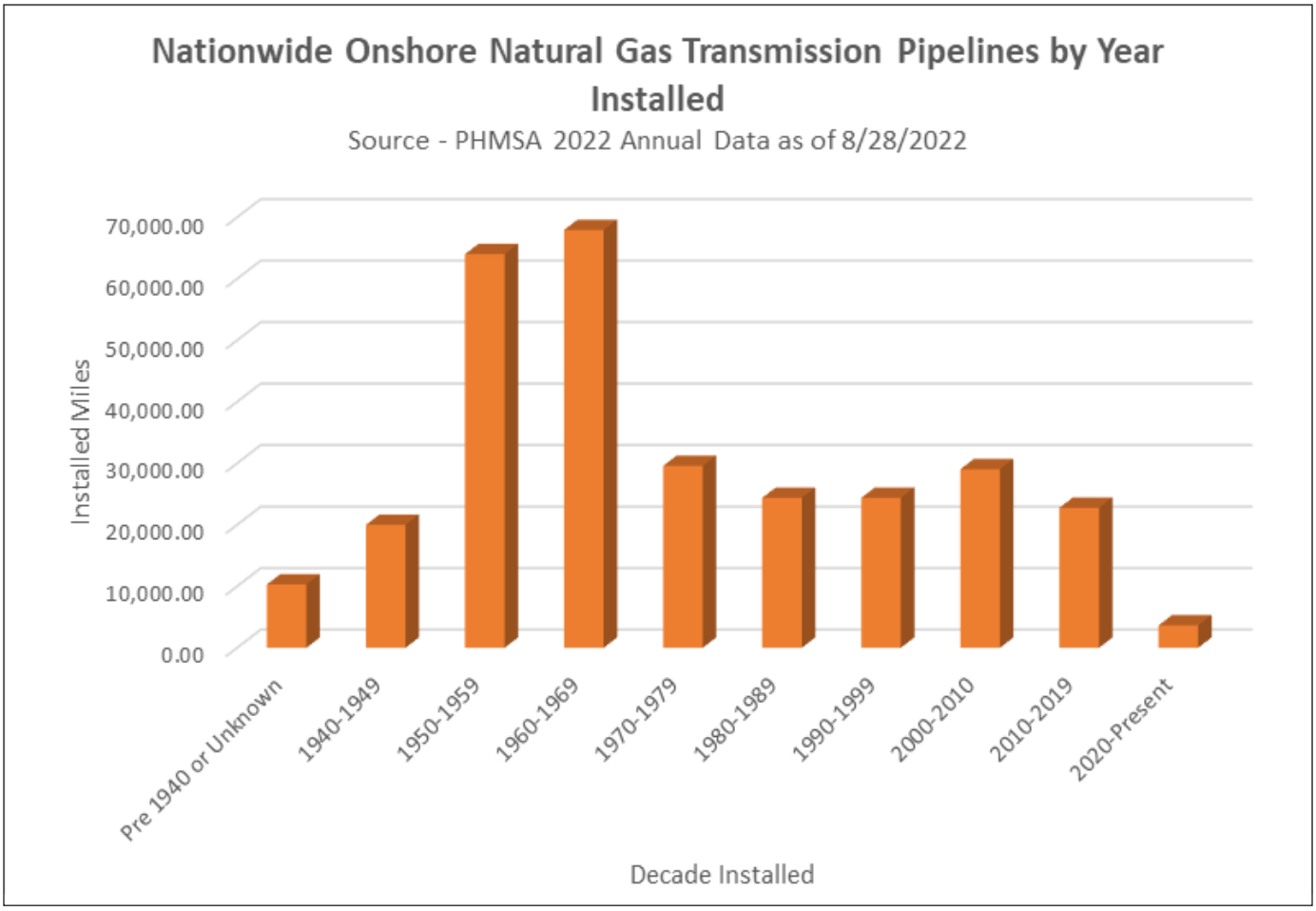

Figure 1

Miles of onshore gas transmission pipelines installed in the United States by decade[3].

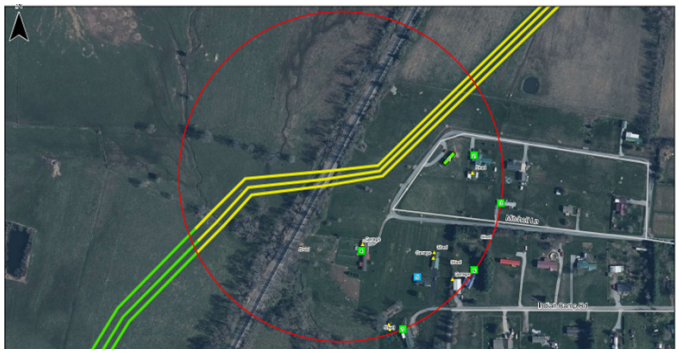

Figure 2

Arial photograph of the mobile home park with location of the pipeline highlighted[4].

Figure 3

Crater left by the pipeline explosion[4].

conditions for the occurrence of the incident at issue. These factors included excessive operating pressures that were not commensurate with the age and conditions of the pipeline along with inappropriate corrosion protection procedures in the form of over-active cathodic protection.

Pipeline Specifications and History

According to provided discovery documents, the pipeline was manufactured in 1957. It was 30 inches in diameter, $^{3}/_{8}$-inch thick, and was made from X-52 carbon steel with an electric flash-welded seam. Additionally, it had a Specified Minimum Yield Strength (SMYS) of 52,000 psi and was being operated at a Maximum Allowable Operating Pressure (MAOP) of 936 psig at the time of the incident. More information about the pipeline's specifications is shown in **Figure 4**.

The pipeline was noted to have experienced a previous rupture 15 years ago about 78 miles north of where the incident rupture occurred. At the time of this previous incident, the pipeline was operating at 907 psi. An investigation report of this incident found that the rupture was

Pipeline Specification	Value
Diameter	30-inch
Material	Carbon Steel
Grade/Specified Minimum Yield Strength (SMYS)[12]	X-52/52,000 psi
Long Seam Weld	Electric Flash-Welded
Manufacturer	
Year Manufactured	1957
Wall Thickness	0.375 inches
Flow Direction (at time of failure)	
MAOP, south flow	936 psig
Operating Pressure (at time of failure)	925 psig
Compressor Station Gas Discharge Temperature (at time of failure)	115 °F
External Coating Type	Coal Tar Enamel
Soil Type	Shale
Cathodic Protection Method	Impressed Current

Figure 4
Pipeline specifications at the rupture origin.

caused by hydrogen-induced cracking that initiated at a hard spot — a region of elevated material hardness.

Fracture Origin

Examination of a segment of the ejected pipe section (**Figure 5**) revealed the presence of chevron marks that were utilized to identify the failure origin (**Figure 6** and **Figure 7**). The failure origin was located 90 inches from a girth weld at approximately the 4 o'clock position of the pipe (seam weld at 12 o'clock). Corrosion pitting was also

Figure 5
The 33-foot-long segment of pipe that was ejected as a result of the explosion[4].

Figure 6
Sectioned segments of the pipeline at the failure origin[4].

Figure 7
The fracture surface of the pipeline at the failure origin[4].

observed near the failure origin and throughout the surrounding area.

The surface of the pipeline segment near the failure origin was ground, polished, and etched to create a grid for the measurement of hardness variation within this area (**Figure 8**). The etched surface revealed a darker region (**Figure 9**) near the failure origin where higher hardness values were measured as compared to areas away from the failure origin (**Figure 10**).

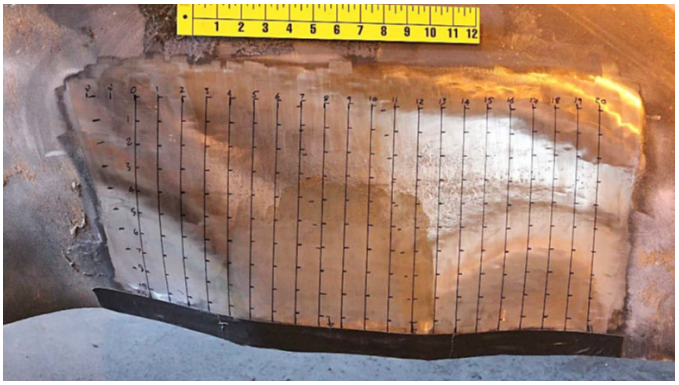

Figure 8
Hardness grid on a polished and etched surface of the pipeline near the failure origin[4].

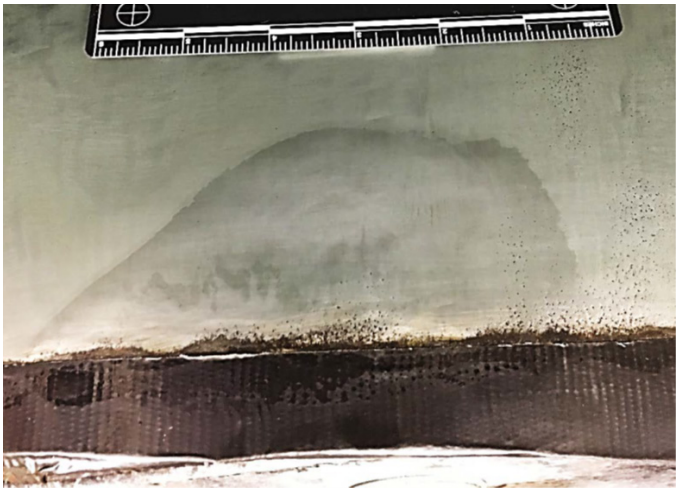

Figure 9
Close-up of the polished and etched surface near the failure origin. Note the presence of the darker region where high hardness values were measured, as shown in **Figure 10**[4].

East Grid

0	1	2	3	4	5	6	7	8	9	10	11	12	13	14	15	16	17	18	19	20
1	169	164	169	165	166	168	169	170	166	179	169	165	161	165	159	161	169	160	168	156
2	161	163	168	166	165	162	173	170	161	167	167	166	167	165	165	161	163	162	160	163
3	167	169	169	164	169	160	176	169	159	172	168	170	164	163	161	171	164	164	160	170
4	168	167	165	165	163	167	168	169	170	173	170	167	171	173	168	162	167	170	163	174
5	167	162	170	170	169	171	177	177	190	174	166	171	154	162	161	162	157	162	164	167
6	164	168	165	164	169	178	186	255	245	181	179	178	165	166	173	167	163	161	172	171
7	166	163	166	164	168	176	251	301	295	283	232	164	163	164	162	164	160	163	157	171
8	162	161	164	203	186	208	289	293	309	305	282	169	154	162	167	164	158	160	155	173
9	150	158	166	194	202	210	291	310	319	313	303	173	165	162	158	162	161	157	159	160
9.5	161	146	164	195	202	211	280	336	326	304	303	245	155	163	155	157	163	167	159	163

West Grid

Fracture Origin

0	1	2	3	4	5	6	7	8	9	10	11	12	13	14	15	16	17
1	163	196	190	167	231	280	287	285	276	236	151	156	159	153	151	149	149
2	151	158	170	162	170	248	250	257	245	149	144	158	160	166	154	149	150
3	164	150	160	162	159	175	174	162	146	153	148	156	160	164	157	156	150
4	159	159	156	157	155	153	149	146	144	148	148	144	152	156	158	149	147
5	153	161	156	152	154	147	148	151	147	147	146	146	154	153	157	153	150
6	153	153	158	153	152	149	156	151	140	149	146	149	149	159	157	155	147
7	156	155	155	152	157	151	153	148	152	151	150	152	153	153	159	152	149

Figure 8: East and West Grid Hardness Values

Figure 10

Results of the conducted hardness testing[4].

A 6-inch x 1.5-inch segment of the pipe containing the fracture origin was cut out, cleaned, and examined under Scanning Electron Microscope (SEM). As shown in **Figure 11**, the fracture origin was observed to exhibit intergranular fracture from the exterior surface to approximately 0.1 inches below the surface, up to ~30% of the nominal thickness of the pipe. A mixed-mode fracture region was observed from 0.1 inches below the exterior surface up to the edge of a shear lip on the inner surface. The presence of intergranular features was noted to decrease with increasing distance from the exterior surface. Based on the above observations, it was concluded that the exterior surface of the pipeline was exposed to an embrittling environment.

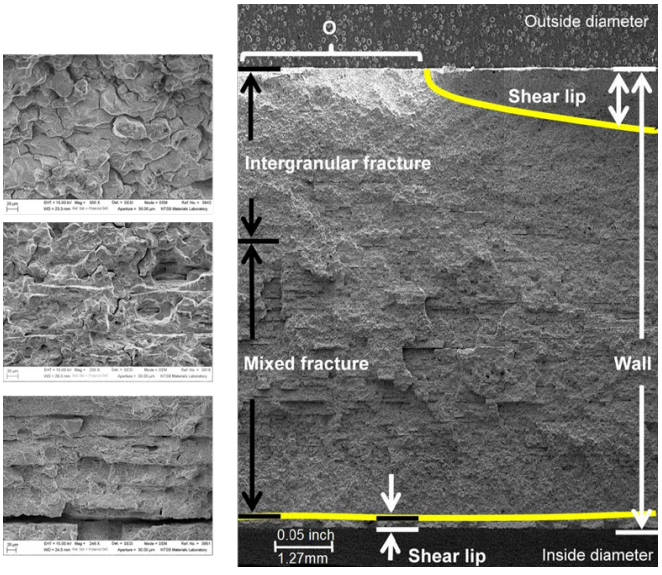

Figure 11

SEM image of the fracture surface at the fracture origin, displaying regions of intergranular and mixed mode fracture[4].

Hard Spots

A "hard spot" is a term used to indicate regions of elevated hardness within a material, typically with these areas displaying hardness values considerably higher than the surrounding metal. In pipelines, hard spots refer to areas of martensite generated from the rapid quenching of the pipeline steel during manufacturing[5].

Hard spots on steel form when heated metal in the austenitic phase is rapidly quenched, forming martensite[6]. It has been reported that pipelines produced from 1952 to 1957 were susceptible to hard spot development as a result of unintentional water leakage onto the production line[5,7]. It is well known in the industry that vintage pipes with high concentrations of hard spots are highly susceptible to brittle failure.

Non-Destructive Detection of Hard Spots

To inspect buried pipelines, pigging operations are performed that incorporate In-Line Inspection (ILI) tools capable of surveying the interior surface of a pipeline for the presence of various metallurgical and environmental conditions that can adversely affect the safety and efficiency of the pipeline.

Magnetic Flux Leakage (MFL) is routinely used for the detection of hard spots. MFL ILI tools work by inducing a magnetic flux into the pipeline while measuring variations in the rate of magnetic flux leakage. A homogeneous metal surface produces a uniformly distributed magnetic flux, while the presence of defects results in an

altered flux field[8]. To detect hard spots, an MFL ILI tool must run a dual, low, or residual field inspection[8].

A review of the maintenance records revealed that eight years before the incident, a pipeline inspection company performed ILI for the detection of hard spots within the pipeline. Their inspection identified 16 hard spots, four of which were excavated and repaired. The remaining 12 did not meet the owner's criteria for excavation; therefore, they were not excavated or repaired.

Following the incident, the pipeline inspection company performed a re-analysis of its original data from the inspection performed eight years before the incident. This re-analysis utilized an improved version of the company's analysis software, which now incorporated AI instead of human operators to identify potential hard spots. As shown in **Figure 12**, this re-analysis revealed a total of 441 hard spots (compared to only 16 that were originally identified), nine of which were located within the same section of pipe that ruptured and one that was located at the failure origin.

According to the manufacturer of ILI tools, such devices have a corresponding probability of detecting an anomaly or defect in the pipeline, known as their Probability of Detection (PoD). This parameter is based on the number of known defects the tool is able to detect. The PoD is reduced based on the depth of the defect, so defects on the outer surface of the pipe will be more difficult to detect[8]. The ILI tool pipeline inspectors used for the original hard spot inspection were noted to have a PoD of 90%, typical of the average tool on the market[8,10,11]. Therefore, the ILI tool used by the pipeline inspectors in their original inspection would have missed 10% of potential critical defects in the pipeline. As this information was supplied to the pipeline owners prior to the original run of the ILI tool, they knew (or should have known) there was a considerable chance that critical defects in the pipeline would have been missed — such as the case with the hard spot at issue.

As a result of this, federal regulations require that pipeline operators perform hard spot inspections every seven years[11,12,13]. According to reviewed documents, the pipeline owners had scheduled another hard spot inspection more than a year before the incident but failed to carry through with this plan. However, even if they had performed this scheduled inspection, they would not have satisfied their due diligence as owners. According to a 2016 publication by PHMSA, "Defaulting to the maximum reassessment interval allowed by code and not analyzing each unique inspection segment for each pipeline threat can lead to failures and undermine an effective integrity management

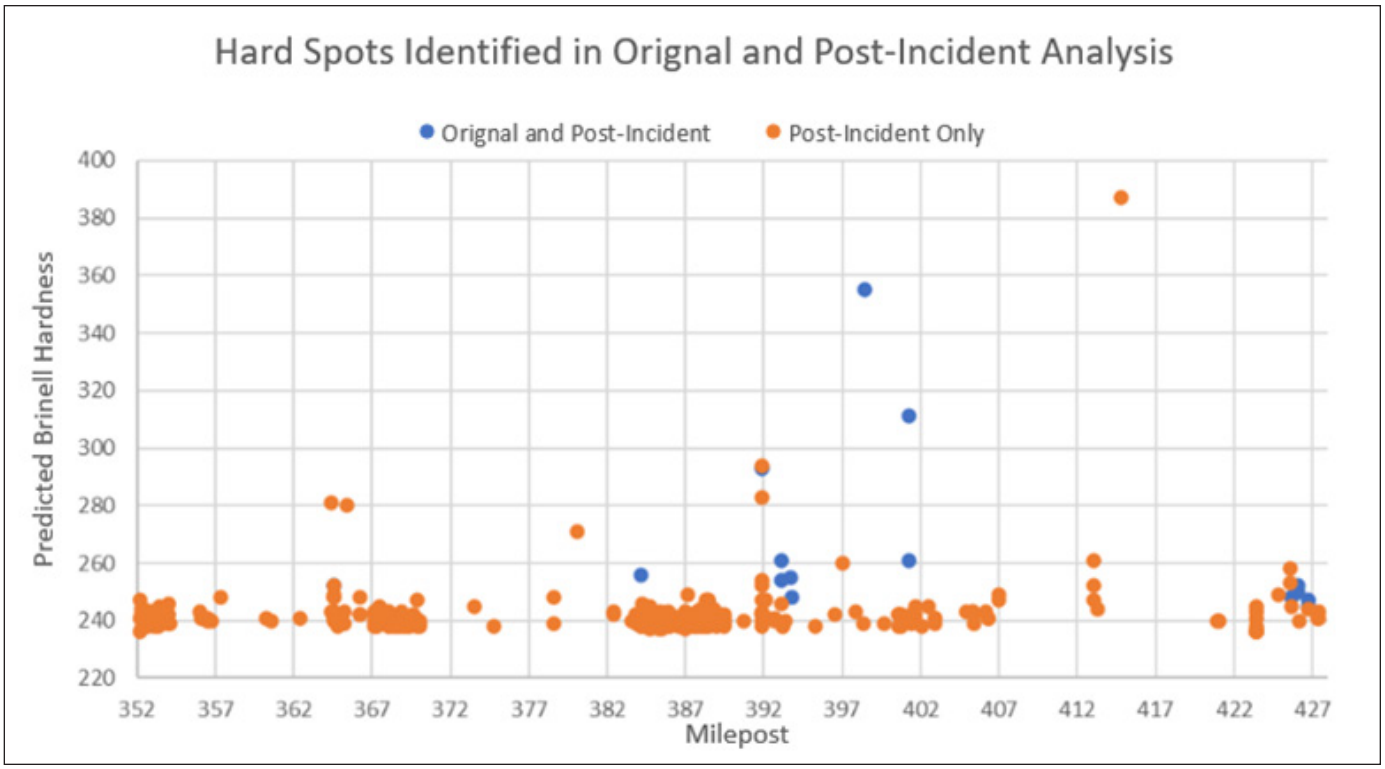

Figure 12
Comparison of hard spots identified in the original and post-incident analysis.

program[14].” As the pipeline at issue was a vintage pipe with a known susceptibility to hard spots, the pipeline owners should have instituted an inspection interval well below the maximum stated interval of seven years in order to account for the increased risk of hard spots presented. Had the pipeline owners run ILI multiple times as required by federal regulations, they would have — in all probability — caught 99% of the defects present in the pipeline, and the incident may likely have been prevented.

Cathodic Protection and the Consequences of Overprotection

Potential sources for the embrittlement observed at the failure origin were investigated. Based upon provided documentation, the production of hydrogen by the cathodic protection system of the pipeline was considered the most likely source of said embrittlement.

Corrosion protection of pipelines is routinely performed via cathodic protection, where the pipeline is electrically connected to a more anodic material. By electrically connecting the pipeline to a more anodic material, the couple undergoes an oxidation-reduction reaction — where the anode transfers its electrons to the cathode. Thus, the anode that is coupled to the pipeline acts as a “sacrificial metal” that takes on the corrosion the pipeline would normally experience[14]. The effectiveness of cathodic protection depends on the difference in electrical potential between the two anode and cathode materials. The material that undergoes electron loss will act as the anode of the galvanic couple while the material that gains electrons will act as the volume of the pipeline.

Cathodic protection of a pipeline can also be accomplished via impressed current. Instead of solely relying on the potential difference between the anode and cathode, an external power source is employed to run either DC or AC current through the system to increase the cathodic current for protecting the cathode from corroding (**Figure 13**). This method is typically applied to large structures (such as pipelines) where the natural potential difference (per unit volume) between anode and cathode would be insufficient to protect the entire structure[15,16].

To ensure that the cathode does not experience corrosion, a minimum level of potential must be maintained. For pipelines, this minimum potential, as dictated by NACE SP0169 and ASTM G218 is ~ -0.85 V[17]. Potentials slightly over or under this recommended level are allowed to account for environmental conditions.

Since the recommended minimum value of applied potential is ~ -0.85 V, some operators erroneously conclude that increasing this potential to even higher values would offer further benefits for the pipeline. While increasing the potential difference to values greater than the recommended minimum value of -0.85 V does increase the corrosion protection of the system, such increased corrosion protection comes with unintended adverse consequences. By increasing the potential of the impressed current, the excess potential causes nearby water in the soil or local environment to undergo electrolysis, releasing atomic hydrogen and hydroxide around the pipeline. The increased level of atomic hydrogen and hydroxide leads to the development of two unwanted phenomena — namely, hydrogen

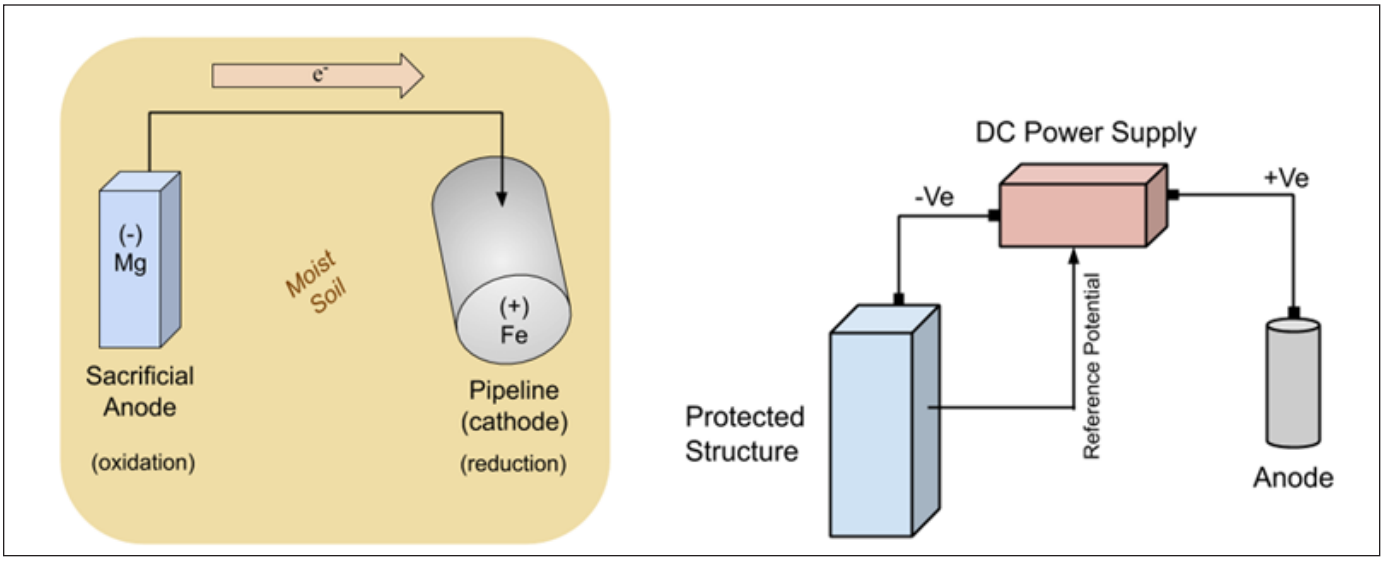

Figure 13

A typical sacrificial anode system (left) and a DC impressed current system (right)[15].

embrittlement and coating disbondment.

Hydrogen Embrittlement (HE) is a complex phenomenon in which atomic hydrogen is absorbed into the metal, reducing the material's strength, toughness, and ductility. This occurs due to a variety of different mechanisms, such as hydride formation, hydrogen-enhanced decohesion mechanism (HEDE), hydrogen-enhanced local plasticity (HELP), and adsorption-induced dislocation emission (AIDE)[18]. While these mechanisms differ dramatically from each other, ultimately, they all manifest as cracking in steel through either strain-controlled plastic flow or stress-controlled decohesion. The strain-controlled mechanism (combined with concentrated plastic flow) typically results in transgranular cracking while stress-controlled decohesion results in intergranular cracking[19]. An increase in hardness allows for higher stresses to be sustained by the steel and for more hydrogen to collect at these regions of elevated stress, thereby increasing decohesion-based hydrogen embrittlement[20].

As hydrogen diffuses through a steel pipeline over time, resulting in its gradual embrittlement, a critical hydrogen concentration level will be reached that causes nominally applied stresses to result in catastrophic failure of the material[21]. Probabilistically, older structures that have been consistently exposed to relatively low levels of hydrogen will eventually reach a critical hydrogen concentration that ultimately results in their failure. As such, it is critical that the occurrence of hydrogen embrittlement be closely monitored to identify and mitigate the risks associated with the aging population of pipelines.

Organic coatings such as coal tar enamel applied to the pipelines are partially permeable to cathodic current[22]. When a cathodic potential over the recommended value is applied, the elevated cathodic current facilitates an increased rate of hydrogen reduction at the surface of the metal, leading to a greater rate of hydrogen embrittlement[15]. In addition, the hydroxide ions produced by electrolysis are absorbed into the organic coating, degrading it and leading to its delamination. The resulting delamination exerts additional stresses on the coating, which, in turn, causes its disbondment from the pipeline. Since organic coatings such as coal tar enamel are permeable by hydrogen, oxygen, and water, these constituents are able to diffuse their way into the disbonded area and corrode the metal or accelerate hydrogen embrittlement[24,25,26]. Coating disbondment can also occur at locations of defects inherent in the coating, such as scratches, holes, and nicks[25,26,27]. Delamination causes the coating to disbond around these defects, which readily allows hydrogen, water, and hydroxide to pool in the coating defect and accelerate the diffusion of hydrogen into the metal, further disbonding of the coating (**Figure 14**)[22].

NACE SP0169 warns about the use of excessive potentials on coated pipelines and instructs that such excessive potentials should be avoided to minimize the occurrence of coating disbondment. This is due to the fact that as the level of cathodic protection is increased, the rate of hydrogen reduction, corrosion, and coating degradation increases[23,24,28,29].

According to available literature, the general consensus in the industry is that polarized (IRF) potentials of -1.05 V and higher (more negative) should be avoided to avoid cathodic overprotection[30]. In addition, ISO 15589-1 instructions for preventing disbondment of pipeline coatings state that the limiting critical potential for all metals should not be more negative than -1.20 V[31]. It is also to be noted that under normal pipeline operating conditions, this stated upper limit of -1.20 V could still be enough to result in high levels of hydrogen reduction, leading to hydrogen induced cracking of steel pipelines[21,27,32,33,34,35,36,37,38,39].

In this case, the pipeline owners utilized a series of cathodic protection test stations located roughly every mile along the pipeline for annual monitoring. These stations measured two types of potentials: the "Pipe-to-Soil" (P/S) potential, which includes the resistance inherent in the soil, and polarized (IRF) potential that is a reading corrected for soil resistance. The IRF is used as the effective cathodic protection level in accordance with ISO standards[31]. The cathodic protection readings at the

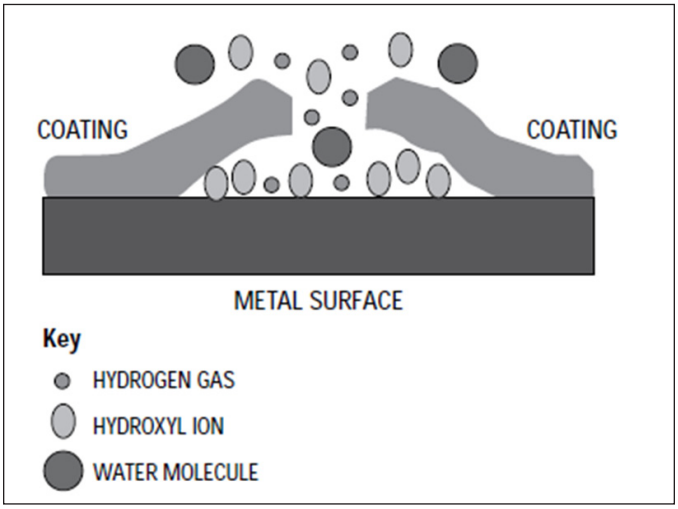

Figure 14
Elements of coating disbondment[27].

milepost where the rupture occurred in the years prior to the incident are shown in **Figure 15**. As can be seen from the data in **Figure 15**, there were numerous locations of low cathodic potential, exceeding the recommended value of -0.85 V with some of the locations exceeding the limit of -1.20 V. These highly negative potentials were kept in place for years, damaging the pipelines and increasing the risk of catastrophic ruptures.

The pipeline owner's standard operating procedure acknowledged that a high level of cathodic protection can cause damage to the pipeline coating as well as the pipe itself. As such, they required that error-corrected potentials (IRF) readings more negative than -1.20 V be investigated. While the pipeline owners at the time of the incident sought to maintain the cathodic protection potential between -0.85 V and -1.20 V, there was no indication that they made any organized effort to investigate and correct the high levels of cathodic protection that were known to be in place at the location of the subject incident as well as numerous other pipeline segments. Further evidence of disregard by the pipeline operators to prevent subjecting the pipeline to potentials above the critical -1.20 V level was obtained through discovery documents — where a corrosion technician employed by the pipeline operators who was interviewed by NTSB stated that he or she did not consider potentials up to -2 V as a cause for concern.

By taking into account the applied level of cathodic overprotection, the pipeline was subjected to, the presence of a hard spot at the failure origin, and the age of the pipeline, it was concluded that decohesion-based hydrogen embrittlement took place which caused the pipeline to fail in an intergranular manner. Based on the body of knowledge available in the previously cited open literature, the owners knew (or should have known) the susceptibility of steel pipelines to elevated cathodic protection levels at or near -1.20 V level, but their lack of due diligence in understanding proper cathodic protection levels led to improper cathodic protection operations at levels detrimental to the structural integrity of the pipeline.

Determination of Maximum Allowable Operating Pressure (MAOP)

One of the methods for determination of Maximum Allowable Operating Pressure (MAOP), as described in 49 CFR 192.619, is to operate at 80% of the hydrostatic burst pressure. Given that the as-manufactured (in 1959) pipeline's hydrostatic burst pressure was 1,170 psi, the operating pressure of the pipeline was set at 936 psi from the onset of operations. At the time of the incident, the operating pressure of the vintage pipeline was 925 psi or ~98.8% of the MAOP of 936 psi. Another method for determination of MAOP, as prescribed by 49 CFR 192.619, is to utilize the following equation:

$$P = \left(2\frac{St}{D}\right) x\ F\ x\ E\ x\ T \qquad \text{EQ. 1}$$

Miles From Subject	4 Years Before		3 Years Before		2 Years Before		1 Year Before		Year of Incident	
	P/S	IRF	P/S	IRF	P/S	IRF	P/S	IRF	P/S	IRF
-6	-1.884	-1.228	-1.811	-1.281	-1.832	-1.231	-1.629	-1.314	-1.443	-1.16
-5	-1.625	-1.201	-1.609	-1.261	-1.654	-1.348	-1.434	-1.22	-1.463	-1.098
-4	-1.652	-1.261	-1.67	-1.299	-1.858	-1.541	-1.453	-1.251	-1.28	-1.199
-3	-1.697	-1.256	-1.707	-1.282	-1.719	-1.321	-1.508	-1.242	-1.6	-1.176
-2	-1.275	-0.856	-1.036	-0.879	-1.006	-0.865	-0.776	-0.729	-0.8	-0.709
-1	-1.94	-1.159	-1.92	-1.15	-1.949	-1.26	-1.651	-1.145	-1.753	-1.079
0	-1.781	-1.096	-1.78	-10.41	-1.947	-1.234	-1.829	-1.081	-1.583	-1.047
1	-4.172	-1.478	-4.188	-1.4	-4.093	-1.536	-3.775	-1.469	-3.645	-1.287
2	-2.732	-1.277	-2.624	-1.175	-2.526	-1.252	-2.039	-1.333	-2.382	-1.154
3	-2.161	-1.14	-2.103	-1.011	-2.084	-1.08	-1.815	-1.066	-1.159	-1.045
4	-2.164	-1.143	-1.963	-1.066	-2.072	-1.103	-1.818	-1.045	-1.892	-1.076
5	-2.016	-1.158	-1.968	-1.093	-2.027	-1.065	-1.721	-1.008	-1.088	-1.037
6	-2.003	-1.187	-1.828	-0.927	-1.925	-0.958	-1.707	-1.058	-1.683	-1.132
7	-2.148	-1.028	-2.126	-1.029	-2.338	-1.034	-1.93	-0.967	-2.327	-1.348
8	-3.423	-1.266	-3.745	-1.254	-2.572	-1.235	-2.531	-1.215	-2.564	-1.347

Figure 15
Year-by-year readings of Pipe-to-Soil (P/S) Potentials (volts) with error correction (IRF) at the subject and nearby cathodic protection stations.

Where P is the design pressure (MAOP), S is the yield strength, t is the nominal wall thickness, F is the design factor, E is the longitudinal joint factor, and T is the temperature derating factor. As the pipeline was operating in a class 2 location (F=0.6), at operating temperatures under 250°F (T=1), and utilized electric flash welded pipes (E=1), the as-calculated MAOP would be 780 psi.

Additionally, the Interstate Natural Gas Association of America (INGAA) released a report that stated:

> *"If there is a likelihood hard spots or arc burns exist, and the coating is inferred to be of poor quality with cathodic protection levels uncontrolled and more negative than -1.2 volts, assess the stress in the pipe. If stress is less than 60% SMYS, cracks are not likely to form. Otherwise, when hard spots are located on the pipeline, measure their hardness levels. If the hardness levels are at or above Rockwell C35, experience indicates hydrogen stress cracking is possible*[40]*."*

The SMYS of X52 steel is 52,000 psi, and 60% of this value is 31,200 psi. Using this new yield stress in the modified hoop stress equation in EQ. (2), the resulting MAOP would be 780 psi, which is similar to the result obtained from EQ. (1).

$$P = \frac{\sigma x t}{r} \qquad \text{EQ. 2}$$

Where P is the MAOP, σ is the SMYS, t is the pipe thickness, and r is the pipe radius.

As required by 49 CFR 192.619, when selecting the proper MAOP, a prudent operator should choose the lowest value amongst MAOPs determined via different methods. As such, the pipeline owners should have selected the MAOP value of 780 psi obtained from EQ. (1) or EQ. (2). This is especially true since the pipeline was a vintage pipe, which was known to include hard spots.

Around 16 years before the incident, the pipeline operators experienced a rupture approximately 78 miles north of the subject location. This rupture occurred at a pressure of 907 psi. This segment of the pipeline was also constructed from the same vintage pipe material that was used in the manufacturing of the subject pipeline. Failure of this segment of the pipeline was attributed to hydrogen-induced cracking at a hard spot. Given the fact that 46 years after its manufacturer the pipeline was experiencing bursts at operating pressures well below the original MAOP, the pipeline operators should have reduced their MAOP of the vintage pipe to 80% of the most recent burst pressure of 907 psi and operated at 726 psi instead of continuing operations at MAOP of 936 psi as if the pipeline was still in its original condition.

Given that the susceptibility of vintage pipelines to hydrogen-induced cracking increases with increased tensile stresses caused by excessive operating pressures — combined with the fact that pipeline owners continued to operate the pipeline at pressures (925 psi) well above the conservative MAOPs (726 psi) required by 49 CFR 192.619 — the pipeline owners failed to operate as a reasonably prudent operator. As such, they directly contributed to the incident at issue. Had the owners lowered the MAOP of its pipeline to a level consistent with recommended design guidelines (726 psi), within a reasonable degree of scientific and engineering probability, the incident would not have occurred.

Summary and Conclusions

Metallurgical analysis of the ruptured pipeline revealed that the failure of the pipeline originated at a location of elevated hardness known as a hard spot. The intergranular nature of the fracture indicated exposure to an embrittling environment. Further analysis of the operating conditions of the pipeline revealed that the embrittling environment was caused by stress-controlled decohesion hydrogen embrittlement that occurred due to excessive hydrogen production resulting from an over-aggressive cathodic protection program.

Ultimately, the vintage pipeline's rupture occurred not only due to the owner's continued use of the pipeline at excessive operating pressures that were above required levels from the onset, but also did not adequately consider the age of the pipeline. The owners knew — or should have known — that the excessive levels of cathodic protection, combined with higher-than-acceptable operating pressures, would eventually compromise the structural integrity of the pipeline due to the long-term effects of hydrogen embrittlement. Had the owners followed established preventive maintenance procedures and operated the pipeline according to regulations, this catastrophic incident would not have occurred.

This failure highlights the fact that the vintage pipelines in the United States are at risk of failure due to hydrogen embrittlement. Regular inspection, replacement of the pipelines, and/or reduction of operating pressure can be utilized to prevent similar catastrophic failures from occurring.

Acknowledgments

The authors would like to thank the legal experts we worked with on this case as well as our dedicated team of forensic engineers and interns.

References

1. DOT-PHMSA, U.S. Department of Transportation Pipeline and Hazardous Materials Safety Administration, 2021. Annual Data www.phmsa.dot.gov/.

2. J.G. Ramírez-Camacho et al, "Assessing the consequences of pipeline accidents to support land-use planning" Safety science, vol. 97, pp. 34-42, Jan. 2017.

3. DOT-PHMSA, U.S. Department of Transportation Pipeline and Hazardous Materials Safety Administration, 2022. Annual Data www.phmsa.dot.gov/ (Accessed: Aug. 28, 2022).

4. NTSB Materials Laboratory Factual Report - Report No. 19-064, National Transportation Safety Board, Washington, D.C., USA, Feb. 6, 2020.

5. A. Bellinger, et. Al, "Multiple Data Inspection of Hard Spots and Cracking." in Proceedings of the 2014 10th International Pipeline Conference. Volume 2: Pipeline Integrity Management. Calgary, Alberta, Canada. September 29–October 3, 2014.

6. M. J. Slaughter, et. al "Pipeline Integrity: The Use of Multiple Technology In-Line Inspection Tool." in Proceedings of the 2002 4th International Pipeline Conference. 4th International Pipeline Conference, Parts A and B. Calgary, Alberta, Canada. September 29–October 3, 2002. pp. 1913-1922.

7. M. J. Rosenfeld, "Joint Efficiency Factors for A.O. Smith Line Pipe" Kiefner & Associates, Worthington, Ohio, Dec. 2012.

8. NACE International, "In-Line Inspection of Pipelines", NACE International, Texas, Houston, NACE Publication 35100, 2016.

9. "In-Line Inspection Tools Specifications" https://apps.neb-one.gc.ca/REGDOCS/File/Download/792731 (Retrieved: Aug 28, 2022).

10. *Specifications and requirements for in-line inspection of pipelines*, Pipeline Operators Forum Standard 100, 2016.

11. Transmission lines: Assessments outside of high consequence areas, 49 C.F.R. § 192.710 (b) 2.

12. How does an operator identify potential threats to pipeline integrity and use the threat identification in its integrity program?, 49 C.F.R. § 192.917 (e) 3.

13. What are the required reassessment intervals?, 49 C.F.R § 192.939 (a).

14. Phmsa "Inspection Reassessment Intervals Guidance for Less than 7 years" October 2016.

15. K. Nanan "The Basics of Cathodic Protection" Corrosionpedia, https://www.corrosionpedia.com/2/1368/prevention/cathodic-protection/cathodic-protection-101 (Accessed: Aug. 28, 2022).

16. "Impressed Current Cathodic Protection" Matcor, https://www.matcor.com/impressed-current-cathodic-protection/ (Accessed: Aug. 28, 2022).

17. Control of External Corrosion on Underground or Submerged Metallic Piping Systems, NACE Standard SP0169, 2007.

18. S. K. Dwivedi "Hydrogen embrittlement in different materials: A review" International Journal of Hydrogen Energy, vol. 43, no. 46, pp 21603-21616, Nov. 2018.

19. C. J. McMahon "Hydrogen-induced intergranular fracture of steels" Engineering Fracture Mechanics, vol. 68, no. 6, pp. 773-788, Apr. 2001.

20. D. Hardie, et al., "Hydrogen embrittlement of high strength pipeline steels" Corrosion Science, vol. 48, no. 12, pp. 4378-4385, Dec. 2006.

21. J. Capelle et al., "Sensitivity of pipelines with steel API X52 to hydrogen embrittlement" International Journal of Hydrogen Energy, vol 33, no 24, pp. 7639-7641, Dec. 2004.

22. D. Kuang, et. al "Study Of Cathodic Protection Shielding Under Coating Disbondment On Pipe-

lines," Corrosion Science, vol. 99, pp. 249-257, Oct. 2015.

23. "Over Protection Explained" Marine Protection Systems, http://www.marineprotectionsystems.com.au/mpswp/wp-content/uploads/2011/06/Over-Protection-Explained.pdf (Accessed: Aug. 28, 2022).

24. S. H. Lee, et. al, "Acceleration and quantitative evaluation of degradation for corrosion protective coatings on buried pipeline: Part II. Application to the evaluation of polyethylene and coal-tar enamel coatings" Process and Organic Coatings, vol. 76, no.4, pp.784-789, Apr. 2013.

25. H. Leidheiser, "De-Adhesion At The Organic Coating/Metal Interface In Aqueous Media," Croatica Chemica Acta, vol. 53, no. 2, pp. 197-209, 1980.

26. E. L. Koehler, "The Influence of Contaminants on the Failure of Protective Organic Coatings on Steel," Corrosion, vol. 33, no. 6, June 1977.

27. N. Kamalanand, et. al, "Role Of Hydrogen And Hydroxyl Ion In Cathodic Disbondment," Anti-Corrosion Methods and Materials, vol 45, no. 4, pp.243-247, Aug. 1998.

28. F. Gan, et. Al, "Cathodic Protection to Mitigate External Corrosion of Underground Steel Pipe Beneath Disbonded Coating," Corrosion, vol. 50, no. 10, pp. 804-816, Oct.1994.

29. F. Kajiyama, "Strategy For Eliminating Risks Of Corrosion And Overprotection For Buried Modern Pipelines," Tokyo Gas Co. Ltd, Tokyo, Japan, 2011.

30. E. Klechka, et al. "Practical Considerations for Upper Limits of Cathodic Protection," Corrosion 2007 Conference and Expo, Nashville, Tennessee, Mar. 2007.

31. Petroleum, petrochemical and natural gas industries — Cathodic protection of pipeline systems — Part 1: On-land pipelines, ISO Standard 15589-1, 2015.

32. M. Cabrini, "Hydrogen Embrittlement and Diffusion of High Strength Low Alloy Steels with Different Microstructures," Insight-Material Science, vol. 2, no. 1, pp. 1-9, Mar. 2019.

33. M. Javidi et al, "Investigating The Mechanism Of Stress Corrosion Cracking In Near-Neutral And High ph Environments For API 5L X52 Steel," Corrosion Science, vol. 80, pp. 213-220, Mar. 2014.

34. P. Liang, et. al, "Stress Corrosion Cracking Of X80 Pipeline Steel In Simulated Alkaline Soil Solution," Materials and Design, vol. 30, no. 5, pp. 1712-1719, May 2009.

35. S. A. Shipilov, et. al, "Structural Integrity Of Aging Buried Pipelines Having Cathodic Protection," Engineering Failure Analysis, vol. 13, no. 7, pp. 1159-1176, Oct. 2006.

36. C. Kim, et. al "The Effects of Hydrogen Embrittlement by Cathodic Protection on the CTOD of Buried Natural Gas Pipeline," Metals and Materials International, vol. 8, no. 2, pp.197-202, Apr. 2002.

37. M. Cabrini, et. al "Hydrogen Embrittlement Behavior Of HSLA Line Pipe Steel Under Cathodic Protection," Corrosion Reviews, vol. 29, no. 5-6, pp. 261-274, Oct. 2011.

38. S. X. Mao, et. al, "Hydrogen Facilitated Anodic Dissolution Type Stress Corrosion Cracking of Pipeline Steels in Coating Disbondment Chemistry," Proceedings of the 1998 2nd International Pipeline Conference. Volume 1: Risk Assessment and Management; Emerging Issues and Innovative Projects; Operations and Maintenance; Corrosion and Integrity Management. Alberta, Canada. June 7–11, 1998. pp. 485-492.

39. A. Q. Fu, et. al, "Effect Of Alternating Current On Corrosion And Effectiveness Of Cathodic Protection Of Pipelines," Canadian Metallurgical Quarterly, vol. 51, no. 1, pp. 81-90, Jul. 2011.

40. "Integrity Characteristics of Vintage Pipelines", Interstate Natural Gas Association of America, Washington, D.C., 2002.

Forensic Engineering Analysis of an Apartment Freezing Sequence Using Heat Flow Equations

By Daniel P. Couture, PEng (NAFE 951S)

Abstract

Four students had staggered departures from their electrically heated third-floor shared residence apartment to travel home for the winter holiday break. Two pipe bursts and two frozen toilets were discovered a week after the last resident had left. The property management group gathered scene evidence and analyzed the cause of the water escape. The investigation revealed that some electric heaters had been turned off, and some bedroom and living room windows were open. A forensic engineering analysis was conducted to qualitatively determine the effects of heater disengagement and open window positions on the apartment temperature drop and to estimate the likely start date of sub-zero Celsius conditions. Heat flow and balance equations for different sets of factors were used to quantitatively assess the instantaneous heat flow trends as the basis for understanding whether certain students carried more burden of liability. The analysis revealed that the open windows were the dominant factor for the freeze-up condition development that led to the bursts.

Keywords

Heat balance, instantaneous heat flux, electrical heating, pipe freeze time, pipe burst, toilet freeze time, open window heat convection, room heat loss, forensic engineering

Introduction

A water supply pipe burst in the kitchen of an upper-floor apartment suite of a student residence (**Figure 1**) of a university in southeastern Ontario on or about December 30, 2009, resulting in subsequent significant water damage.

Investigation

The author was engaged to evaluate the circumstances and time sequence of the pipe freeze-up incident. The site had long since been repaired at the time of engagement such that there was no opportunity to inspect and confirm the original conditions. A series of photographic prints taken on December 30, 2009 at the site (as well as reports with opinions formulated by other engineers) was provided for review by the author. All company names and resident names have been obscured to respect conditions of confidentiality.

Suite Configuration

The plan view of Suite 36 showed a living room, dining room, four bedrooms, two washrooms (one with a shower/tub), central kitchen, and storage room. It was configured with a connecting wall to another suite on the longer living room wall and dining room side adjacent to the door. The relative dimensions of the rooms are laid out approximately in **Figure 2**. The living room and dining room had large windows, and every bedroom had a moderately sized window. The bathrooms each had a small window.

The rooms were heated with baseboards powered by electricity. The details of heating methods and the names

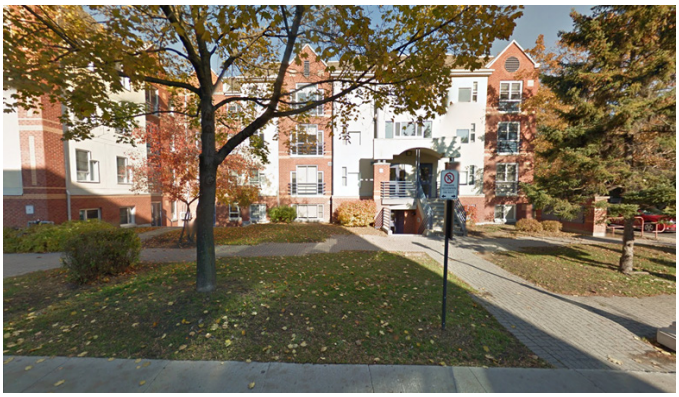

Figure 1
South elevation of University residence apartment block.

Daniel P. Couture, PEng, 9033 Leslie St., Units 18/19, Richmond Hill, ON L4B 4K3 Canada, daniel.couture@arconforensics.com

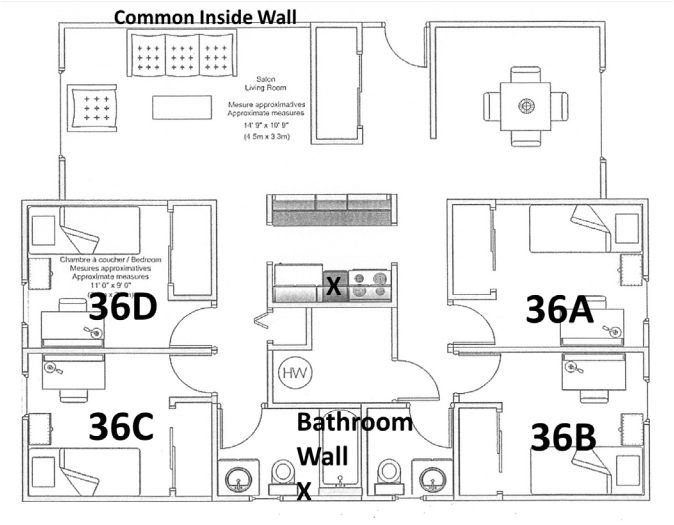

Figure 2
Suite plan showing where the pipes split (marked as X).

of their occupants were (counting clockwise from above left in the suite plan):

- Dining room — 1,750 watts (W) (6,000 BTU/h) electric baseboard, with a thermostat;
- Living room — 1,500W (5,100 BTU/h) baseboard, controlled by the dining room thermostat;
- Bedroom 36A (Allan) — 1,000W (3,400 BTU/h) baseboard, with a thermostat;
- Bedroom 36B (Bob) — 1,250W (4,260 BTU/h) baseboard, with a thermostat;
- Bathroom 1 — 300W (1,000 BTU/h) baseboard with a thermostat;
- Bathroom 2 with shower/tub — 300W (1,000 BTU/h) baseboard with a thermostat.
- Bedroom 36C (Charlie) — 1,250W (4,260 BTU/h) baseboard, with a thermostat; and
- Bedroom 36D (Dave) — 1,000W (3,400 BTU/h) baseboard, with a thermostat.

The total available heating power in Suite 36 was 8,350W (28,500 BTU/h).

Origins of the Water Escape

Based on the site photographs, one origin of the water escape was on the upstream side of the yellow-handled shut-off valve in the hot water copper supply line below the kitchen sink. **Figure 3** depicts a longitudinal split in the pipe adjacent to the soldered joint with the valve as well as a second short piece of pipe with a similar longitudinal split taken from behind the drywall in the exterior wall cavity behind a toilet. The short piece was assumed to be the second origin.

The water in the toilet tank and the bowl of both bathrooms had frozen with one tank shown in **Figure 4**. The float was immobilized in ice and the overflow pipe displaced. The interior wall of this tank was insulated with white closed-cell polystyrene with a smooth skin surface.

Door, Window, and Thermostat Positions

The status of the windows and heating devices on December 30, 2009 was generally confirmed during the examinations for discovery, in which principal parties to litigation were questioned under oath.

- The windows of the dining room and living room

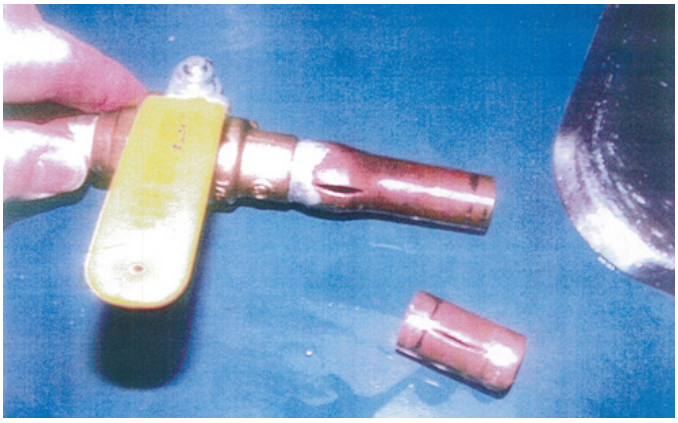

Figure 3
The two longitudinal splits in water supply pipes.

Figure 4
One of two toilet tanks with ice formation.

were open;

- Room 36C had its thermostat turned off and the window in open position with the door closed;
- Room 36D had its thermostat turned off and the window in open position with the door closed;
- The positions of doors, windows, and thermostats elsewhere were not remarked in the security or emergency response records; and
- No suite temperature measurements were taken by university security personnel at the time of the water escape.

Time line

From the examinations for discovery transcripts, the following sequence was established:

- Charlie had left the apartment on December 19, closed his door, left the thermostat in the off position, and opened the window in Room 36C;
- Allan had left the apartment on December 20. There was no evidence that he left the thermostat off or the window open in Room 36A;
- Bob left the apartment on December 23 at 10 or 11 a.m., and there was no evidence that he left the thermostat off or the window open in Room 36B;
- Dave and Bob opened the windows in the living room and dining room on the morning of December 23, prior to Bob's departure;
- Bob stated that he had closed these windows prior to leaving;
- Dave was the last to leave (at 3 a.m. on December 24), and had closed his door/left the thermostat in the off position and the window open in Room 36D;
- Dave claims not to have looked to see if the windows in the living room and dining room were open or closed when he left.

Considerations & Assumptions

The following factors and assumptions were made, in part due to the limited site access:

1. For construction, the exterior walls of the unit had typical drywall and brick construction dimensions, the interior walls of the suite were made with typical wood stud and drywall techniques, the ceiling was formed of drywall backed by insulation leading to an unheated attic, and one full interior wall (along the living room and dining room by the suite's entrance door) was not exposed to the exterior;
2. The rooms had 2.5-meter-high (8-foot-high) ceilings and dimensions shown in **Figures 5a** and **5b**. The windows of the suite were about 9 meters (29.5 feet) above grade;
3. The minimum internal temperature of a room with a window open was the exterior temperature. Once a room equilibrated with the exterior temperature, the room tracked the exterior efficiently

Room	Outside Wall Height (m)	Outside Wall Width (m)	Outside Wall Area (m^2)	Glazed Area (m^2)	Actual Wall Area (m^2)	Ceiling Area (m^2)
Living	2.5	3.5	8.75	3.24	5.51	15.75
Dining	2.5	3.5	8.75	3.24	5.51	19.25
36A	2.5	2.8	7.00	1.35	5.65	9.18
36B	2.5	6.2	15.5	1.35	14.15	9.18
36C	2.5	6.2	15.5	1.35	14.15	9.18
36D	2.5	2.8	7.00	1.35	5.65	9.18
Bath 1	2.5	1.6	4.00	0.4	3.60	6.6
Bath 2	2.5	3.2	8.00	0.4	7.60	3.2

Figure 5a
Estimated wall, glazed and ceiling areas for the rooms (metric).

Room	Outside Wall Height (ft)	Outside Wall Width (ft)	Outside Wall Area (sq ft)	Glazed Area (sq ft)	Actual Wall Area (sq ft)	Ceiling Area (sq ft)
Living	8.2	11.5	94	34.9	59.3	169.5
Dining	8.2	11.5	94	34.9	59.3	207.2
36A	8.2	9.2	75.3	14.5	60.8	98.8
36B	8.2	20.3	166.8	14.5	152.3	98.8
36C	8.2	20.3	166.8	14.5	152.3	98.8
36D	8.2	9.2	75.3	14.5	60.8	98.8
Bath 1	8.2	5.3	43	4.3	38.7	71
Bath 2	8.2	10.5	86	4.3	81.8	34.4

Figure 5b
Estimated wall, glazed and ceiling areas for the rooms (U.S. customary).

with only a minor lag when the exterior temperature changed;

4. Air will flow underneath closed bedroom doors, and this air will be at exterior temperatures once the room has equilibrated;

5. The interior wall of a room with an open window acted as an unheated exterior wall for the remainder of the suite;

6. All kitchen ventilation fans and bathroom fans were off;

7. The baseboard heaters were either fully on or fully off based on typical models. When the non-programmable thermostats were set to "off" in the narrative, that meant the units were unpowered rather than set to a minimum heating value such as 5°C (41°F);

8. Electrical power was available at all times to Suite 36;

9. Toilet tanks were porcelain ceramic with a polystyrene liner, which insulated against heat loss such that water in the tank took much longer to freeze than water in exposed copper pipes;

10. At least 25 mm (1 inch) of ice had formed on the top of the toilet tank, and the same thickness had formed within the bowl;

11. External conditions were represented by Heating-Degree-Day values obtained from International Airport and the Experimental Farm records for December 2009, and the daily outside mean temperature profile for the period[1] was that in **Figure 6**.

Analysis

Nature of the Pipe Bursts

Two sections of copper pipe with longitudinal splits within bulged areas were found at the scene. The splits were caused by localized pipe freeze-up events under the sink in the kitchen in the center of the apartment and in the exterior wall behind one of the bathrooms.

Both were created when locally formed ice fronts within the pipes trapped pockets of water. The mechanism of failure has to do with the water rather than the ice. The trapped water is incompressible, such that as the available volume shrinks, the pressure in the pocket increases past the yield point stress of the copper tube, initiating the permanent bulge deformation pattern and finally causing the longitudinal split. Recent experiments have shown that

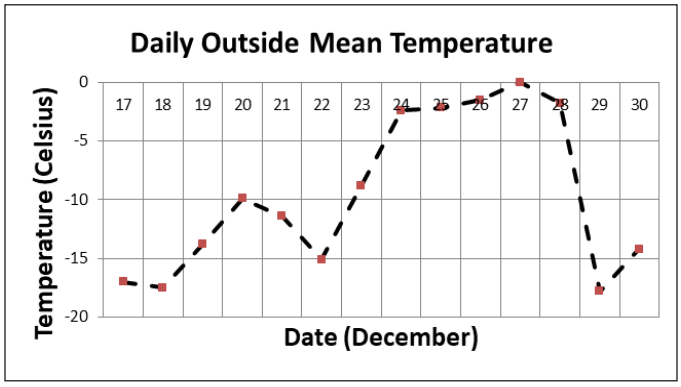

Figure 6
Daily outside mean temperature from Environment Canada, December 2009.

pressures in excess of 7,500 p.s.i. are needed to burst 12 mm (½-inch) diameter copper tubes[2]. Such pressures are not found in a domestic water supply in regular operation.

Consideration of the Requirements to Freeze the Toilet Tank

The time required to create 25 mm (1 inch) of ice on the top of the toilet tank in the bathroom was estimated from first principles. A standard toilet tank, measuring 200 by 300 by 500 mm (7.9 by11.8 by 19.7 inch), would have an approximate volume of 0.03 cubic meters (30 liters) (1835 cubic inches) and a ceramic surface area of 0.52 square meters (5.6 sq.ft).

The well-known steady state heat flow formula,

$$q / A = U x ((t(i) - t(o)) \quad \text{EQ. 1}$$

derives q/A, in which q is the heat in Watts and A is the square area in metres across which the heat flows (from hot to cold), according to thermodynamic laws. The other side of the equation involves U, the overall coefficient of heat transmission, multiplied the difference between two temperatures, t(i) inside and t(o) outside, which drives the flow. U is calculated with the sum of the reciprocals of the conductance values, C:

where C_1, C_2, C_3 = conductance values for materials 1, 2, and 3 in a given wall

$$U = 1/C_1 + 1/C_2 + 1/C_3 + ... \quad \text{EQ. 2}$$

Employing equation (1), with 1000 W/m^2-K (176 BTU/h-ft^2-°F) for porcelain and 1.8 W/m^2-K (0.317 BTU/h-ft^2-°F) for styrofoam, the author determined a value of q of 11.5W (39 BTU/h).

For a temperature decrease from 5°C to -1°C (41°F to 30°F), and a 2.5 liter volume (0.66 US gallon) of ice weighing 2.5 kg (5.5 lb), 825 kiloJoules (778 BTU) are required to cool the water to 0°C (32°F) and 1,588 kiloJoules (1,498 BTU) to crystallize it under typical freezing conditions. In the context of the very slow cooling of the insulated tank, the calculated time to freeze a 25-mm (1 inch) thick top layer was 138,800 seconds, equivalent to 38 hours or about one and a half days. Supercooling and nucleation effects were ignored for this estimate

If this process started with 10°C (50°F) water, this time would increase to approximately 60 hours or two and a half days. The range for the freezing completion means that the initiation occurred from two and a half days to one and a half days prior to the tank inspection on December 30.

Suite 36 Heat Flow Snapshot Analysis Model — Case Descriptions

A system heat flow model of the suite was created to give a snapshot of conditions at a particular instant, based on assumptions about the construction of the exterior walls and windows. Sequential snapshots at the daily mean temperature gave insight into the heat flow trends, and were a proxy for the temperature trend of the suite — because no direct temperature measurements had been made at the time of the incident. The goal was to establish if the suite was cooling or not at the time of the snapshot.

The sources of heat gain within Unit 36 were the baseboard heaters set in the individual rooms, the common living room and dining room, and bathrooms. Heat gain from residents was not included. Heat loss would be through the external walls and upward through the ceiling, with some counteractive gain from the common wall with another apartment but very little from the concrete floor slab of the suite. Convection through windows was factored in. At any given time, the instantaneous heat balance could be estimated for a given HDD value. For single side wind impact on a building window, the airflow[3,4] is calculated by:

$$F = 3.6 \times 500 \times A_{ow} \times V^{1/2} \quad \text{EQ. 3}$$

in which the following variables were applied:

$$V = C_t + C_w \times V_{met}^2 + C_{st} \times H_{window} \times abs(T_i - T_e)$$

F (m^3/h): air flow
A_{ow} (m^2): window opening area
C_t = 0.01: wind turbulence factor
C_w = 0.001: wind speed factor
C_{st} = 0.0035: stack effect factor
H_{window} (m): free area height
V_{met} (m/s): meteorological wind speed at 10 m height
T_i : room air temperature, °C
T_e: outdoor air temperature, °C

An estimate of the sensible heat required to bring outdoor winter air to room temperature given by the Energy Cost Formula[5]. Once the air flow is calculated for the snapshot conditions, the F value is substituted as follows:

$$H_s = F \times \rho \times C_p (T_i - T_o) \quad \text{EQ. 4}$$

When further simplified for ρ of 1.20 kg/m3 and Cp of 1.005 kJ/kg, the equation becomes

$$H_s = 1.21 \times F\ (T_i - T_o) \quad \text{EQ. 5}$$

in which F is the flow rate in L/s converted from equation (2) above.

Heat transmission coefficient values for different materials[5], were used to determine a blended number for the exterior and interior walls of the suite. For example, a U-value of 1.41 W/m^2-K (0.248 BTU/h-ft^2-°F) was derived for an exterior wall with a proportion of glazing, and a U-value of 1.04 W/m^2-K (0.183 BTU/h-ft^2-°F) was calculated for the ceilings.

Nine cases, encompassing possible configurations of the heat gain and loss for the system were set. The most extreme condition, an interior temperature of 18°C (64.4°F) and an exterior temperature of -21°C (-6°F), equivalent to a heating-degree-day (HDD) value of 39, was used to evaluate the regular case. The heat losses for the suite walls were 4,090W (14,000 BTU/h) and for the suite ceiling were 4,149W (14,150 BTU/h). For the listed heating capacity of the room as 8,350W (28,500 BTU/h), there would be a slight positive remainder of 111W (378 BTU/h), indicating that the suite would hold the 18°C (64.4°F) temperature. This confirmed that the assumptions were reasonable for a first principles assessment, with an acceptable range of error.

As the starting point for each case, the extreme condition heat balance was calculated, and then extended over the range of HDD values for the time period starting on December 17. In Cases 1 and 2 (see **Figure 7**), the baseboard heaters in Room 36D and Room 36C were turned off, to determine how this would change the heat flow patterns. Case 3 examined the consequences to heat flow of turning both heaters (36D and 36C) off.

To include the effects of opening windows, equations, including such factors as the height of the window above grade (assumed to be 9 meters, 29.5 feet), wind turbulence, stack effects, area of window opening and air flow volume, were used to calculate the heat flow through such an opening. The process was driven by the difference between room air temperature and outdoor air temperature.

For Cases 4 and 5, the effects of opening the window to 10% and 20% for Rooms 36C and 36D, respectively, were modeled, for a series of days beginning on December 17, using the HDD value. The number of air changes per hour for the rooms was estimated and compared with the flow of air to known devices, such as kitchen and bathroom fans, as a reference point to better understand these effects.

In Case 6, the window opening model was deployed with both the dining room and living room windows open, at either 10% or 20%, beginning on December 24, with the heating elements engaged in Rooms 36C and 36D, with those windows closed. Case 7 was similar, but turned off the heating elements in Rooms 36C and 36D from December 17 to December 30, again with those windows closed.

Case 8 put the known positions of the windows and heating elements in the sequence given by the narrative,

Case	Living Room Window	Dining Room Window	Room 36A Heater	Room 36A Window	Room 36B Heater	Room 36B Window	Room 36C Heater	Room 36C Window	Room 36D Heater	Room 36D Window
1	Closed	Closed	On	Closed	On	Closed	On	Closed	Off	Closed
2	Closed	Closed	On	Closed	On	Closed	Off	Closed	On	Closed
3	Closed	Closed	On	Closed	On	Closed	Off	Closed	Off	Closed
4	Closed	Closed	On	Closed	On	Closed	Off	Open	On	Closed
5	Closed	Closed	On	Closed	On	Closed	On	Closed	Off	Open
6	Open	Open	On	Closed	On	Closed	On	Closed	On	Closed
7	Open	Open	On	Closed	On	Closed	Off	Closed	Off	Closed
8	Open	Open	On	Closed	On	Closed	Off	Open	Off	Open
9	Open	Open	On	Closed	On	Closed	On	Closed	Off	Open

Figure 7
Case conditions for the heat flow model.

that is with the window open and the element off in Room 36C beginning December 19, with the window open and the element off in Room 36 D beginning December 24, and the dining room and living room windows open after the latter date. All windows were set simultaneously open at either 10% or 20% in the model.

Finally, Case 9 was created to assess the question about the status of the 36C heater, and whether its operation might have prevented the freeze up.

Model Calculation Results

In Case 1, (room schematic shown in **Figure 8**) for an extreme day with an HDD of 39 (-21°C outside, 18°C inside), the wall area is 74.5 m^2 (798 sq.ft) with U value of 1.41 W/m^2-K, such that q/A is 54.9, while the ceiling area is 102.28 m^2 (1100 sq.ft) with U value of 1.04 W/m^2-K such that q/A is 40.6. For the walls, q calculates as 4,089W (14,000 BTU/h), while for the ceilings, q is 4,148 W (14,150 BTU/h). The estimated total heat loss will be 8,239W (28,100 BTU/h), following Equation (1) above.

When the 1,000W (3,400 BTU/h) heating source was removed, the main room loses 1,195W (4,100 BTU/h) to the space of Room 36D, while Room 36C will transfer 713W (2,430 BTU/h) to the space through the three interior walls which have 53% more conductance. However, losses to the ceiling of Room 36D (normally about 372W (1,270 BTU/h)) will stop, such that the net additional outflow with these settings is 1,908 less 372, or 1,536W (5,240 BTU/h).

The new main room outflow becomes 8,239 plus 1,536, or 9,775W (33,300 BTU/h), which is much higher than the 7,350W (25,000 BTU/h) available from the remaining baseboard heaters. In particular, Room 36C now loses 1,936W (6,600 BTU/h), much more than its 1,250W (4,260 BTU/h) source. The effect of having more wall area of higher conductance becomes apparent.

> *Case 1 Summary:* The main room begins to cool as soon as the heat source in Room 36D is interrupted, in a 39 HDD situation, with a 2,425W (8,270 BTU/h) deficit. The corner Room 36C begins to cool as soon as the heat source in Room 36D is interrupted.

For Case 2, the results follow the format of Case 1, except that the position of the non-functional baseboard heater changed to the corner room (see **Figure 9**), Room 36C, taking out 1,250W (4,260 BTU/h).

> *Case 2 Summary*: The main room begins to cool as soon as the heat source in Room 36C is interrupted, in a 39 HDD situation. The deficit of 821W (2,800 BTU/h) is less significant than that of Case 1, in part because there would be a smaller area of higher conductance wall involved.

Whenever a room would lose its source of heat gain, the exterior wall to that room would move toward equilibrating with the outside temperature. This process made that exterior wall become "invisible," such that the interior walls of the room became the new exterior walls of the main room. By switching walls constructed to meet the demands of exterior walls (U = 1.41 W/m^2-K) for drywall and stud constructed interior walls with higher coefficient

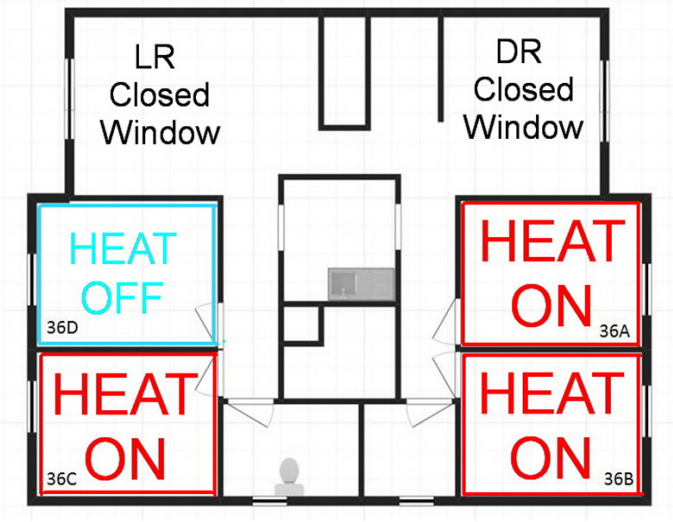

Figure 8
Case 1 suite diagram – heat source off in 36D.

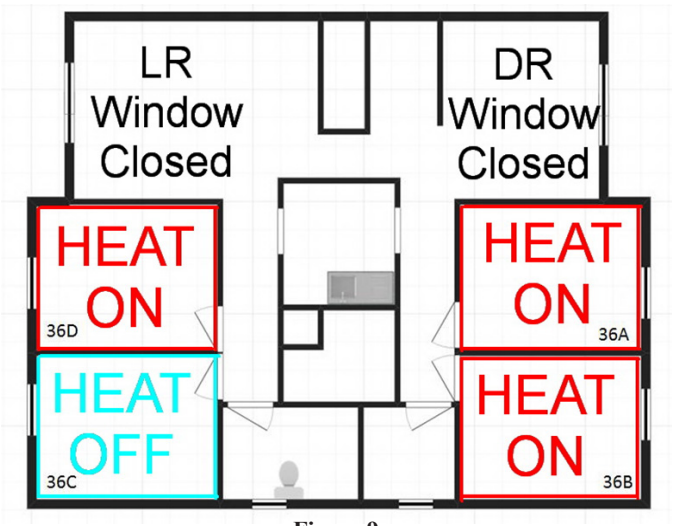

Figure 9
Case 2 suite diagram – heat source off in 36C.

of heat transfer (U = 2.15 W/m²-K), the dynamics for the heat transfer of the main room changed significantly.

Case 3 combines Cases 1 and 2, such that the corner of the suite loses its heat sources, as shown in **Figure 10**. The principle applies once again — the interior wall now acting as an exterior wall copes poorly with the situation, such that the net outflow falls slightly to 8,204W (28,000 BTU/h) compared to 8,238W (28,100 BTU/h). However, only 6,100W (20,800 BTU/h) are available to heat the suite, resulting in a deficit of 2,104W (7,200 BTU/h).

> *Case 3 Summary*: The main room begins to cool as soon as the heat sources in Rooms 36C and 36D are interrupted in a 39 HDD situation. The deficit of 2,104W (7,200 BTU/h) is smaller than that of Case 1, but larger than that of Case 2, due to the different areas of higher conductance wall in the calculations.

The corner Room 36C allegedly had its window open and baseboard heater off (**Figure 11**) from December 19 through December 30, and this was examined in Case 4. For example, using equation (5) assuming 10% window opening with a velocity 1.14 m/s (3.74 ft/s), with a volume of 72 L/s (152 cubic feet per minute) calculates a convection loss of 3,210W (11,000 BTU/h) for an HDD of 35.8 on December 29th. When combined with the through-wall heat loss of 1,175W (4,000 BTU/h), the net heat loss value for the suite was 4,294W (14,600 BTU/h). The equivalent air changes per hour for Room 36C was 11.3 on that date.

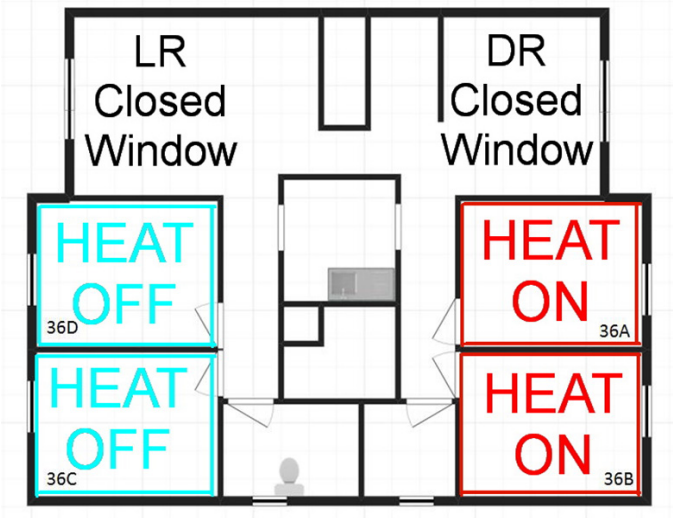

Figure 10
Case 3 suite diagram — heat sources off in both 36C and 36D.

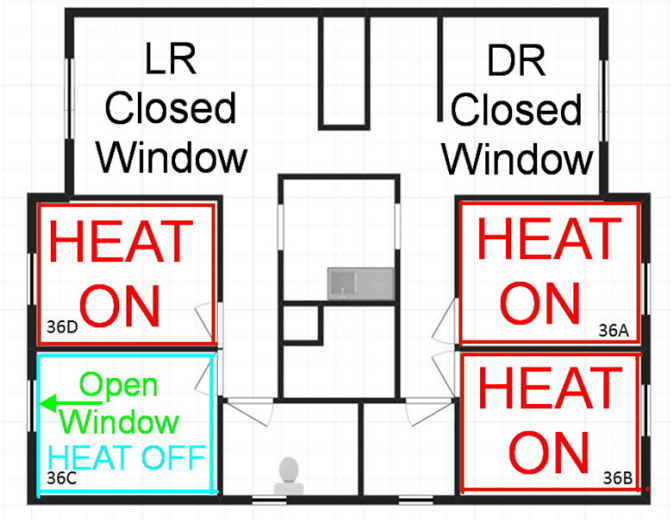

Figure 11
Case 4 suite diagram — window open and heat source off in 36C.

> *Case 4 Summary*: Room 36C begins to cool as soon as the heat source is interrupted and the window is opened, as calculated on a daily basis beginning on December 19, and shown in **Figure 12**. The additional heat loss is about three and a half times larger, and the situation would lead to a disruption of the suite heating dynamics — since between 1,700 and 4,300W (5,800 to 14,600 BTU/h) are required to keep the room at 18°C (64.4°F). This deficit means that the room will cool quickly to the exterior temperature and then track this with a lag. The effect of the percentage opening (10% or 20%) is seen in the cooling trend magnitude.

For Case 5, an adjustment of the wall area from 14.15 square meters (152 sq. ft.) to 22.75 square metres (244 sq. ft.) occurs when the interruption happens, to account

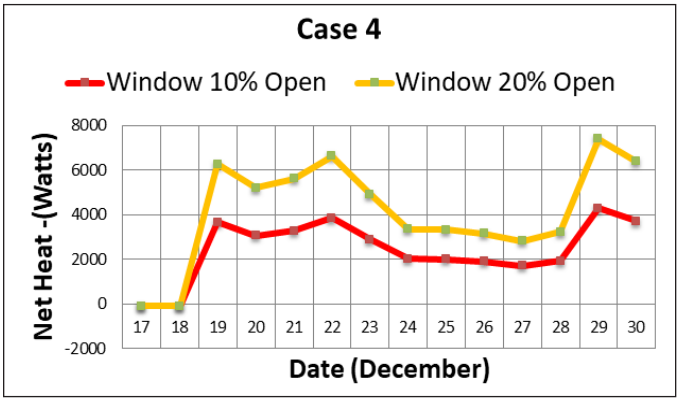

Figure 12
Net heat loss trend by date for Case 4 conditions: window open and heat source off in 36C.

for the equilibration process that begins on three sides: – two walls adjoining the main room and the third adjoining Room 36C (**Figure 13**). The baseboard heater copes well up to and including December 23.

Case 5 Summary: Room 36D begins to cool, behaving in a manner similar to Room 36C in Case 4, as soon as the heat source is interrupted and the window is opened, as calculated on a daily basis beginning on December 24. The additional heat loss is about twice the expected value for a given HDD value, and the situation would lead to a disruption of the dynamics throughout the suite, since between 2,000 and 4,900W (6,820 to 16,700 BTU/h) are required to keep the room at 18°C (64.4°F). This deficit means that the room will cool quickly to the exterior temperature and then track this with a lag, as shown in **Figure 14**.

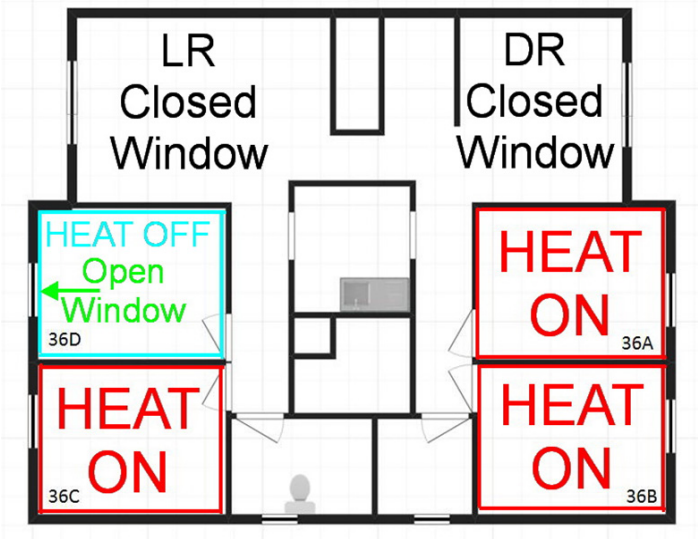

Figure 13
Case 5 suite diagram — window open and heat source off in 36D.

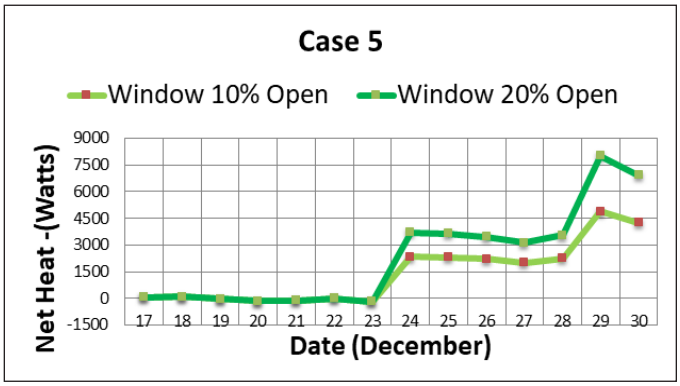

Figure 14
Net heat loss trend by date for Case 5 conditions:
window open and heat off in 36D beginning December 24.

Case 6 mimics having two large windows open while the occupants continue to heat the premises, beginning December 24 (**Figure 15**). Of course, the immediate effect is that the two baseboard thermostatically controlled heaters in these rooms move to 'ON' setting and remain there.

Case 6 Summary: The living and dining rooms begin to cool as soon as the windows are opened, as calculated on a daily basis beginning on December 24. With between 2,300 and 14,000W (7,840 and 47,700 BTU/h) required to keep the room at 18°C (64.4°F), the cooling trend is affected by the large variance as it responds to the exterior temperature changes. This deficit means that the room will cool most quickly to the exterior temperature on December 29 and 30, when compared to preceding days.

Case 7 follows the set-up of Case 6 except that the elements in Rooms 36C and 36D are turned off, but their windows are kept closed (**Figure 16**). Only when the windows are opened does the heat deficit go well beyond the suite's heating system 6,100W (20,800 BTU/h) heating capability with about four air changes per hour. A comparison of these cases is shown in **Figure 17**.

Case 7 Summary: Removing the heating elements makes the situation dramatically worse in the first few days. The results are similar to Case 6 with a large heat deficit as soon as the windows are opened on December 24. Between 3,000 and 16,200W (10,200 and 55,250

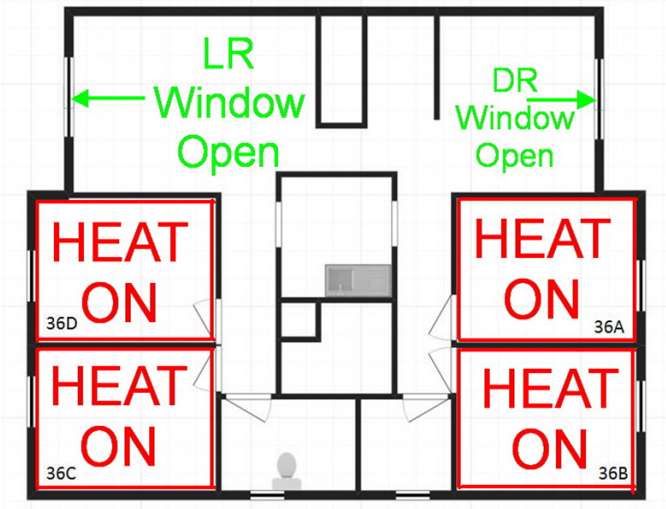

Figure 15
Case 6 suite diagram — windows open
in living room and dining room.

BTU/h) are required to keep the room at 18°C (64.4°F), due to the response to the exterior temperature changes. The room will cool most quickly to the exterior temperature on December 29 and 30.

The known conditions from the sequence described in the summary of the examination for discovery evidence narrative were the basis for Case 8. The heater interruption only causes the heat flow deficit of 1,475W (5,000 BTU/h) to occur on December 29, with a deficit of 711W (2,420 BTU/h) the next day. In sharp contrast, the open window of Room 36C (**Figure 18**) brings the net heat value to a deficit of 2,300W (7,840 BTU/h) on the first day the windows were open in that room.

The heat deficit stays below 3,000W (10,230 BTU/h) until December 24, when three more sets of windows are opened in the suite (Room 36D, living room and dining room), and the deficit falls to 7,300W (24,900 BTU/h). It changes to 5,200W (17,700 BTU/h) on the warm day of December 27 and then drops dramatically to 22,500W (76,700 BTU/h) on December 29, and remains at 19,000W (64,800 BTU/h) the next day when the water escape was discovered.

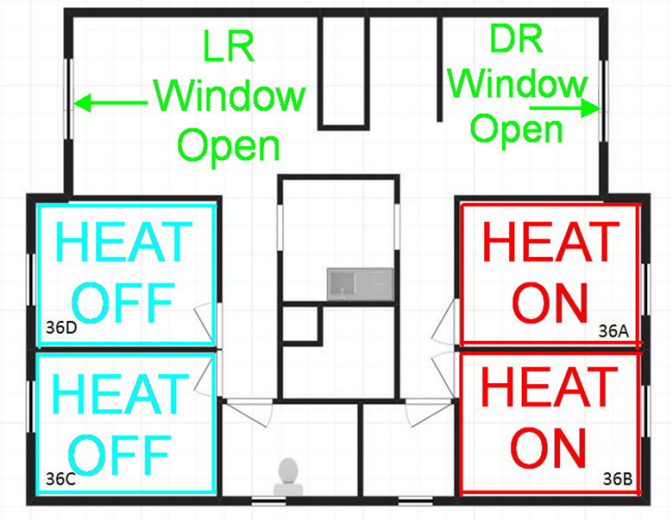

Figure 16
Case 7 suite diagram — heat source off in both 36C and 36D, windows open in living room and dining room.

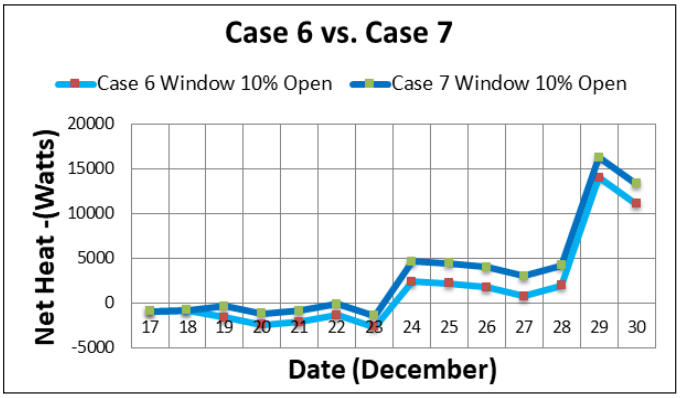

Figure 17
Comparison of net heat loss trends by date for Cases 6 and 7, living room and dining room windows 10% open.

Case 8 Summary: The suite began to cool as soon as Charlie opened his window and turned off the heat in Room 36C on December 19 (see **Figure 18**), instilling a heating deficit range of 700 to 2,300W (2,400 to 7,840 BTU/h) for the whole suite, depending on the HDD value. The heating deficit was exacerbated on December 24 by the opening of the windows in 36D by Dave and the living room and dining room by Dave and Bob as well as the interruption of the baseboard heater in Dave's room. The suite temperature then equilibrated with the outside after December 24, rendering the suite pipes susceptible to freezing on December 28 (when the temperature dropped to -21°C or -6°F) because the water in the pipes started from a cold temperature other than 18°C (64.4°F), as would be expected in a heated suite.

DISCUSSION

Heat Flow Model Trends

The model's cases break out the separate effects of the heating source interruption and the exchange of outdoor air through open window(s). The minor relative importance of the baseboard heaters being turned off was shown in contrast to the drastic impact of the opening of

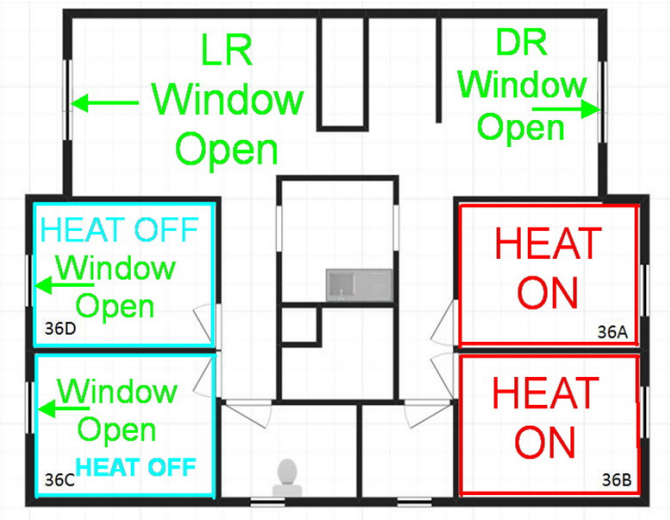

Figure 18
Case 8 unit diagram — heat source off in both 36C and 36C, windows open in 36D, 36C, living room and dining room.

four sets of windows to 10% positions on December 24. The chart in **Figure 19** reveals that the suite was in a heating deficit condition from the first day, December 19, that the window of Room 36C was opened 10%, its baseboard heater turned off, and the volume of air in the suite was changing about once per hour.

The alleged actions of Charlie of opening the window in Room 36C and turning off the baseboard heater in that room created the precursor conditions of a heat deficit that developed in the suite. The now unavailable 1,250W (4,260 BTU/h) may have prevented the cooling of the main portion of the suite to below freezing, and there would have been no convective cooling losses associated with the air changes in that room. Opening these windows and closing and locking the room door initiated the freeze-up process by lowering the average temperature of the suite in the days coming up to December 24.

The immediate effect of Dave opening the window to his room, and to Dave and Bob leaving the living room and dining room window open was a threefold increase in the heating deficit to 7,300W (24,900 BTU/h) and a quintupling of the air change cycle to five main room volumes per hour. The temperature of the suite cannot do anything except decrease to match the exterior low temperatures, which ranged from -7°C (19.4°F) on December 24 to -21°C (-6°F) on December 30.

The effect of having the corner room act as part of the exterior world would have made for cold spots on that side of the suite. For example, the adjacent inside of the exterior wall would cool down, and the air space behind the washrooms would cool laterally, providing the impetus for one of the pipe bursts if the ice front was moving from 36D toward the toilet of one of the bathrooms.

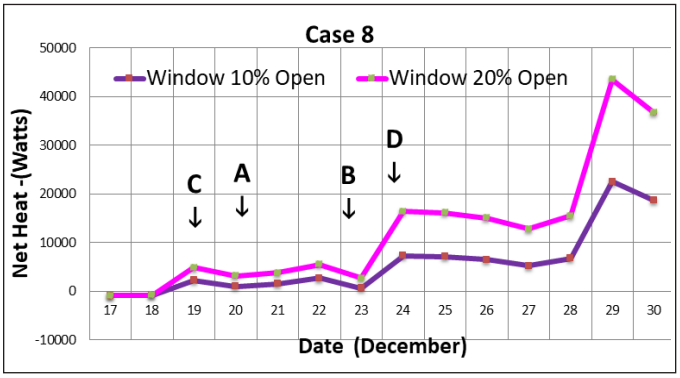

Figure 19
Graph of Case 8 showing the net heat flow by date with heat off in Room 36C and 36D; windows at 10% or 20% open in living room, dining room, Room 36D and Room 36C. Departure dates are labelled by resident initial and arrow.

The model dynamics suggested that the suite began its cooling on December 19 and experienced a steady average decrease in temperature until the night of December 29, when the deficit was too much for system. In other words, the starting point temperature was low enough on December 28 that the equilibration with the exterior on December 29 could create an effective freeze-up of the pipes within the kitchen and the exterior bathroom wall.

The relative effect of shutting down baseboard heaters was demonstrated to be less than that of opening windows, and to the layman, this makes sense and speaks to everyday experience. The attempt to heat the downtown of a Canadian city in winter with two baseboard heaters was futile.

Limitations of the Heat Flow Model

The calculations are limited to being a best estimate of the site conditions in the absence of evidence from inspection by other parties on the construction techniques in existence at the time of the incident. A quantitative viewpoint provided the baseline for a qualitative assessment of the trend of whether the suite was cooling or staying put. The analysis is sensitive to the factors used — in particular, the calculated area of exterior walls and glazing and the blended coefficients of heat transmission for the exterior and interior walls. Decreasing the area of the walls or the ceiling will lower the value of q, while an increase of the coefficient will increase the heat loss of the suite. The heat flow calculations are susceptible to compounding errors from the underlying assumptions. The assessment was restricted by budgetary constraints, so employing a commercially available heat flow software package was not practical.

Pipe Burst Circumstances

There are many reported instances of pipes that froze but did not burst. It is not a “sure thing” that pipes will burst under freezing conditions. A special subset of circumstance may be required to initiate the bursting process, which is an extreme reaction of the water supply system to a severe drop in temperature.

Generally, a large-volume insulated vessel will take longer to freeze than a small-volume bare copper pipe. Given the dynamics of heat flow in the suite from the model, it is more likely that the toilet freeze-up occurred approximately two days prior to its discovery on the night of December 30. In other words, the toilet tank had to

begin to freeze on or before December 28, but the exposed copper pipes would have begun to freeze prior to that date.

One of two pipe bursts occurred within an exterior wall. It is well-known that air spaces act as insulators. Since the air gap within is acting as one of the heat-resistive layers in the wall cross-section, it has a role in keeping a pipe within the space above the freezing point. The Ontario Building Code specifically states that pipes that are installed in areas that can freeze must be protected against freezing. It was assumed that in the original design of the building, this area was not one that was anticipated to fall below freezing. On the other hand, insulation along the exterior behind the pipe would have kept some of the heat in the suite rather than letting it escape.

The main source of the water escape was in the kitchen underneath the sink within a cabinet. This hot water pipe was within that air space which would have not been subjected to direct contact with outdoor air, given the distance from the kitchen to either the dining room or living room windows. The cabinet would act to delay onset of freezing from air contact until the adjacent room had significantly dropped in temperature. Therefore, a lag would be expected between the minimum temperature occurrence and the development of freezing conditions under the sink.

Case 9 — Model of Heat Flux with Room 36D Window Shut and Heating Element On

The freezing of the pipes would have begun within 12 hours of the last tenants' departure from the suite at 3 a.m. on December 24, that is, about 3 p.m. on December 25, taken with the evidence of the frozen toilet tank, which required a minimum of 38 hours to a maximum of 60 hours to freeze.

Putting some context to the incident, an unheated sealed detached home beginning at 18°C (64.4°F) will cool to -6°C (21F) in 24 hours (about 1°C per hour) depending on the methods of construction, based on Arcon's measurements during winter power failures in Toronto.

The fact that the windows were open was more relevant to the development of the incident, since this provided uncontrolled exchange of outdoor air, while the absence of baseboard heaters in the rooms meant that the whole suite would have a larger heating deficit. Case 3 demonstrated that the absence of these heaters in Rooms 36C and 36D will cause the main room to be more sensitive to the exterior temperature, and that it will cool down. By adding the open windows, however, the modeled process of cooling was accelerated considerably.

Figure 19 reveals that the suite was in a heating deficit condition from the first day (December 19) that the window of Room 36C (Charlie's) was opened 10%, and its baseboard heater turned off. Case 8 represents the reported configuration discovered with the water escape.

The alleged actions of Charlie set in place the precursor conditions of heat deficit to develop in the suite, by lowering the average temperature of the suite in the days coming up to December 24, when the actions by others precipitated the process. Closing the room door, which was included in the author's analysis as part of the wall of Room 36C, did not retard the cooling process.

The author was asked to consider, "Whether having the window shut and the heating element on in the room would have prevented or lessened the water damage from the frozen pipes that was ultimately discovered on December 30, 2009."

In response, another engineer opined that, based on the total baseboard capacity in the living room, dining room and bathrooms of 3,850W (13,100 BTU/h), that 'the 1250W heater in Charlie's bedroom would have been incapable at preventing or lessening the large drop in indoor temperature in the common open space. Having the bedroom door closed would have prevented any movement of warm bedroom air to the adjoining corridor.'

Case 9 of the model was created to assess this statement, and the configuration is shown in **Figure 20**. With just the heating element added on, the net heat deficit for the suite occurs on December 29, and had a value of 665W (2,270 BTU/h) loss, not typically enough to freeze the pipes in a day. The closing of the window shifts the first net heat loss value to 5,000W on December 24 (**Figure 21**), considerably less than the 7,300W (24,900 BTU/h) seen in our Case 8. The maximum heat deficit becomes 18,500W (63,000 BTU/h) on December 29, compared to 22,500W (76,700 BTU/h) in Case 8.

The effects of Charlie's actions were not inconsequential to the overall circumstances. Rather, they interfered with the dynamics of the heat flow within the suite, and caused the base conditions of the main suite to alter to a lower temperature such that it was more susceptible

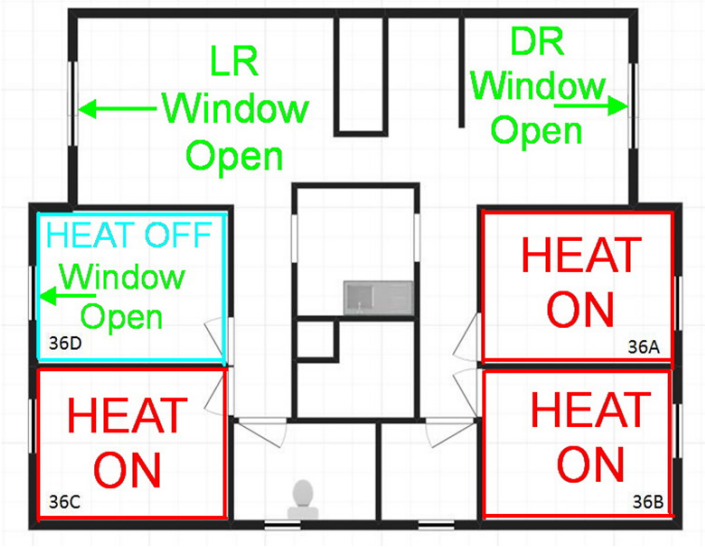

Figure 20
Case 9 suite diagram — heat source off in 36D, windows open in 36D, living room and dining room.

to the freeze-up.

Had Charlie not opened his window, he might have prevented the main suite from cooling as quickly during the post-December 24 period, but it remained unclear whether it would have prevented localized freeze-up damage.

The problems in the bathroom are possibly associated with Charlie's corner room not having adequate heat after December 19, rather than due to the bathroom door being opened. The wall behind the bathroom connects to Room 36C, and would have been subject to the heat losses seen in Room 36C.

Opening the doors to Rooms 36C and 36D provides a path for air to circulate, which would increase the ability of air change cycles to occur and increase the heat flow. Rooms 36C and 36D had about eight to 10 room volume changes of air per hour occurring even with the door closed and their windows at 10% open position (see Cases 4 and 5). Open doors would quicken the air circulation process and let equilibrium conditions develop faster, such that air in the main room would circulate more than seen in our Case 8, and reach the outdoor temperature sooner. Having doors open for Rooms 36C and 36D would correspondingly hurry along the freeze-up of the water pipes.

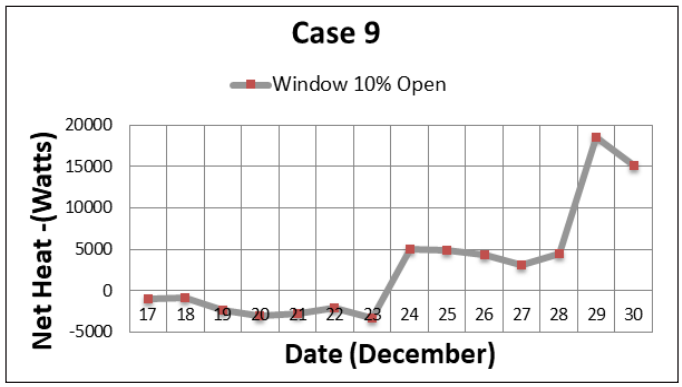

Figure 21
Net heat trend by date with Case 9 conditions: Heat off in Room 36D; Room 36D, living room and dining room with windows 10% open.

Conclusions

A thermodynamic heat flow snapshot model was developed from first principles to assess the status of gain or loss trend at any time, as a proxy for the temperature in the suite. The model revealed that a combination of factors led to the water escape circumstances. The most significant factor was that the living room and dining room windows were left open on December 24, 2009, with a strong contribution from the cessation of heating and the open windows of Rooms 36D and 36C.

A contributing factor for the development of the precursor conditions was the activity of Charlie in Room 36C, who left the window open and the baseboard heater turned off on December 19. The actions of Charlie were not inconsequential because the model showed they set the stage for the freeze-up incident by lowering the temperature within the suite.

After December 24, based on the HDD records, the model indicated that the suite had a large heating deficit that left it unprepared for the cold snap to -21°C (-6°F) on December 28. The insulated toilet tank freeze-up provided an independent source of information on the timing, and put the tank freeze-up event at two to three days before December 30, that is December 27 to December 28. The bare copper pipes would freeze before the toilet tank so they must have frozen before December 27.

The thermodynamic heat flow model supported an inference that the pipes most likely began to freeze about 3 p.m. on December 25, that is approximately 12 hours after the last tenant, Dave, exited at 3 a.m. on December 24.

The bathroom supply pipe froze from the inside out, rather than from the outside exposure, in a space that was not insulated, but these "no-heat" conditions may not have been anticipated at the time of the building design and construction.

References

1. Environment Canada Historical Data, Daily Data Report, December 2009. [Online] https://climate.weather.gc.ca/climate_data/daily_data_e.html

2. J. Certuse, PE, DFE (NAFE 708F) private communication, ISE Engineering experimental data, June 2017.

3. Ventilation for buildings – Calculation methods for the determination of air flow rates in buildings including infiltration. CEN/TC 156 – prEN 15242:2006, BSI Secretariat.

4. IEA Annex 20 – Air Flow Patterns Within Buildings, International Energy Agency, 1993, pp 14-20.

5. Neil B. Hutcheon and Gustav O.P. Handegord, Building Science for a Cold Climate, Construction Technology Centre Atlantic Inc. Fredericton, NB. 1989

Appendix A: Calculations of Constants Used in the Analysis and Charts of Heat Loss

Thermal Resistance Values, K-m^2/W

$16.6 \rightarrow for\ drywall/plasterboard$
$8.3 \rightarrow vertical\ surface\ in\ still\ air$
$6.1 \rightarrow horizontal\ surface\ in\ still\ air$
$6.1 \rightarrow air\ space\ in\ a\ wall$

$k = 2.15 \rightarrow for\ inside\ wall\ of\ wood\ stud\ and\ plasterboard\ (two\ layers)$

$To\ calculate\ U\ value, Thermal\ Transmittance, \frac{W}{(m2 \cdot K)}$

Where C_1, C_2, C_3 = resistance values for materials 1, 2, and 3 in a given wall

$U = 1/C_1 + 1/C_2 + 1/C_3 + ...$

U values calculated for the suite:

$1.41 \rightarrow combined\ for\ the\ exterior\ walls\ and\ windows$
$3.2 \rightarrow for\ windows\ in\ the\ suite, storm\ type$
$1.04 \rightarrow for\ stud\ walls$

To convert from W/m^2-K to BTU/hr-ft^2-°F, divide by 5.678:

$0.248 \rightarrow combined\ for\ the\ exterior\ walls\ and\ windows$
$0.563 \rightarrow for\ windows\ in\ the\ suite, storm\ type$
$0.183 \rightarrow for\ stud\ walls$